AD-A084 786 ILLINOIS UNIV AT URBANA-CHAMPAIGN DEPT OF MECHANICAL --ETC F/G 20/4
AN EXPERIMENTAL AND THEORETICAL INVESTIGATION OF MULTIPLE DUCTE--ETC(U)
JAN 80 H L PETRIE, A L ADDY DAAG29-76-G-0200
UNCLASSIFIED UILU-ENG-80-4002 ARO-13737.2-EX NL

1 OF 2
AD
A084786

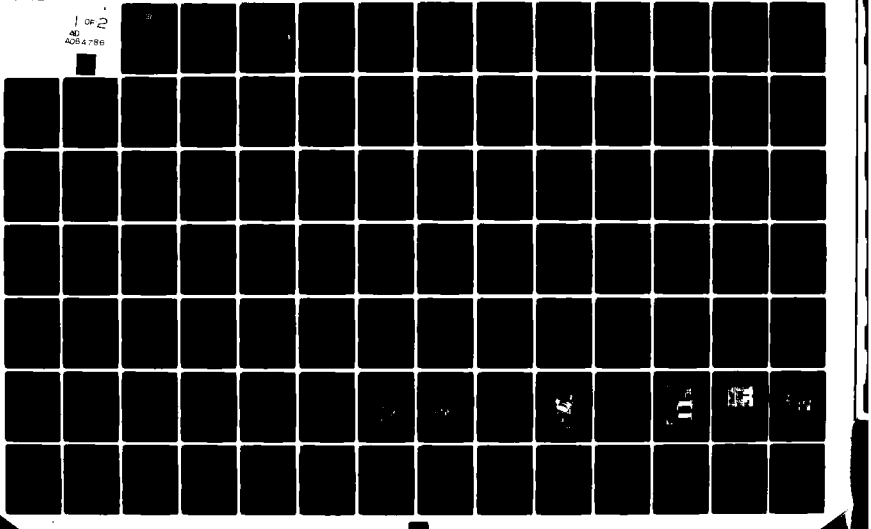

MECHANICAL ENGINEERING LABORATORY
UILU-ENG-80-4002
DEPARTMENT OF MECHANICAL
AND INDUSTRIAL ENGINEERING
UNIVERSITY OF ILLINOIS AT URBANA-CHAMPAIGN
URBANA, ILLINOIS 61801

FINAL TECHNICAL REPORT

AN EXPERIMENTAL AND THEORETICAL INVESTIGATION OF MULTIPLE DUCTED STREAMS WITH A PERIODIC OR A STEADY SUPERSONIC DRIVER FLOW

by
H. L. PETRIE
A. L. ADDY

JANUARY 1980

Supported by
U.S. Army Research Office
Research Grant DAAG 29-76-G-0200
and the
Department of Mechanical and Industrial Engineering

Errata

to Report
"An Experimental and Theoretical Investigation
of Multiple Ducted Streams with a Periodic
or a Steady Supersonic Driver Flow"

On page 25, change the last two lines on the page from

"Section 6.0, the APPENDIX, contains ..."

to

"APPENDIX A, contains ..."

On page 144, change the second and third lines from the bottom from

"... to drive a supersonic-subsonic configuration during ..."

to

"... to drive a supersonic-subsonic ejector configuration during ..."

Unclassified

SECURITY CLASSIFICATION OF THIS PAGE (When Data Entered)

REPORT DOCUMENTATION PAGE

READ INSTRUCTIONS BEFORE COMPLETING FORM

1. REPORT NUMBER: UILU-ENG-80-4002
2. GOVT ACCESSION NO.: AD-A084 786
3. RECIPIENT'S CATALOG NUMBER: ----

4. TITLE (and Subtitle): An Experimental and Theoretical Investigation of Multiple Ducted Streams with a Periodic or a Steady Supersonic Driver Flow
5. TYPE OF REPORT & PERIOD COVERED: Final Technical Report 1976-80
6. PERFORMING ORG. REPORT NUMBER: UILU-ENG-80-4002

7. AUTHOR(s): H. L. Petrie, A. L. Addy
8. CONTRACT OR GRANT NUMBER(s): DAAG 29-76-G-0200

9. PERFORMING ORGANIZATION NAME AND ADDRESS: Dept. of Mechanical and Industrial Engineering, University of Illinois at Urbana-Champaign, Urbana, Illinois 61801
10. PROGRAM ELEMENT, PROJECT, TASK AREA & WORK UNIT NUMBERS: 11162

11. CONTROLLING OFFICE NAME AND ADDRESS: U.S. Army Research Office, Post Office Box 12211, Research Triangle Park, NC 27709
12. REPORT DATE: Jan 80
13. NUMBER OF PAGES: 160

14. MONITORING AGENCY NAME & ADDRESS(if different from Controlling Office): 1) Final rept. 1976-1980,
15. SECURITY CLASS. (of this report): Unclassified
15a. DECLASSIFICATION/DOWNGRADING SCHEDULE: NA

16. DISTRIBUTION STATEMENT (of this Report)

Approved for public release; distribution unlimited.

DTIC ELECTE MAY 28 1980 D

17. DISTRIBUTION STATEMENT (of the abstract entered in Block 20, if different from Report)

(18) ARO (19) 13143.3-EX

C

18. SUPPLEMENTARY NOTES

The findings of this report are not to be construed as an official Department of the Army position unless so designated by other authorized documents.

19. KEY WORDS (Continue on reverse side if necessary and identify by block number)

Supersonic Ejector
Mixing Flows
Steady Flow
Periodic Flow

20. ABSTRACT (Continue on reverse side if necessary and identify by block number)

An experimental and theoretical investigation of a supersonic-subsonic, two-dimensional planar, constant area ejector with a periodically pulsed or a steady driver flow is discussed. A large scale fluidic oscillator was developed to partially pulse the driver flow at frequencies up to 250 Hz. A wide range of ejector flow conditions were experimentally investigated with three values of ejector mixing duct length-to-width ratios. Driver flow frequencies of 142 Hz and 250 Hz were used in the ejector experiments and a

DD FORM 1 JAN 73 1473 EDITION OF 1 NOV 65 IS OBSOLETE

Unclassified

SECURITY CLASSIFICATION OF THIS PAGE (When Data Entered)

AD A084 786

complete set of steady driver flow experiments was conducted. A one-dimensional, quasi-steady control volume analysis was successfully employed to model these ejector flows.

Unsteady ejector flows were found to be modeled well by the quasi-steady analysis. Both steady and unsteady ejector flow performance parameters were accurately predicted by the one-dimensional analysis with the exception of the pressure recovery characteristics observed. Experimentally determined compression ratios were about 25% lower than predicted by the analysis. The pulsation of the driver flow was found to have little effect on ejector operation. Mixing and entrainment characteristics did not appear to be altered by the pulsed driver. Pressure recovery was enhanced but only slightly. The steady driver ejector flows were quite unexpectedly found to be unstable and highly disturbed under most flow conditions. It was felt this may have negated the effects of the pulsed driver flow. The Strouhal number of pulsed driver flows was not felt to be high enough to significantly effect the dynamics of mixing between high speed ducted streams.

AN EXPERIMENTAL AND THEORETICAL INVESTIGATION OF MULTIPLE DUCTED STREAMS WITH A PERIODIC OR A STEADY SUPERSONIC DRIVER FLOW*

by

H. L. Petrie†

A. L. Addy††

January 1980

Supported by

U.S. Army Research Office
Research Grant DAAG 29-76-G-0200

and the

Department of Mechanical and Industrial Engineering
University of Illinois at Urbana-Champaign
Urbana, Illinois 61801

---

* This report is based on the M.S. thesis of H. L. Petrie

† Graduate Research Assistant

†† Professor of Mechanical Engineering

ACKNOWLEDGMENTS

We wish to acknowledge the support provided for this research by the U.S. Army Research Office under grant number DAAG 29-76-G-0200. Mr. James J. Murray of the U.S. Army Research Office served as the Technical Monitor of this grant.

TABLE OF CONTENTS

NOMENCLATURE

Symbols

A	Area.
C_p	Specific heat at constant pressure.
C_v	Specific heat at constant volume.
d	Jet diameter.
$f_1( )$, $f_2( )$, ...	Gas dynamic functions defined in the text.
F	Force.
g	The acceleration due to gravity.
h	Specific enthalpy.
L	Mixing duct length.
M	Mach number.
Mw	Molecular weight.
P	Pressure.
Q	Heat.
R	Universal gas constant.
St	Strouhal number.
t	Time.
T	Absolute temperature.
V	Magnitude of velocity.
w	Mass flowrate.
w_{sp}	Secondary to primary mass flowrate ratio.
W	Mixing duct width.
W_{ss}	Work, shaft and shear.
X	Longitudinal or flow-direction coordinate.

Symbols (cont.)

Z	Elevation.
γ	Ratio of specific heats.
ρ	Density.
ω	Frequency.

Subscripts

0	Stagnation state.
$1,2,3$	System locations.
cs	Control surface.
m	Mixed.
p	Primary flow.
s	Secondary flow.
x	Quantity in the flow coordinate direction.

Superscripts

$*$	Choked flow quantity.
$\overline{\quad}$	Mean value.

Acronyms

APPR	Approximate flow regime.
MR	Mixed flow regime.
SR	Supersonic flow regime.
SSR	Saturated supersonic flow regime.
UCAE	Unsteady constant area ejector program.

LIST OF FIGURES

1.0 INTRODUCTION

This investigation of multiple ducted streams with a periodic driver flow was conducted to determine if the periodic driver flow was an effective mechanism to improve the momentum and energy exchange and to enhance mixing between compressible high speed ducted streams. The ducted system investigated was a two-dimensional planar, constant area, air-to-air, supersonic-subsonic ejector. A large scale fluidic oscillator was developed to generate the periodic pulses in the primary driver flow. A theoretical analysis based on the assumptions of a one-dimensional, quasi-steady, inviscid flow was developed and compared with experimental results. An extensive experimental program examining both steady and periodic driver flows in the ejector was carried out.

1.1 STATEMENT OF THE PROBLEM

The impetus of this investigation is rooted in fluid-dynamic problems encountered in the development of high energy chemical laser systems. The high Mach number, low pressure streams entering the laser cavity do not readily mix. This results in a short lasing zone and restricted laser power output. The introduction of an unsteady flow into this flow could potentially enhance the mixing between these multiple high speed compressible laser cavity streams by causing large disturbances and vorticity in these flows.

The high temperature, low pressure, corrosive laser cavity flow must be pumped, after exiting the cavity, to the prevailing ambient pressure condition. As discussed later, ejector-diffuser systems are well suited

for this task, despite the fact that the ejector-diffuser is a heavy, bulky, and inefficient addition to the laser system. Walker [1][†] discusses topics involved in laser-ejector system integration such as packaging multiple ejectors, diffuser requirements, and staging considerations. The opinion was expressed by Walker, et al., that advances in ejector packaging and investigations of the effects of laser system parameters on ejector operation could lead to improved ejector system performances; however, any significant improvement in ejector performance is most likely to be the result of advances in ejector technology.

The overall goals of this research program were to investigate how a periodic driver flow influenced ejector performance parameters and whether a periodic driver flow in an ejector significantly enhanced mixing and momentum exchange between the ducted, high speed, compressible primary and secondary streams.

The investigation had the following specific objectives:

1. To develop an understanding of the mechanisms, processes, and interactions involved in ducted multiple stream flows with a periodic driver;
2. To develop and evaluate a theoretical model for such a system;
3. To determine if a periodic driver flow demonstrates the potential to make ejector systems more compact and/or efficient;

[†]Numbers in brackets refer to entries in REFERENCES.

4. To develop a large-scale fluidic oscillator with no moving parts, frequency adjustability, and small losses;
5. To add to the limited technology and data base of such flows.

1.2 GENERAL BACKGROUND AND LITERATURE SURVEY

Ejectors are non-mechanical devices used to pump, compress, mix, and convey fluids. Ejector applications include high vacuum systems, ram-jet combustors, thrust augmentation nozzles, nuclear reactor core flow recirculation pumps, and chemical laser pumping systems to name just a few. Ejector system configurations range from one axisymmetric primary driver flow nozzle concentrically directing its flow into a constant area cylindrical mixing tube to a bank of hypermixing nozzles directing skewed driver flows into a variable area rectangular duct [1,2,3].

The basic mechanisms of ejector operation are viscous interaction and mixing between the primary driver and secondary induced flows. Thrust augmentation and the pumping and compression of a secondary flow are the result of the momentum and energy transfer from the primary to secondary flow within the mixing duct of the ejector [4]. During ejector start-up the momentum of the primary driver flow is imparted to the fluid within the mixing duct; this causes a flow towards the open end of the duct. The resulting pressure drop at the inlet end of the mixing duct induces a secondary flow to enter the duct. The primary and secondary flows interact and mix, ideally reaching a fully uniform state at the exit plane of the ejector mixing duct.

A number of analytical methods, differing in levels of sophistication, have been applied successfully to ejector flows. Finite difference techniques were used by Gilbert and Hill [5] to model a two-dimensional planar, variable area, slot nozzle ejector. Hasinger [6] has applied a one-dimensional analysis to a number of ejector mixing modes including constant area, constant pressure, and a defined pressure profile along the mixing duct. Tai [7] has developed a computer code that for given entrance conditions and a wall static pressure distribution determines the ejector wall contour by finite difference techniques. A one-dimensional inviscid analysis was applied by Addy and Mikkelsen [8] to the supersonic-subsonic, constant area ejector. This analysis is based on the method of Fabri and Paulon [9]. The quasi-steady flow ejector analysis developed during this investigation is based on the steady flow ejector analysis of Addy and Mikkelsen. More detailed analyses by Chow and Addy [10,11] and Chow and Yeh [12] of supersonic-subsonic ejector flow use the method of characteristics to determine the initial supersonic primary flowfield and a one-dimensional model of the secondary flow. Viscous effects, variable area inlet sections, and special consideration of low secondary mass flow rates are incorporated into these analyses.

Supersonic-supersonic, constant area ejector-diffuser flow was modeled with a one-dimensional control volume approach by Mikkelsen, Sandberg, and Addy [13]. The one-dimensional theory predicted maximum ejector compression ratios 15 to 20 percent higher than the corresponding experimental values. The supersonic-supersonic, constant area ejector was particularly susceptible to secondary flow separation

which requires a more sophisticated analysis than the one-dimensional theory used.

One-dimensional analyses of ejector flow are limited, in a strict sense, to constant area ducts. Constant pressure and specified pressure distribution mixing modes can be treated by one-dimensional analyses [6,8] but rely on more sophisticated analyses or empiricism to obtain the required wall contour. Viscous interaction between primary and secondary ejector streams can noticeably effect the secondary mass flowrate [10,11,12] under certain flow conditions but one-dimensional analyses do not consider or predict such flow field details. Despite these limitations, theoretical predictions based on the simple one-dimensional approach are generally in good agreement with experimental results.

Extensive bibliographies of ejector literature and papers have been compiled by Addy and Mikkelsen [8,13].

Ejector pumping systems have their advantages and disadvantages when compared to conventional mechanical systems. A detailed comparison of ejector and mechanical pumping systems has been made by Baker and McDermit [14]. The no-moving-parts simplicity and the simple geometry of ejector systems facilitates protective cooling, lining, or coating of wetted ejector surfaces. Ejectors can be fabricated from most materials without difficulty. Thus ejectors often see service where high temperature corrosive fluids are involved, such as in chemical lasers. Ejectors start quickly and respond rapidly to adjust to changing flow conditions. Ejector applications which require large secondary flowrates and high pressure recovery are accomplished by the packaging of ejectors in parallel

and/or series. A diffuser is generally used to further improve the pressure recovery of an ejector system. Such ejector-diffuser systems tend to be heavy and bulky and to require considerable quantities of high pressure primary flow to pump the secondary fluid. Optimum performance of ejector systems is usually limited to a small range of operating conditions and requires total system integration to achieve.

This investigation is based on the premise that a periodic driver flow may enhance the modes of flow interaction beyond those which exist in a steady flow ejector. Turbulent mixing and entrainment, the basic mechanisms involved in steady ejector flows, have been the subject of numerous investigations [15-22]. Experimental evidence indicates that large scale eddies, which evolve from surface waves generated by turbulence induced instabilities at a fluid interface, act as the primary mechanism of entrainment in turbulent shear flows. The rate of entrainment and mixing layer growth depend directly on the intensity of the large scale eddies and indirectly on factors which determine the frequency of eddy generation and the speed of their decay. These large scale structures in the turbulent mixing layers have often been found to be coherent and periodic in nature.

Numerous approaches have been taken to enhance mixing by exciting instabilities in the shear layer of air jets. Crow and Champaign [23] used loudspeakers in a plenum chamber upstream of the exit of a round jet discharging into the atmosphere in an attempt to force latent periodic structures that may exist in the turbulence of the jet mixing layer. Increased entrainment rates and turbulence levels, particularly at the

periphery of the jet, were observed. The virtual origin of the mixing region was shifted approximately two jet diameters upstream with a 2% fluctuation of the exit velocity. Becker and Massoro [24] investigated the instability of an axisymmetric jet with external acoustic stimulation. Pure tones and noise produced both large increases in the mixing layer spread rate and large ring vortices that disintegrated into small scale turbulent eddies. Glass [25] located a reflecting surface near the exit of an overexpanded supersonic jet. Disturbances which were believed to be generated in the shock cells of the supersonic flow, were directed towards the jet exit. Periodic vortex shedding was observed at frequencies as high as 10 kHz. The spread rate and velocity decay of the jet were noticeably increased. McCormack, Cochran, and Crane [26] also obtained increased mixing rates and a shortened potential core by mechanically vibrating a two-dimensional slot nozzle that was discharging air into the atmosphere.

Fully and partially pulsed jets were used in a number of investigations to study the effects unsteady flow had on jet mixing and turbulence. Binder and Favre-Marient [27] used a rotating butterfly valve to pulse an axisymmetric air jet; RMS velocity deviations from the mean of up to 30% were produced at frequencies up to 200 Hz. Centerline velocity decay and spread rates reached their asymptotic values much faster than for the steady jet and the intensity of the turbulence increased more rapidly and remained at higher levels well after pulsations had died away downstream. Bremhorst and Harch [28] fully pulsed an axisymmetric subsonic air jet using mechanically driven rollers that only allowed air flow during approximately 1/3 of each revolution. The entrainment capabilities of the

jet were significantly increased. Olivari [29] examined an axisymmetric jet that was almost fully pulsed. A fluidic back pressure amplifier that used a rotating cam to modulate the control port was used to pulse the flow. Turbulence intensity increased significantly but mixing between the jet and the surrounding fluid was not significantly increased over that of the steady jet. It appears that the Strouhal number, $St = \omega d/V$, is a critical parameter in the above studies. Olivari, et al., had St values of 8.25×10^{-3} and 22×10^{-3} but the other studies, cited above, had St values from 69×10^{-3} to 800×10^{-3}. In general an increase in the Strouhal number causes an increase in the entrainment of a jet and a more rapid decay of the jet core velocity.

Viets [30] developed an alternative approach to stimulate jet entrainment. A fluidic nozzle was used to induce a jet to oscillate transverse to the flow direction. The jet spread rapidly and takes on a serpentine appearance prior to jet breakup. Platzer, Simmons, and Bremhorst [31] compared the effects on the entrainment of the surrounding fluid of a transverse oscillating jet, fully pulsed jets, and co-axial jets with a partially pulsed core. The fully pulsed jets entrained the most ambient fluid and the partially pulsed and transverse oscillating jet entrained approximately the same amount. All three unsteady jets entrained substantially more flow than a corresponding steady jet.

Ejectors have been the subject of a number of pulsed flow investigations [32-35]. The primary driver flow was fully pulsed by a rotating valve mechanism in each of these studies. "Slugs" of primary flow are discharged into a duct producing compression waves in front of the "slug" and

rarefaction waves behind it. The piston-like wave action of the primary flow "slugs" effectively induced a secondary flow into the duct. The normal mode of energy and momentum exchange in these "wave energy exchangers" is ideally isentropic and more efficient than the irreversible mixing mechanism operating in steady flow ejectors. The secondary-to-primary mass flowrate ratio of the pulsed flow ejector was much larger than the mass flowrate ratio of the corresponding steady flow ejector in certain cases. Since the secondary or induced flow stagnation pressure and the exit plane static pressure were atmospheric, nothing is known of the pressure recovery capabilities or the effects of the back pressure on the performance of this pulsed ejector.

In some cases steady flow ejectors have been found to resonate under certain pressure conditions. Quinn [36] has examined the effects of these screech tones on ejector performance. It appears that resonance may have fixed the frequency of shear layer vortices, thus strengthening them. Increased entrainment and mixing between the secondary and primary flows were observed.

Experimental evidence strongly suggests mixing between multiple ducted streams and ejector performance can be improved by an unsteady periodic driver flow. All but a few of the investigations described above were concerned with a significantly different flow situation than is considered in this investigation; however, turbulent mixing and/or entrainment are essential to each one.

2.0 THEORETICAL ANALYSIS OF THE CONSTANT AREA SUPERSONIC-SUBSONIC EJECTOR WITH A PERIODIC DRIVER FLOW

A one-dimensional, quasi-steady analysis was used to model the unsteady ejector flow. A computer code, UCAE, was written to perform this analysis on either experimentally determined input conditions or on a default set of conditions including a periodic sinusoidal driver flow. Figure 2.0-1 indicates the location of the stations and control volume used in the overall analysis. The analysis assumes that uniform supersonic primary and subsonic or sonic secondary streams enter the mixing duct at Station 1, interact and mix, and exit the duct as a uniformly mixed subsonic flow at Station 3. Part of the quasi-steady analysis is based on the method of Fabri and Paulon [9] for the steady flow analysis of an ejector.

2.1 EJECTOR FLOW REGIMES

Four ejector flow regimes are considered in this analysis. These flow regimes are characterized by the secondary-to-primary static pressure ratio at Station 1, P_{s1}/P_{p1}, and whether or not the flow conditions at Station 1 are independent of the back pressure. The "saturated supersonic" regime, SSR, can exist when $P_{s1}/P_{p1} \geq 1.0$ and $M_{s1} = 1.0$. If $P_{s1}/P_{p1} > 1.0$, the secondary flow expands against the primary as these streams enter the mixing duct and the minimum secondary flow area is at Station 1. The "supersonic" regime, SR, can exist when $P_{s1}/P_{p1} < 1.0$ and, as discussed later, when the secondary flow is choked at an aerodynamic throat formed between the primary flow and the duct wall. An "approximate" regime, APPR, is used to model flows which are ideally in the supersonic regime

but due to computational difficulties are most practically modeled by assuming $P_{s1}/P_{p1} \simeq 1.0$.

The three regimes mentioned above can occur only if the back pressure, P_{m3}, is sufficiently low. If the back pressure is too high, the secondary flow cannot be choked in the supersonic and saturated supersonic regimes and the $P_{s1}/P_{p1} \simeq 1.0$ condition used in the approximate regime is no longer a good assumption. The "mixed" regime, MR, exists when the back pressure is too high to allow the other regimes to operate. In the mixed regime the subsonic secondary flow conditions at Station 1 are dependent on the back pressure imposed at the exit plane, Station 3. SR, SSR, and APPR flow conditions at Station 1 are always independent of the back pressure.

The flow characteristics which distinguish one flow regime from another are "break-off" conditions. By changing ejector operating conditions, ejector flow can "break-off" from one flow regime to another. For example, SSR flow breaks-off with MR flow at $M_{s1} = 1.0$ and $P_{s1}/P_{p1} \geq 1.0$, the "break-off" conditions. If M_{s1} is somehow decreased from its "break-off" value of 1.0, the flow breaks-off from SSR to MR flow. The theoretical analysis determines ejector flow parameters at break-off points between the mixed regime and back pressure independent regimes.

For the given input data, the solution procedure used to determine ejector flow conditions at Stations 1 and 3 depends on the basic character of the flow that is possible at Station 1. Each of the four flow regimes considered in this analysis requires a different computational approach. The determination of the flow regimes which can exist within

the ejector is the initial step taken in the analysis. This initial determination requires consideration of the possible secondary-to-primary static pressure ratio at Station 1, P_{s1}/P_{p1}. The back pressure imposed at the exit plane of the ejector is also used to determine which one of two possible regimes exist, MR or a back pressure independent regime.

If $P_{s1}/P_{p1} \geq 1.0$, the regime of operation is either the saturated supersonic or mixed regime. In either case, the secondary flow expands against the primary flow as both streams enter the mixing duct. The minimum secondary flow area is at Station 1 so $0 \leq M_{s1} \leq 1$. When the secondary flow is choked, $M_{s1} = 1$, the regime is saturated supersonic; otherwise, the mixed regime must exist, $M_{s1} < 1$. The mixed regime occurs when the back pressure is too high to allow secondary choking.

Both the supersonic and mixed regimes are possible when $P_{s1}/P_{p1} < 1.0$. The primary flow expands against the secondary as each stream enters the duct. It is assumed, after Fabri and Paulon [9], that the primary and secondary streams remain distinct during their initial interactions and that if the back pressure is sufficiently low, the secondary flow is choked at an aerodynamic throat formed between the primary flow and the duct wall. If secondary choking does occur at some location, Station 2, within the duct, see Fig. 2.1-1, the ejector operates in the supersonic regime. An ejector with an unchoked secondary flow is operating in the mixed regime.

SR, SSR, and MR flows do not include all the possible input conditions which require a separate computational solution procedure. The supersonic and saturated supersonic regimes "break-off" into the mixed regime if the secondary flow becomes unchoked, however, the saturated supersonic regime

computationally does not necessarily "break-off" into the supersonic regime at the conditions: $M_{s1} = 1$ and $P_{s1}/P_{p1} = 1$. If a supersonic regime flow is considered, one would expect that as P_{s1}/P_{p1} is increased the location of the choked secondary flow, Station 2, would approach Station 1 as P_{s1}/P_{p1} approached a value near 1. Thus, M_{s1} should approach M_{s2} or a value of 1. The computational procedure for the supersonic regime solution involves a search algorithm in which M_{s1} is successively incremented and used as a calculation parameter. Typically for a certain set of input conditions, a value of $P_{s1}/P_{p1} = 1$ is encountered with $M_{s1} < 1$. A supersonic regime solution is no longer obtained and the flow conditions are not at supersonic-saturated supersonic break-off values. The lowest value of M_{s1} at which this occurs is defined as the critical secondary Mach number, M_{crit}, and marks the break-off of another computationally distinct regime within the supersonic regime. It has been found that supersonic regime solutions may exist for $M_{crit} < M_{s1} < 1$. These solutions all have values of P_{s1}/P_{p1} very near to 1.0 which is also the break-off condition between the regimes of supersonic and saturated supersonic flow. It appears that solutions in this regime can be well approximated by assuming $P_{s1}/P_{p1} = 1$. This "approximate" regime appears to be the result of the sensitivity of the flow at these conditions and the need for greater numerical accuracy. The computational procedure in the supersonic regime involves a search technique and requires iterations to determine a solution by the Fabri criterion at each step of the overall search. It appears that a substantial increase in the overall number of iterations would be required to obtain an accurate SR solution that, at these flow conditions, probably does not significantly differ from the APPR solution.

Theoretically the supersonic, saturated supersonic, and approximate regimes all break-off into the mixed regime flow when the imposed back pressure is greater than the theoretical value at the break-off conditions. However, as previously mentioned, when the back pressure is lower than the break-off value, the flow conditions at Station 1 are unaltered from their break-off values and are independent of the back pressure. Figure 2.1-2 is a sketch to scale of the solution surfaces determined by the analysis for the ejector configuration which was examined experimentally. Break-off values establish the loci of break-off points along which the SR, APPR, and SSR surfaces intersect the MR surface. In the analysis and in Fig. 2.1-2, P_{s0}/P_{p0} is an input flow condition, P_{m3}/P_{s0} is the non-dimensional back pressure boundary condition, and M_{s1} is the dependent variable.

2.2 OVERALL CONTROL VOLUME ANALYSIS

The control volume used in the overall analysis is indicated in Fig. 2.0-1. It was assumed that piecewise uniform flows enter the duct at Station 1 and exits subsonically at Station 3 as a uniformly mixed flow. A unique solution is obtained by determining from the input flow conditions which of the flow regimes is possible when the back pressure is sufficiently low. Flow conditions at Station 1 can then be determined. If the back pressure is greater than the break-off value, the mixed regime exists and a unique solution is found by satisfying the back pressure boundary condition. The conservation principles are applied to the overall control volume, Fig. 2.0-1, to determine both the exit plane conditions

at the break-off point and the mixed regime solutions. The overall control volume analysis has a unique solution for the back pressure independent regimes, i.e., the break-off solution. The analysis cannot, for instance, find the exit plane Mach number, M_{m3}, when the back pressure is less than the break-off value.

The theoretical analysis with an unsteady driver flow was carried-out under the assumption of quasi-steady flow. The periodic input flow conditions were subdivided into time increments and the theoretical analysis was performed during each time increment as if the flow were steady and independent of other time increments. Approximate integral averages of the performance parameters can then be obtained.

The following assumptions are made in the analysis:

1. Quasi-steady flow $\frac{\partial(\ )}{\partial t} = 0$ for each time step;
2. Piecewise uniform flow at Station 1;
3. Fully mixed uniform flow at Station 3;
4. Frictional effects within the duct are negligible;
5. No shear or shaft work;
6. Gravitational potential energy changes are negligible;
7. The flow is adiabatic and non-reacting within the duct;
8. Primary and secondary gases are calorically perfect;
9. The primary nozzle base area is negligible; and
10. Flows are brought isentropically from their stagnation states to Station 1.

Continuity may then be expressed as:

$$\oint_{cs} \rho \bar{V} \cdot d\bar{A} = 0 \qquad (2.2\text{-}1)$$

or

$$\rho_{p1} V_{p1} A_{p1} + \rho_{s1} V_{s1} A_{s1} = \rho_{m3} V_{m3} A_{m3} \tag{2.2-2}$$

If the mass flowrate, $w = \rho AV$, is employed, the continuity equation may be written as:

$$w_s + w_p = w_{m3} \tag{2.2-3}$$

or

$$w_{sp} + 1 = w_{m3}/w_p \tag{2.2-4}$$

where $w_{sp} \equiv w_s/w_p$ is the mass flowrate ratio.

The mass flowrate function is:

$$\frac{w}{PA}\left[\frac{R}{Mw} \cdot T_0\right]^{1/2} = M\left[\gamma\left[1 + \left(\frac{\gamma-1}{2}\right)M^2\right]\right]^{1/2} \equiv f_1(\gamma,M) \ . \tag{2.2-5}$$

Expressing the mass flowrate ratio, w_{sp}, in terms of the mass flowrate function yields:

$$w_{sp} = \frac{P_{s1}}{P_{p1}} \cdot \frac{A_{s1}}{A_{p1}}\left[\frac{Mw_s}{Mw_p} \cdot \frac{T_{p0}}{T_{s0}}\right]^{1/2} \frac{f_1\left(\gamma_s, M_{s1}\right)}{f_1\left(\gamma_p, M_{p1}\right)} \ . \tag{2.2-6}$$

Conservation of momentum in the X or flow direction may be expressed as:

$$\Sigma F_x = \oint_{cs} V_x(\rho \, \overline{V} \cdot d\overline{A}) \ . \tag{2.2-7}$$

The momentum equation for the overall control volume is:

$$P_{p1}A_{p1} + P_{s1}A_{s1} - P_{m3}A_{m3} = \rho_{m3}A_{m3}V_{m3}^2 - \left(\rho_{p1}A_{p1}V_{p1}^2 + \rho_{s1}A_{s1}V_{s1}^2\right) . \tag{2.2-8}$$

Using the relationship

$$\rho V^2 = P\gamma M^2 \tag{2.2-9}$$

Eq. (2.2-8) can be written as:

$$\frac{P_{s1}}{P_{p1}} \cdot \frac{A_{s1}}{A_{p1}} \left(1 + \gamma_s M_{s1}^2\right) + \left(1 + \gamma_p M_{p1}^2\right) = \frac{P_{m3}}{P_{p1}} \cdot \frac{A_{m3}}{A_{p1}} \left(1 + \gamma_m M_{m3}^2\right) . \quad (2.2\text{-}10)$$

Substituting Eq. (2.2-6) for P_{s1}/P_{p1} and expressing P_{m3}/P_{p1} in terms of the mass flowrate function, Eq. (2.2-5), produces:

$$f_2\left(\gamma_m, M_{m3}\right) = \frac{f_2\left(\gamma_p, M_{p1}\right) + f_2\left(\gamma_s, M_{s1}\right) \left[\frac{Mw_p}{Mw_s} \cdot \frac{T_{s0}}{T_{p0}}\right]^{1/2} \cdot W_{sp}}{\left[\frac{Mw_p}{Mw_m} \cdot \frac{T_{m0}}{T_{p0}}\right]^{1/2} \left(1 + W_{sp}\right)} \quad (2.2\text{-}11)$$

where the function $f_2(\gamma, M)$ is defined as:

$$f_2(\gamma, M) \equiv \frac{\left(1 + \gamma M^2\right)}{M\left[\gamma\left(1 + \frac{\gamma - 1}{2} M^2\right)\right]^{1/2}} . \quad (2.2\text{-}12)$$

Solving Eq. (2.2-12) for M produces:

$$M = \left[\frac{-\left(f_2^2 - 2\right) \pm \left[\left(f_2^2 - 2\right)^2 + 2\left(\frac{\gamma - 1}{\gamma}\right)\left(f_2^2 - \frac{2\gamma}{(\gamma - 1)}\right)\right]^{1/2}}{(\gamma - 1)\left[f_2^2 - \frac{2\gamma}{(\gamma - 1)}\right]}\right]^{1/2} . \quad (2.2\text{-}13)$$

Only the subsonic solution of Eq. (2.2-13) is used.

The energy equation can be written in the form:

$$\frac{\partial Q}{\partial t} - \frac{\partial W_{ss}}{\partial t} = \oint_{cs} \left(h + \frac{V^2}{2} + gZ\right)(\rho \, \bar{V} \cdot d\bar{A}) . \quad (2.2\text{-}14)$$

Under the foregoing assumptions, the energy equation simplifies to:

$$\oint_{cs} h_0(\rho \, \bar{V} \cdot d\bar{A}) = 0 \quad (2.2\text{-}15)$$

where $h_0 \equiv h + V^2/2$. For adiabatic flow, the overall control volume analysis energy relation is:

$$h_{0s} w_s + h_{0p} w_p = h_{0m3} w_{m3} \quad . \tag{2.2-16}$$

Using Eq. (2.2-4) and that $h_0 = C_p T_0$ produces:

$$\frac{T_{m0}}{T_{p0}} = \frac{1}{\left(1 + w_{sp}\right)} \frac{\left(C_p\right)_p}{\left(C_p\right)_m} \left[1 + w_{sp} \frac{\left(C_p\right)_s}{\left(C_p\right)_p} \frac{T_{s0}}{T_{p0}} \right] \tag{2.2-17}$$

Dalton's law of partial pressures is assumed to be applicable to the mixing process within the control volume as a means of determining the mixed flow gas properties at Station 3. Mass flowrate ratios are used to express the mass fractions in the relations for a constant volume mixing process. This is perhaps the most unrealistic part of the quasi-steady approach for non-constant property flows. The properties of the "slugs" of flow currently entering the duct are used to determine the exit plane properties at the same point in time. These conditions at Station 3 are then assumed to be the back pressure conditions affecting the flow at Station 1. If amplitudes and/or phase lags are small this will not result in a significant error. The mixed flow properties expressed in terms of w_{sp} and the primary and secondary gas properties are:

$$\frac{\left(C_p\right)_p}{\left(C_p\right)_m} = \frac{1 + w_{sp}}{1 + w_{sp} \dfrac{\left(C_p\right)_s}{\left(C_p\right)_p}} \tag{2.2-18}$$

$$\frac{Mw_m}{Mw_p} = \frac{1 + w_{sp}}{1 + w_{sp} \left(\dfrac{Mw_p}{Mw_s} \right)} \tag{2.2-19}$$

$$\gamma_m = \left[1 - \left(\frac{\gamma_p - 1}{\gamma_p}\right)\frac{\left(1 + w_{sp} \cdot \frac{Mw_p}{Mw_s}\right)}{\left[1 + w_{sp} \cdot \frac{\gamma_s}{\gamma_p}\frac{(\gamma_p - 1)}{(\gamma_s - 1)}\frac{Mw_p}{Mw_s}\right]}\right]^{-1} \qquad (2.2\text{-}20)$$

Using the relationship

$$C_p = \frac{\gamma R}{Mw(\gamma - 1)} \quad ,$$

the ratio of specific heats can be expressed as

$$\frac{(C_p)_s}{(C_p)_p} = \frac{\gamma_s}{\gamma_p} \cdot \frac{(\gamma_p - 1)}{(\gamma_s - 1)}\frac{Mw_p}{Mw_s} \quad . \qquad (2.2\text{-}21)$$

Thus the mixed flow gas properties are defined in terms of γ_s, γ_p, Mw_s, Mw_p, and w_{sp}.

The non-dimensional form of the back pressure boundary condition, P_{m3}/P_{s0} can be found using Eqs. (2.2-4) and (2.2-5). The result is

$$\frac{P_{m3}}{P_{s0}} = \frac{P_{m3}}{P_{p1}} \cdot \frac{P_{p1}}{P_{p0}} \cdot \frac{P_{p0}}{P_{s0}}$$

$$\frac{P_{m3}}{P_{s0}} = \frac{(P_{p1}/P_{p0})}{(P_{s0}/P_{p0})} \cdot \left[\frac{T_{m0}/T_{p0}}{Mw_m/Mw_p}\right]^{1/2} \left(\frac{A_{p1}}{A_{m3}}\right)(1 + w_{sp}) \frac{f_1(\gamma_p, M_{p1})}{f_1(\gamma_m, M_{m3})} \qquad (2.2\text{-}22)$$

The preceding relations are used to formulate a solution procedure for the back pressure independent and mixed flow regimes. In this procedure, it is assumed that $(\gamma_p, \gamma_s, M_{p1}, P_{m3}/P_{s0}, A_{p1}/A_{m3}, Mw_s/Mw_p, T_{s0}/T_{p0})$ are known. In the mixed regime, unknowns include $(w_{sp}, P_{s1}/P_{p1}, M_{m3}, M_{s1}, T_{m0}/T_{p0})$. The problem for the back pressure independent regimes has some of these variables specified from the outset.

In the saturated supersonic regime, $M_{s1} = 1.0$; in the approximate regime, $P_{s1}/P_{p1} \simeq 1.0$. The static pressure ratio, P_{s1}/P_{p1}, can be determined for a value of M_{s1} by the Fabri criterion in the supersonic regime; in this regime, M_{s1} is used as a calculation parameter. As presented, the problem is not closed. There are five mixed regime unknowns but only three conservation equations and the back pressure boundary condition are available to determine them. The back pressure independent regimes have four unknowns and three equations. One basic unknown must be specified as a calculation parameter. The secondary-to-primary stagnation pressure ratio has been chosen as the calculation parameter. The pressure ratio, P_{s0}/P_{p0}, is fundamental to both flows and can be experimentally measured versus time without difficulty. Thus P_{s1}/P_{p1} can then be determined from the isentropic relation:

$$\frac{P_{s1}}{P_{p1}} = \frac{\left[1 + \left(\frac{\gamma_s - 1}{2}\right) M_{s1}^2\right]^{\gamma_s/1-\gamma_s}}{\left[1 + \left(\frac{\gamma_p - 1}{2}\right) M_{p1}^2\right]^{\gamma_p/1-\gamma_p}} \cdot \left(\frac{P_{s0}}{P_{p0}}\right) \qquad (2.2\text{-}23)$$

for a given M_{s1}; the problem is closed.

2.3 SUPERSONIC REGIME ANALYSIS

A control volume analysis, see Fig. 2.1-1, which is based on the method of Fabri and Paulon [9] has been used to determine supersonic regime secondary flow conditions at Station 1. Due to the interaction between the primary and secondary streams within the duct, the assumption is made that the secondary flow chokes within the duct at Station 2 and that the secondary and primary flows separately co-exist to fill the duct.

The pressure ratio, P_{s1}/P_{p1} is found for an assumed value of M_{s1} by applying the conservation of mass and momentum between Stations 1 and 2. M_{s1} is determined by iteration by a search routine until the value of P_{s1}/P_{p1} obtained from the Fabri criterion agrees with the value resulting from input conditions: M_{p1}, P_{s0}/P_{p0}, and the assumed M_{s1}.

The following assumptions have been made:

1. The primary and secondary streams remain distinct and uniform between Stations 1 and 2;
2. The mean pressures of the primary and secondary flow may differ at any cross section;
3. $P_{s1}/P_{p1} < 1.0$;
4. $M_{s2} = 1.0$;
5. The flow is isentropic;
6. The body forces are negligible;
7. The wall friction can be neglected;
8. No shear or shaft work;
9. The primary nozzle base area is negligible; and
10. The flows are brought isentropically from their stagnation states to Station 1.

The area ratio, A_{s1}/A_{s2}, can be expressed with the area ratio function, A/A^*,

$$A/A^*(\gamma,M) = \frac{1}{M}\left[\frac{2}{(\gamma+1)} \cdot \left[1 + \frac{(\gamma-1)}{2} M^2\right]\right]^{\gamma+1/2(\gamma-1)} \equiv f_3(\gamma,M) \quad (2.3\text{-}1)$$

as

$$A_{s1}/A_{s2} = A/A^*\left(\gamma_s, M_{s1}\right)$$

since $M_{s2} = 1$. The flow area available to the primary at Station 2 and the determination of M_{p2} follow directly from the conservation of mass; the relationship is

$$A/A^*\left(\gamma_p, M_{p2}\right) = A/A^*\left(\gamma_p, M_{p1}\right) \cdot \frac{A_{p2}}{A_{p1}}$$

or

$$f_3\left(\gamma_p, M_{p2}\right) = f_3\left(\gamma_p, M_{p1}\right)\left[\frac{1 - \frac{\left(1 - A_{p1}/A_{m3}\right)}{\left[A_{s1}/A_{s2}\right]}}{A_{p1}/A_{m3}}\right] \tag{2.3-2}$$

M_{p2}, found numerically, must be greater than M_{p1}.

Conservation of momentum between Stations 1 and 2 produces:

$$P_{s1}A_{s1}\left(1 + \gamma_s M_{s1}^2\right) + P_{p1}A_{p1}\left(1 + \gamma_p M_{p1}^2\right) = P_{s2}A_{s2}\left(1 + \gamma_s\right) + P_{p2}A_{p2}\left(1 + \gamma_p M_{p2}^2\right) \tag{2.3-3}$$

Dividing by $P_{p1}A_{p1}$ and rearranging for computational simplicity, the expression for P_{s1}/P_{p1} is:

$$\frac{P_{s1}}{P_{p1}} = \frac{\left(\frac{P_{p2}/P_{p0}}{P_{p1}/P_{p0}}\right) \cdot \left(\frac{A_{p2}/A_p^*}{A_{p1}/A_p^*}\right) \cdot \left(1 + \gamma_p M_{p2}^2\right) - \left(1 + \gamma_p M_{p1}^2\right)}{\left(\frac{1 - A_{p1}/A_{m3}}{A_{p1}/A_{m3}}\right)\left[\left(1 + \gamma_s M_{s1}^2\right) - \left(\frac{P_{s2}/P_{s0}}{P_{s1}/P_{s0}}\right) \cdot \left(\frac{1 + \gamma_s}{A_{s1}/A_s^*}\right)\right]} \tag{2.3-4}$$

With the input values of $\left(\gamma_s, \gamma_p, M_{p1}, A_{p1}/A_{m3}\right)$ and an assumed trial value of M_{s1}, Eq. (2.3-4) can be solved after determining M_{p2} from Eq. (2.3-2) and the isentropic relations. The supersonic regime solution for flow conditions at Station 1 has been completed when a value of M_{s1} is found that results in convergence of the values of P_{s1}/P_{p1} determined from Eqs. (2.2-23) and (2.3-4).

2.4 COMPUTATIONAL PROCEDURE

The steps in the computational procedure are:

1. To determine which back pressure independent regime can exist, if the back pressure is sufficiently low, at the assumed value of the calculation parameter, P_{s0}/P_{p0};
2. To use the appropriate Station 1 conditions and the overall control volume analysis to determine the resulting exit plane break-off conditions; and
3. To perform an iteration for a mixed regime solution if the back pressure condition imposed at the exit plane is greater than the break-off value determined in item 2 above.

The first step taken to determine which back pressure independent flow regime can exist is to determine the flow conditions at which the supersonic and approximate flow regimes break-off from one another. M_{crit}, the break-off value between these regimes of the secondary flow Mach number at Station 1, is found by carrying out the supersonic regime analysis in Section 2.3 with assumed values of M_{s1}. The minimum value of M_{s1} which produces $P_{s1}/P_{p1} = 1.0$ from Eq. (2.3-4) is the critical Mach number, M_{crit}. The search for M_{crit} is not difficult because P_{s1}/P_{p1} increases monotonically with M_{s1} in the supersonic regime. The corresponding break-off value of P_{s0}/P_{p0} is found using the relation

$$\left(\frac{P_{s0}}{P_{p0}}\right)_{crit} = \frac{P_{p1}/P_{p0}}{P_{s1}/P_{s0}} \cdot \frac{P_{s1}}{P_{p1}} \qquad (2.4\text{-}1)$$

where the isentropic relations and $P_{s1}/P_{p1} = 1.0$ are used.

The possibility of a SSR flow can be determined by assuming $M_{s1} = 1.0$ and solving for the resulting value of P_{s1}/P_{p1}. The relation is

$$\frac{P_{s1}}{P_{p1}} = \frac{\left(\frac{P_{s1}}{P_{s0}}\right)\left(\frac{P_{s0}}{P_{p0}}\right)}{\left(P_{p1}/P_{p0}\right)} \quad . \tag{2.4-2}$$

If $P_{s1}/P_{p1} \geq 1.0$, either the saturated supersonic or mixed flow regime must exist. When $P_{s1}/P_{p1} < 1.0$ and $P_{s0}/P_{p0} > \left(P_{s0}/P_{p0}\right)_{crit}$, the flow regime must be either approximate or mixed. Either the supersonic or the mixed regime exist for values of P_{s0}/P_{p0} lower than $\left(P_{s0}/P_{p0}\right)_{crit}$. Thus, as previously discussed, back pressure independent flow conditions at Station 1 are determined.

The overall control volume analysis is then used to determine the flow conditions at Station 3. This is accomplished by solving in order Eqs. (2.2-23), (2.2-6), (2.2-20), (2.2-21), (2.2-18), (2.2-19), and (2.2-17) for P_{s1}/P_{p1}, w_{sp} and mixed flow gas properties. $P_{s1}/P_{p1} \simeq 1.0$ is assumed for APPR flow so Eq. (2.2-23) is used to determine M_{s1}. M_{m3} is found by solving Eqs. (2.2-11) and (2.2-13). Only the subsonic solution of Eq. (2.2-13) is considered. The break-off back pressure ratio, P_{m3}/P_{s0}, is determined by using Eq. (2.2-22). If the imposed back pressure ratio is greater than this break-off value, the mixed regime exists. In the mixed regime, an iterative procedure is necessary to find the value of M_{s1} which causes P_{m3}/P_{s0} to converge to the given value. Each iteration for a MR solution must start with Eq. (2.2-23) and then proceed with the overall control volume analysis as discussed above.

A computer code, UCAE, was written to perform this analysis. Section 6.0, the APPENDIX, contains UCAE and a sample input and output.

2.5 PARAMETRIC STUDY

A parametric study of theoretical ejector results was made with UCAE for a wide range of P_{s0}/P_{p0} values. The input conditions used for this parametric study correspond to the experimental setup. Values of w_{sp}, P_{s1}/P_{p1}, M_{s1}, and P_{m3}/P_{s0} at the break-off conditions of the back pressure independent regimes with the mixed regime are plotted versus P_{s0}/P_{p0} in Figs. 2.5-1, 2.5-2, 2.5-3, and 2.5-4. The lowest value of P_{s0}/P_{p0} plotted in these figures corresponds to M_{s1} = .001, the minimum value considered by UCAE.

The mass flowrate ratio, Fig. 2.5-1, is a smooth monotonic function of P_{s0}/P_{p0}, increasing with P_{s0}/P_{p0} in all three back pressure independent flow regimes. The slight change in slope between the SR and SSR segments of the curve occurs gradually over the APPR segment of the curve.

The static pressure ratio, P_{s1}/P_{p1}, is a linear function of P_{s0}/P_{p0} for SSR flow but is nonlinear for SR flow, see Fig. 2.5-2. Discontinuities exist in the P_{s1}/P_{p1} solution at the SR-APPR break-off and the APPR-SSR break-off. The SR-APPR discontinuity is due to the P_{s1}/P_{p1} = 1.0 approximation for APPR flow and insufficient numerical accuracy, as previously discussed. The APPR-SSR discontinuity is due to the constant secondary choked flow area in SSR flow which imposes an additional constraint on the nature of the solution. This is more apparent in the plot of M_{s1} versus P_{s0}/P_{p0}, Fig. 2.5-3.

Figures 2.5-4 and 2.5-1 shows the relationship existing between ejector pressure recovery and mass flowrate performance. Large mass flowrates are obtained in the saturated supersonic regime at the sacrifice of

the pressure recovery. The converse is true for supersonic regime flows at lower values of P_{s0}/P_{p0}.

Figures 2.5-3 and 2.5-4 are the normal projections of the loci of break-off points between the mixed and back pressure independent flow regimes, as shown in Fig. 2.1-2, onto the $\left(P_{s0}/P_{p0},\ M_{s1}\right)$ and $\left(P_{s0}/P_{p0},\ P_{m3}/P_{s0}\right)$ planes, respectively.

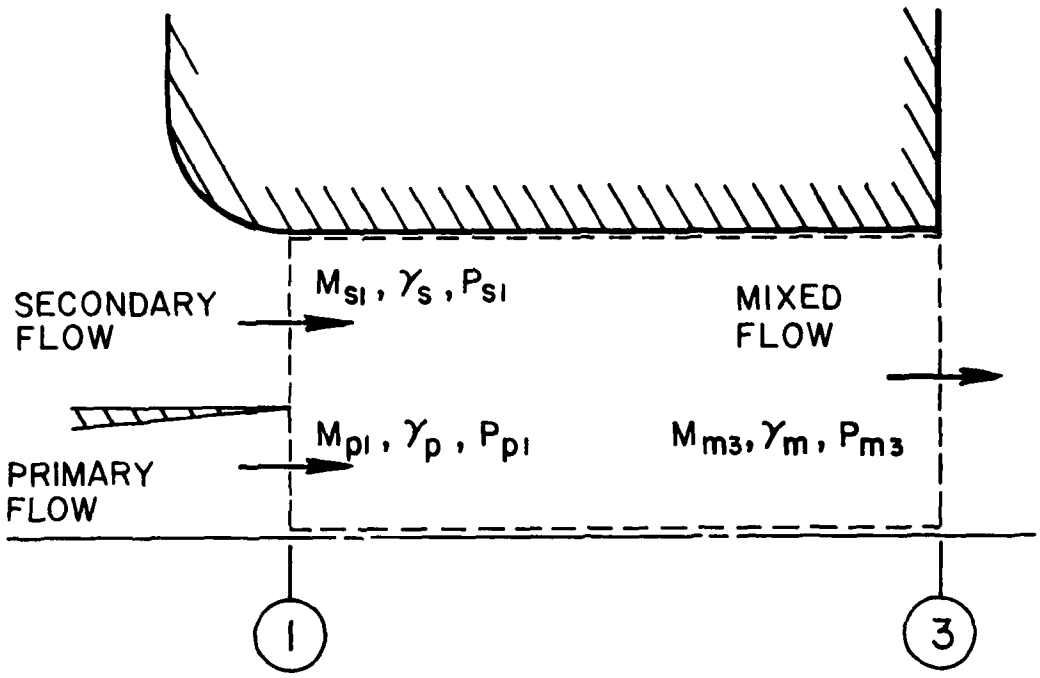

Figure 2.0-1 Control volume used in the overall analysis

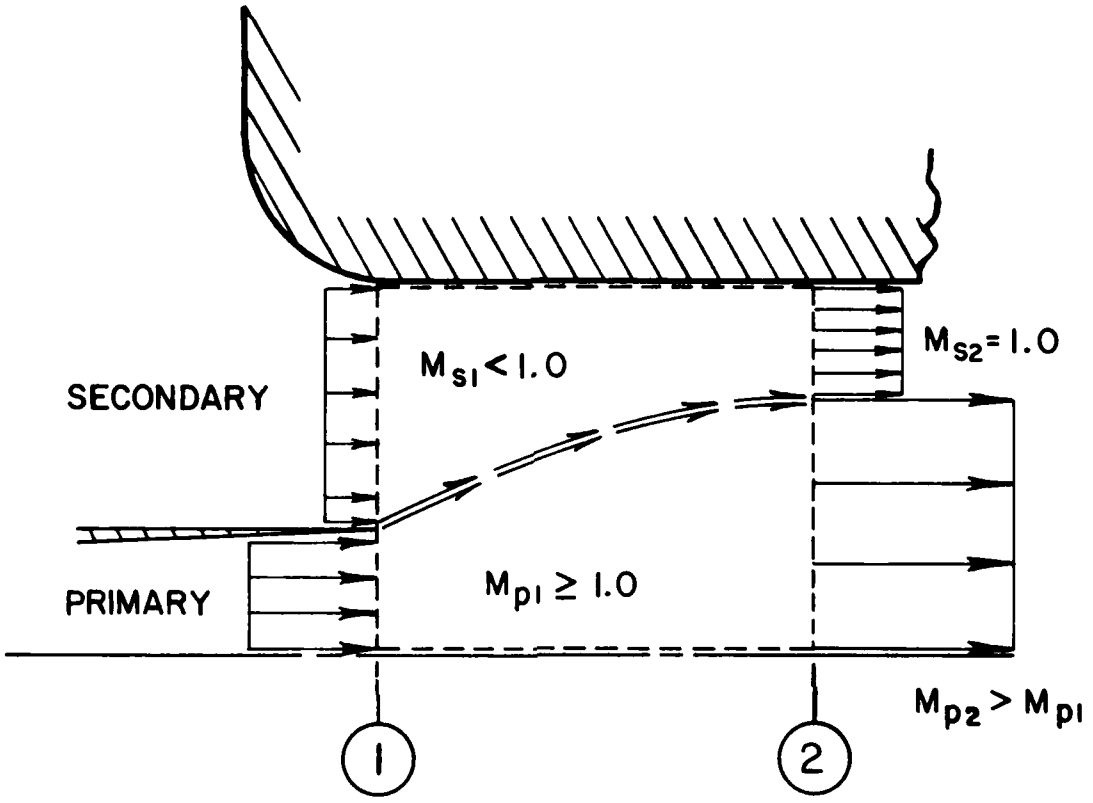

Figure 2.1-1 Control volume used in the supersonic regime analysis

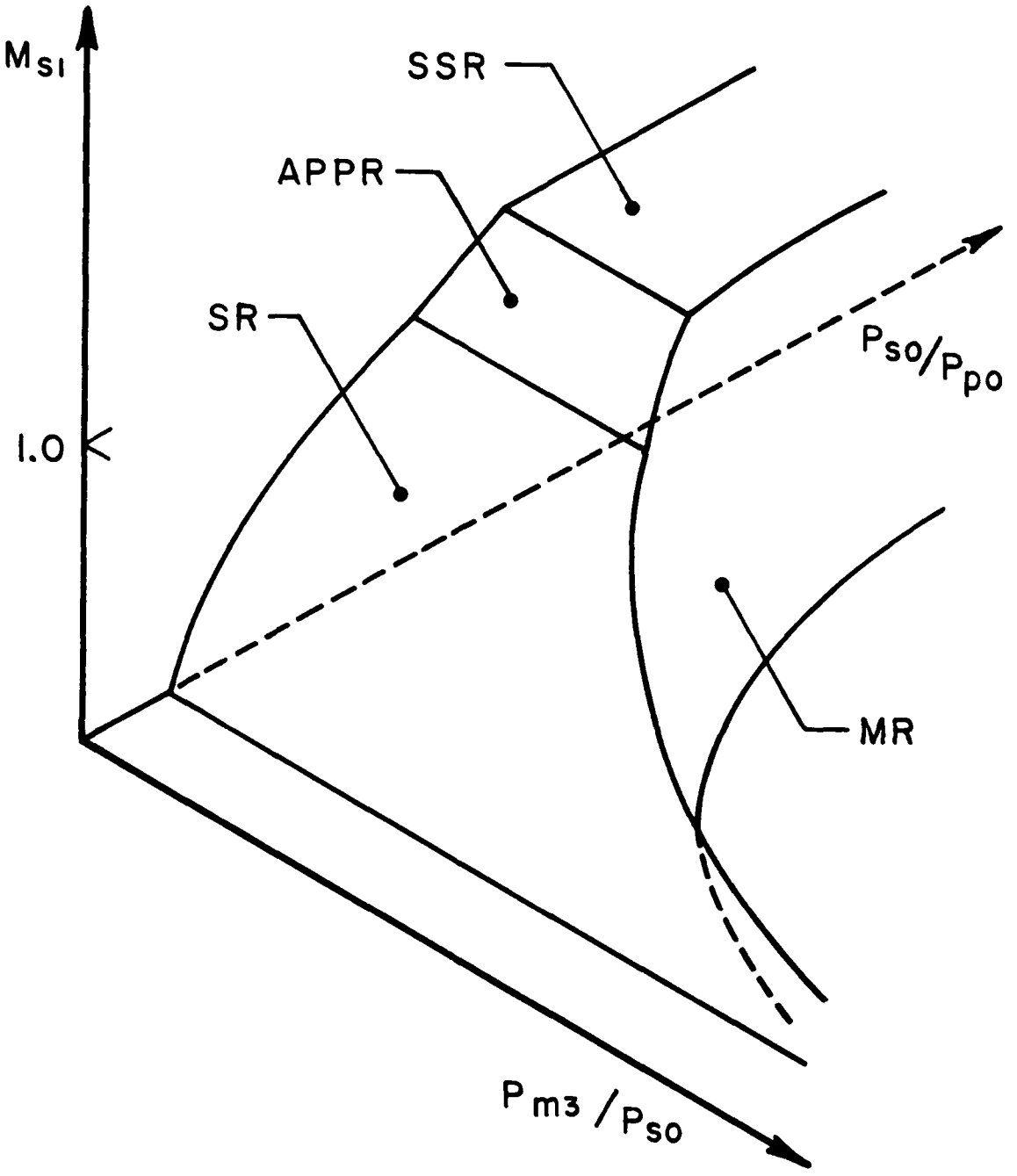

Figure 2.1-2 The one-dimensional inviscid analysis solution surfaces

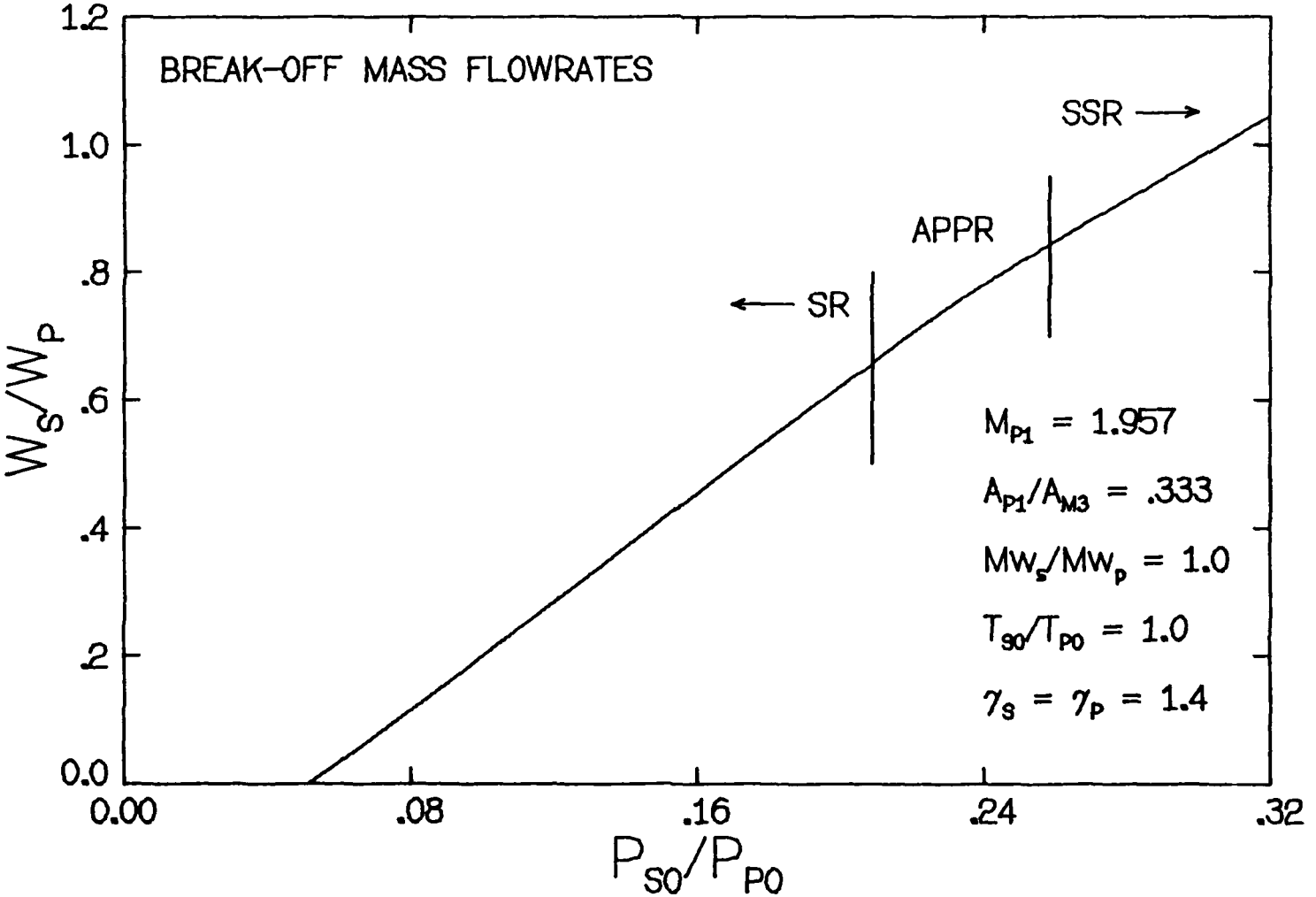

Figure 2.5-1 Theoretical mass flowrate characteristics of the back pressure independent flow regimes versus P_{s0}/P_{p0}.

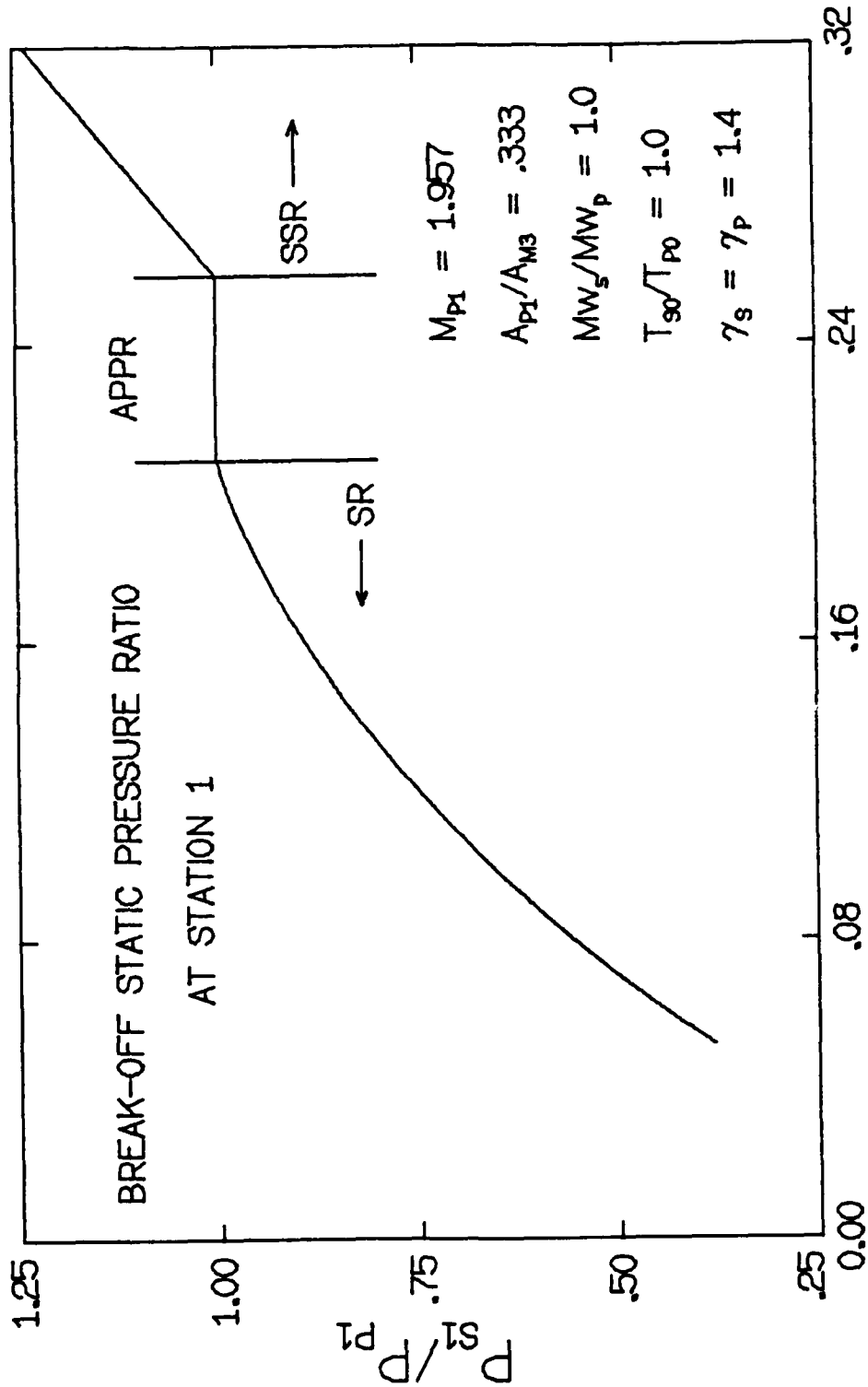

Figure 2.5-2 Theoretical characteristics of P_{s1}/P_{p1} for the back pressure independent flow regimes versus P_{s0}/P_{p0}

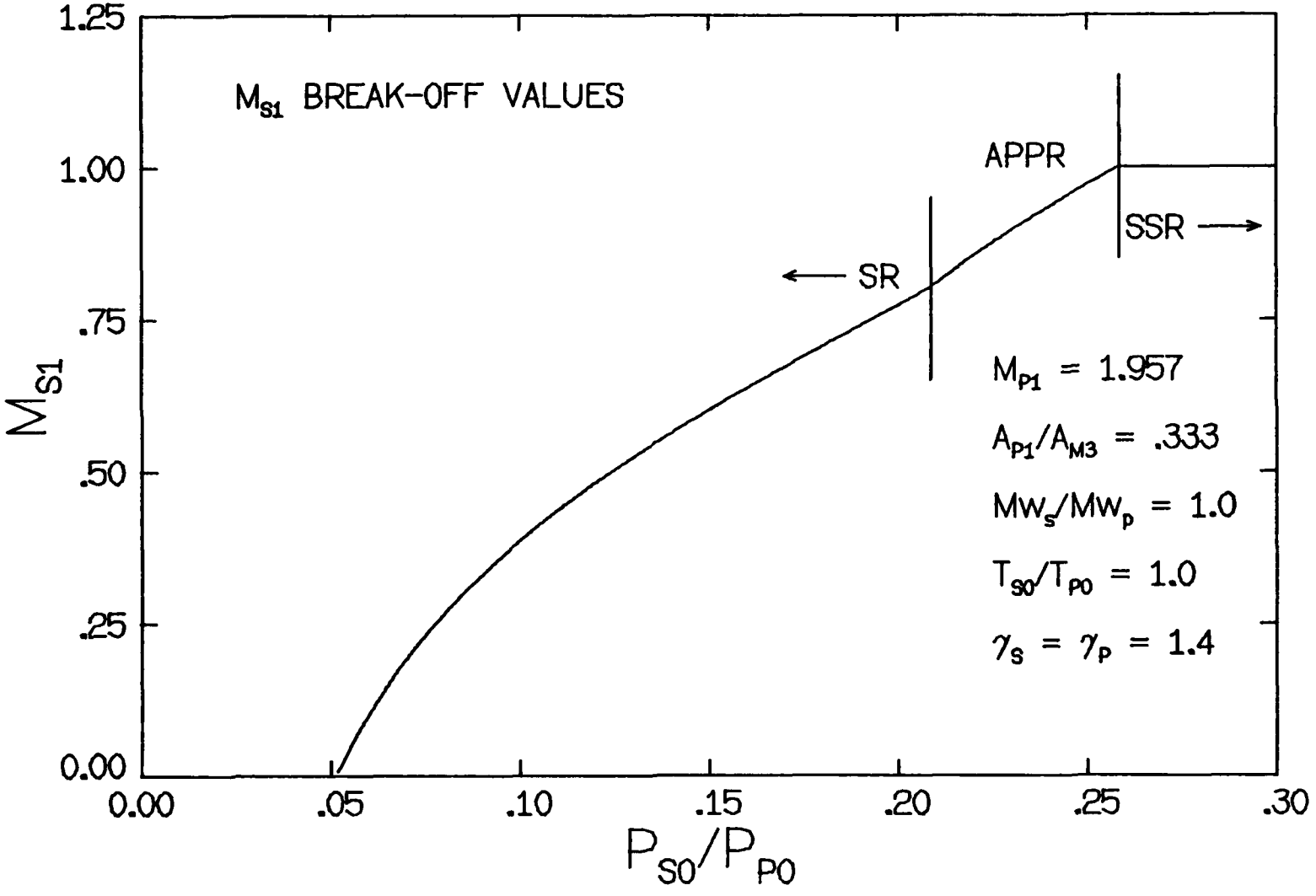

Figure 2.5-3 Theoretical values of M_{s1} for the back pressure independent flow regimes versus P_{s0}/P_{p0}

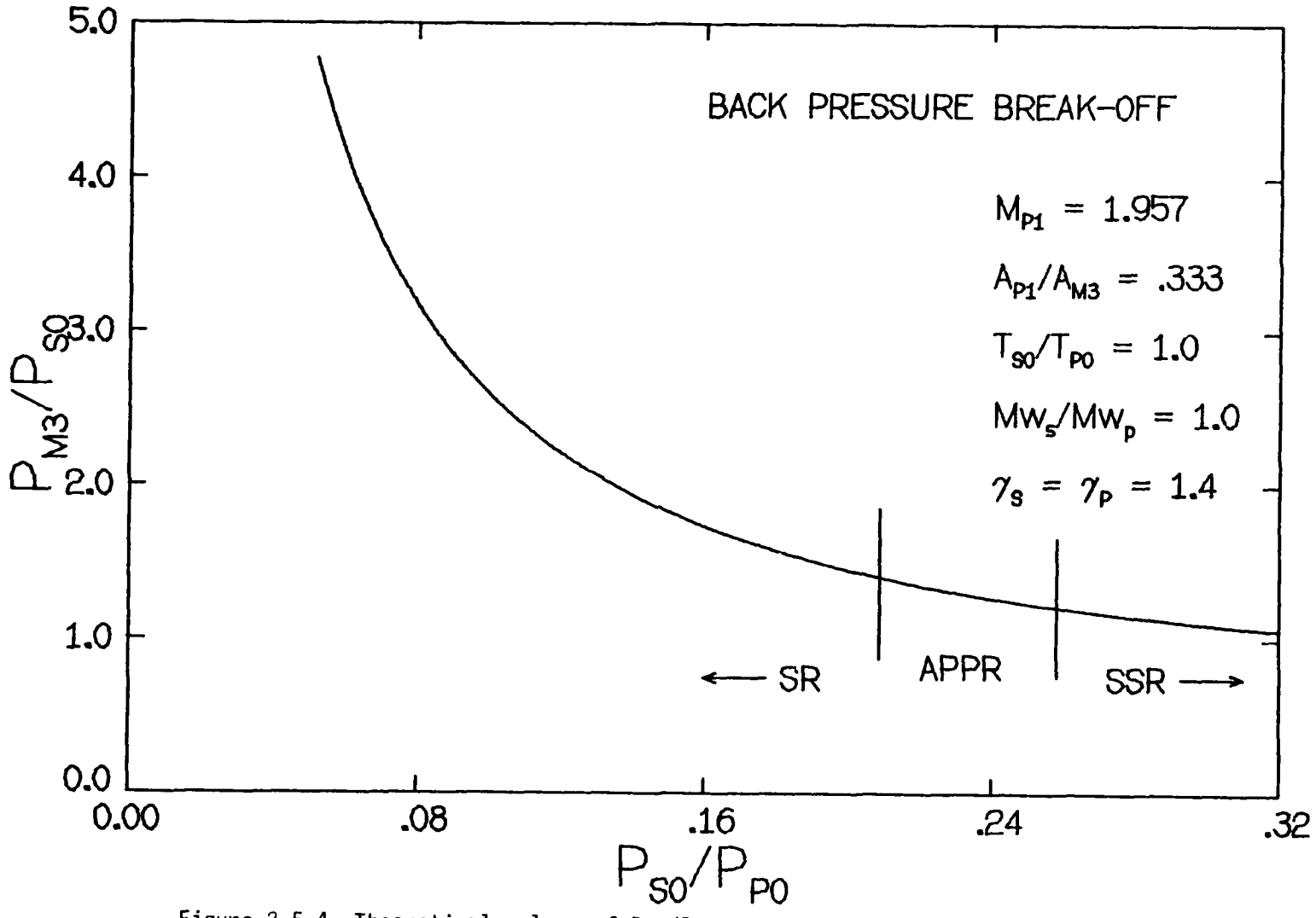

Figure 2.5-4 Theoretical values of P_{m3}/P_{s0} at which SR, APPR, AND SSR flows break-off to MR flow versus P_{s0}/P_{p0}^{m3}

3.0 THE EXPERIMENTAL PROGRAM

A series of small-scale cold air flow experiments were conducted at the University of Illinois Mechanical Engineering Laboratory to determine what effects a continuous periodic driver flow had on the performance and flow characteristics of a two-dimensional, planar supersonic-subsonic ejector. A wide range of operating conditions were examined with both steady and unsteady primary driver flows.

3.1 EXPERIMENTAL APPARATUS

Filtered and dried compressed air at a maximum pressure level of 850 kPa was supplied from a compressor connected to a 100 m^3 storage tank farm. Steady-state operation was possible for experiments requiring mass flowrates of approximately 1 kg/s or less of compressed air. This air supply system was the source of primary flow in all ejector experiments.

The continuous flow test facility, which was used to run these experiments, consists of two test stands and a central control panel. Each test stand has a two and a three inch compressed air supply line. The stagnation pressure in either line can be adjusted independently at the control panel by air operated control valves. Two sets of U-tube manometers on the control panel are used to measure pressure differences across VDI standard nozzles to determine mass flowrates. Control panel switching allows the selection of U-tube manometers with fluid specific gravities of 1.0, 2.95, or 13.7. A Wallace and Tiernan Series 1500 0-150 psia pressure gage with a .0667% full scale accuracy was used to

measure pressures at various line and test locations and to calibrate some pressure transducers. A Wallace and Tiernan precision manometer and a control panel regulated vacuum source were also used for pressure transducer calibration. Each test stand has 20 pressure taps connected to a 40 tube mercury manometer board. The manometer board was used to measure the secondary stagnation pressure and to obtain a quick visualization of the approximate static pressure distribution within the ejector mixing duct.

The ejector primary flow was taken from a 2-inch supply line on one of the test stands. A VDI standard nozzle, located upstream of the test stand, was used to measure primary mass flowrates. The supply line was reduced to 1¼ inch pipe at the test stand source. A hose fitting was machined from a standard 1¼ inch pipe nipple so that nylon reinforced flexible tubing could be used to connect the primary flow directly to the ejector inlet for steady experiments or to the inlet of a large-scale fluidic oscillator for the unsteady driver flow experiments. Figure 3.1-1 is a schematic of the experimental apparatus which details primary and secondary flow lines.

The secondary flow was induced through a smooth elliptical inlet nozzle from the atmosphere. A VDI standard nozzle block, located in the middle of a 2.13 m length of seamless 2-inch tubing, was used to determine the secondary mass flowrate. The flow was throttled with a gate valve to the desired stagnation pressure after it had passed through the VDI nozzle and a .35 m^3 holding tank. A four port manifold was used to distribute the flow to the secondary inlets on the ejector unit. The

threaded holes seen in Figs. 3.1-2 and 3.1-3 are the secondary flow inlet ports.

The holding tank, mentioned above, was used to avoid mass flowrate measurement errors typically encountered when a metering orifice or nozzle is used in the measurement of an unsteady flow. The deviation due to unsteady or pulsatile flow of the metering device discharge coefficient from steady flow values is not well understood. Investigations [37,38] have shown that frequency, amplitude, wave form, and the pressure difference across a flow metering device all have to some degree an effect on the discharge coefficient in a periodic flow. A decoupling of the dynamic pressure difference across the metering device with the velocity through it as well as vortex shedding phenomena due to the unsteady flow are suspected of erroneously altering mass flowrate measurements. Pressure drops across a metering nozzle or orifice in a periodic flow are not representatively measured by U-tube manometers.

For experiments conducted with pulsating flow, the holding tank adds sufficient capacitance to the secondary flow system so that pulsations are damped in the flow to a negligible level at the VDI standard nozzle. The holding tank that was used has more than adequate volume to damp the flow according to the Hodgson number criterion discussed by Ower and Pankhurst [39].

Pulsation of the primary flow was achieved with a large-scale fluidic oscillator. No moving parts, simplicity, small losses, and frequency and amplitude variability were reasons for using a fluidic device to produce the pulsations in the driver flow. An initial effort during this program

involved the selection and development of a fluidic oscillator configuration to produce the pulsating primary ejector flow. Scale models of promising fluidic oscillator geometries were fabricated from styrofoam for performance testing using the hydraulic analogy. The hydraulic analogy is a convenient way to study and visualize unsteady compressible flow; thus it provided a qualitative means to understand the factors influencing the oscillator performance [40]. The particular oscillator configuration used in the air flow experiments was chosen because of its capability to self excite, its pressure level insensitivity, frequency stability, its large amplitude pulses, and the ease with which its operating frequency can be varied. Essentially the same oscillator configuration was used by Halbach, Otsap, and Thomas in a fluidic temperature sensor [41].

This oscillator consists of a fluid jet which impinges on a knife-edge, a feedback loop, and a resonance chamber; the body of the oscillator is shown in Fig. 3.1-4. A jet impinging on a knife-edge is in a bi-stable condition; the jet tends to flip to one side of the knife-edge or the other. This flipping action results in a pressure pulse moving through the portion of the oscillator fed by the jet. Pulses are either reflected back to the jet at the end of the resonance chamber or looped back to the jet through the feedback loop; in either case, the interaction with the jet causes the jet to flip to the other side of the knife-edge. The resonance chamber has an opening at the reflecting end, as shown in Fig. 3.1-5, through which the periodic primary driver flow enters the ejector. Flexible tubing made up a part of the resonance chamber between the ejector inlet and the oscillator body. Similarly, the feedback loop was completed

outside of the body of the oscillator with flexible tubing and a machined 180° turn. Oscillator frequencies were adjusted by changing the lengths of the resonance chamber and the feedback loop tubing. Stagnation pressure probes were located in the hose fitting connecting the source flow to the oscillator inlet and in the hose fitting at the reflecting end of the resonance chamber. The latter stagnation pressure probe was located immediately upstream of the ejector primary flow inlet.

The oscillator knife-edge can be moved along its centerline, see Fig. 3.1-4, so that the distance between the oscillator inlet and the knife-edge can be varied. However, the oscillator knife-edge was always positioned for the maximum oscillator inlet to knife-edge distance allowed by the geometry of the oscillator body. Hydraulic analogy findings indicated that this position, for the given fixed oscillator inlet and exit flow areas, would probably produce the largest amplitude pulses [42]. This knife-edge position avoided possible vibration problems which an extended knife-edge could have created. However, this oscillator configuration was limited to only one pulse amplitude for a given operating frequency and oscillator inlet stagnation pressure.

A planar two-dimensional, constant area, supersonic-subsonic ejector was built for this investigation. The primary flow enters the ejector mixing duct through a continuous slope converging-diverging nozzle designed for a uniform Mach 2 exit plane flow by the method of characteristics with a boundary layer displacement thickness correction. From a stagnation pressure traverse across the exit plane of this nozzle, a reasonably uniform flow was found with Mach numbers in the range: $1.98 \leq M \leq 2.01$. This

was a pleasant surprise because the nozzles were cut rather thin near the exit plane to minimize the base area between primary and secondary flows; see Figs. 3.1-3 and 3.1-6. The machining process left the nozzle blocks slightly warped and it was necessary to straighten them. To correct sealing problems, multiple assembly-disassembly operations were initially required. Based on static pressure measurements taken after the final assembly of the ejector, the centerline exit plane Mach number was found to be approximately $M_{p1} \simeq 1.96$.

The ejector unit itself consists of two types of assemblies. A base assembly in which secondary and primary flows are brought to their confluence point, Fig. 3.1-6, and three aluminum mixing duct assemblies, Fig. 3.1-7. The base assembly was made primarily from stainless steel to improve its dimensional stability, to increase its mass, and to reduce vibration. The supersonic primary flow enters at the center of the mixing duct inlet interleaved between two subsonic secondary streams. The nominal width, W, of the constant area rectangular mixing duct; i.e., the distance across both secondary and the primary streams, is 33.07 mm. The distance from the primary flow centerline to a secondary flow wall, half of the width, is 16.54 mm and is indicated in Fig. 3.1-6. The height of the mixing duct, the dimension normal to the page in Fig. 3.1-6, is 15.24 mm. The primary to mixing duct flow area ratio is 1/3. Static pressure taps are located along the centerline of each of the four mixing duct walls. The first four pressure tap locations are at intervals of X/W = 1/3 the duct width, W = 33.07 mm. The remainder of the taps are at one duct width intervals in the X or flow direction starting at X/W = 2.0.

The base assembly pressure taps and the secondary stagnation pressure probes can be seen in Figs. 3.1-6 and 3.1-3. Static pressure taps are located in the center of the primary and secondary flow inlets at Station 1 and on the primary flow centerline of each mixing duct assembly very near the exit plane. The three mixing duct assemblies produce total duct length-to-width ratios of 5, 9, and 13, when mounted on the base assembly. The L/W = 5 combination was found to be too short to be of practical interest. The shortest duct assembly was modified so that it could be attached to the longest mixing duct. Thus, a mixing duct of L/W = 16.374 could be investigated.

A back pressure valve and muffler were connected to the exit plane of the ejector. The back pressure valve was always kept open and was not used to adjust the exit plane pressure. The valve was mounted on a sealing plate, thus providing a chamber into which the ejector flow discharged. The muffler attached directly to the back pressure valve. A stagnation pressure probe was mounted on the sealing plate and was used to measure the stagnation pressure at the center of the exit plane and at a point 3/8 of the duct width off of center.

Figures 3.1-8 and 3.1-9 are two views of the assembled flow system. The oscillator is located on the right in both figures; the resonance and feedback tubes were set-up for a 142 Hz operating frequency. The back pressure valve and muffler are located on the left. The holding tank is behind the oscillator.

An electronic data acquisition system capable of recording four channels simultaneously was used to collect the data for all unsteady

experiments. Pressures were measured with CEC type 4-312 strain gage pressure transducers. These transducers were mounted in case assemblies or line adapters. Scanivalve "zero" volume line adapters were used; these line adapters were designed for use with CEC type 4-312 transducers and are designed to minimize the volume around the transducer diaphragm within the adapter. Figure 3.1-10 is a cross-sectional view of the Scanivalve "zero" volume line adapter with a transducer in place. Each transducer had a cap custom fitted to its diaphragm in accordance with Scanivalve specifications. Pressure waveform distortion due to adapter and pressure line capacitance was minimized by using the Scanivalve adapters and by keeping the connecting pressure lines as short as possible. A 20 mm long piece of #16 gage flexible tubing was used to connect these transducer line adapters to the pressure taps on the ejector unit. All distances between ejector pressure taps and transducer diaphragms were less than 75 mm. CEC type 1-183 signal conditioners were used to excite, balance, and calibrate the transducers as well as to provide an amplified output. Figure 3.1-11 is a schematic of the instrumentation system used.

The signal conditioner output was recorded with a Biomation 1015 waveform recorder. This unit is capable of recording four channels simultaneously at sampling rates as high as 100 kHz. Both analog and digital output were available from the Biomation, thus allowing the examination of data on an oscilloscope before initiating the recording of the digital output on tape. The digital output from the Biomation was recorded with a Memodyne model 2146 digital cassette recorder. A Datos 305 data interface was used to present the Biomation digital output in an

acceptable form with formatting to the Memodyne recorder. A Data Works Model 1700 was used to do this for some of the initial experiments.

A Texas Instruments Silent 700 ASR terminal was used to transmit the recorded data to a CDC CYBER 175 computer.

3.2 EXPERIMENTAL PROCEDURE

Cold flow air experiments were conducted to study and compare steady and unsteady ejector performance characteristics. All experiments were conducted at stagnation pressure ratios, P_{s0}/P_{p0}, that would produce supersonic regime flow at sufficiently low values of P_{m3}/P_{s0}. As can be seen in Figs. 2.1-2 and 2.5-4, the maximum pressure recovery in the back pressure independent flow regimes, which occurs at the break-off point with MR flow, is noticeably less for SSR and APPR flows than SR flow. Since this investigation is concerned with high pressure recovery applications of ejector systems, the objectives of this investigation can most efficiently be met by investigating only the SR flow range of values of P_{s0}/P_{p0}. Also, a pressurized secondary system would have been required to investigate SSR and APPR flows. It can also be seen in Fig. 2.1-2 that higher P_{m3}/P_{s0}, according to the theoretical analysis, are obtained in MR flow than SR flow. Thus MR flow, near break-off with SR flow, was investigated to obtain a more complete understanding of ejector performance near break-off.

The effects of a pulsing driver flow, its frequency, the back pressure, and the mixing duct length on ejector performance and the behavior of the flow within the mixing duct were investigated for evidence of

significant variations in mixing and pressure recovery processes as well as ejector entrainment characteristics. Ejector flow data were also taken to determine how well the analysis predicts flow conditions at Station 1 for both steady and periodic primary flow.

3.2.1 Steady Flow Experimental Procedure

An extensive set of steady flow experiments was conducted in order to gain a detailed knowledge of the ejector operating characteristics and to form a basis with which an unsteady driver flow could be judged.

Preliminary experiments were conducted to determine at what values of P_{m3}/P_{s0} SR flow began to break-off to MR flow and how w_s/w_p decreased as P_{m3}/P_{s0} was increased beyond the break-off value. These experiments were accomplished by adjusting the stagnation pressures to different levels so that their ratio, P_{s0}/P_{p0}, remained constant while the back pressure condition, P_{m3}/P_{s0}, varied. During these experiments P_{m3} remained approximately constant. The mass flowrate ratio proved to be quite sensitive to the back pressure; it decreased as P_{m3}/P_{s0} increased once the ejector flow had passed break-off conditions and was in the mixed regime. It was learned that the mixing duct static pressure profile could be used as a reliable indicator of whether or not break-off of SR to MR flow had occurred and to what extent. This was helpful in conducting the experiments since the flow began to break-off at lower values of P_{m3}/P_{s0} and more gradually than predicted from the theoretical analysis.

Back pressure independent flow conditions were investigated for values of P_{s0}/P_{p0} in the approximate range: $.048 \leq P_{s0}/P_{p0} \leq .180$. The mixing

duct static pressure distribution was used to insure that the ejector flow was in the supersonic flow regime. The pressures: P_{p1}, P_{s1}, P_{s0}, P_{m3}, and the mixing duct static pressure distribution were recorded by photographing the manometer board. A precision pressure gage was used to measure the primary and exit plane stagnation pressures. The necessary VDI nozzle data were also recorded to determine the mass flowrates. This entire set of experiments was conducted for mixing ducts with length-to-width ratios, L/W = 9.0, 13.0, and 16.374.

Static pressure measurements versus time were recorded to establish approximately the intensity and scale of the turbulence within the mixing duct. As a result of the unexpected nature of these preliminary transient measurements, a series of experiments was conducted following the procedures planned for the periodic driver flow experiments. The static pressures were recorded simultaneously at pressure taps on the primary flow centerline and on the subsonic secondary flow wall along the length of the mixing duct. These data sets were recorded at values of P_{s0}/P_{p0} = .070 and .160 in the L/W = 13.0 mixing duct and at values of P_{s0}/P_{p0} = .100 and .160 in the L/W = 9.0 mixing duct. The exit plane stagnation pressures were also recorded. Static pressures within both the L/W = 13 and 9 mixing ducts at P_{s0}/P_{p0} = .070, .100, .130, and .160 were examined on an oscilloscope display which was triggered by the Biomation. The mixing duct flow was examined at several duct locations for side to side symmetry. The secondary stagnation pressure, P_{s0}, was examined for steadiness.

Most of the experiments were conducted in the mixed regime near the experimental break-off point with the supersonic regime. This was done

because the ejector flow began to break-off from SR flow at values of P_{m3}/P_{s0} that were significantly lower than the theoretically predicted values and because the sharp theoretical break-off between SR and MR flows and the rapid decrease of M_{s1} in the mixed regime, as shown in Fig. 2.1-2, experimentally were found to be a smoother transition followed by a more gradual decline of M_{s1} and w_{sp}. Thus, truly back pressure independent SR flow mass flowrate ratios, which were obtained at the sacrifice of pressure recovery, were not significantly greater than MR flow values obtained at higher P_{m3}/P_{s0}. MR flow near break-off was examined in order to obtain a more complete picture of ejector performance.

Another set of experiments was conducted for values of P_{s0}/P_{p0} = .070, .100, .130, and .160 with L/W = 9.0 mixing duct to determine how the mass flowrate ratio decreased as P_{m3}/P_{s0} was increased above the break-off value. The exit plane static pressure, P_{m3}, was digitally recorded and then averaged to determine an effective value of P_{m3}/P_{s0}. In all other respects the experimental procedure was the same as that used in the preliminary runs discussed at the beginning of this section; however, the number of experiments conducted was more extensive.

3.2.2 Periodic Flow Experimental Procedure

Periodic driver flow ejector experiments were conducted at driver frequencies of 142 Hz and 250 Hz. More experiments were conducted with the L/W = 9.0 mixing duct than the two longer ducts because it was desired to determine whether or not ejector performance with a shorter mixing duct could be improved by a periodic driver. The mixing duct with

L/W = 16.374 duct was only investigated for the back pressure independent mass flowrate ratios with the 142 Hz driver.

Preliminary experiments were conducted to correlate the stagnation pressure upstream of the oscillator inlet to the mean value, $\overline{P_{p0}}$, of the stagnation pressure in the resonance chamber of the oscillator slightly upstream of the ejector primary inlet. With this correlation, $\overline{P_{p0}}$ could accurately be set by adjusting the steady oscillator inlet stagnation pressure. This correlation was found to be constant within .5% over the range of pressures of interest and repeatable within calibration accuracy. $\overline{P_{p0}}$ was approximately 90% of the oscillator inlet stagnation pressure at both driver frequencies. It is through this correlation procedure that a representative or effective value of P_{s0}/P_{p0} is obtained for comparison of periodic and steady driver ejector flow results.

The use of an overbar to indicate the mean will be dropped with the mean value being understood. Proper reference to time is made for instantaneous values.

The procedures outlined for the steady flow experiments using the electronic data sampling equipment were followed. This includes static pressure measurements along the length of the ducts and mass flowrate break-off experiments. These procedures were repeated completely with the 142 Hz driver; for the 250 Hz driver flow, experiments were conducted with only a mixing duct with L/W = 9.0.

Experiments were run at both driver frequencies measuring P_{p0}, P_{p1}, and P_{s1} simultaneously over the range of P_{s0}/P_{p0}. This was done so that the ratios P_{s1}/P_{p1} and P_{p1}/P_{p0} could be observed with time. P_{p1} could

also be compared with P_{p0} to determine how oscillator pressure pulses may have been altered by passage through the C-D nozzle at the primary flow inlet.

3.3 EXPERIMENTAL RESULTS

Steady driver ejector flow performance parameters have been compared, in the following discussion, with the one-dimensional theory and with periodic driver ejector flow performance parameters. The comparison with theory has been done to identify trends in ejector performance over the range of flow conditions and mixing duct lengths and to test the theory. The quasi-steady analysis cannot be expected to predict periodic driver ejector flow conditions better than the one-dimensional analysis predicts steady driver ejector flow conditions. The effects of a periodic driver on ejector flows are judged by the comparisons made with steady driver ejector flows and with the predictions of the quasi-steady analysis.

3.3.1 Steady Flow Experimental Results

The back pressure independent performance parameters of the steady flow ejector were found to follow closely the trends predicted by the one-dimensional analysis with the exception of the back pressure ratio, P_{m3}/P_{s0}, at the break-off point. In Fig. 3.3.1-1, it can be seen that the experimental and theoretical values of P_{s1}/P_{p1} agree reasonably well. The value of M_{p1} used in the theoretical analysis was determined experimentally from P_{p1}/P_{p0} and the isentropic relations [43]. The two longer mixing ducts produced values of P_{s1}/P_{p1} which were consistently below the theoretical curve; the shortest mixing duct produced values

which were slightly above the theoretical curve. This suggests that M_{s1} and w_{sp} should be smaller for the shorter duct. Figure 3.3.1-2 does indicate that lower w_{sp} values occurred with the shorter L/W = 9.0 duct over most of the range of P_{s0}/P_{t0}. However, the mass flowrate characteristics of the shortest mixing duct do not follow the theoretical curve as well as the two longer ducts, the experimental results are below and above the theoretical curve. It was also observed that the shorter duct had to be operated at lower back pressure conditions before performance parameters began to level off as supersonic regime back pressure independence was approached. The back pressure ratio, P_{m3}/P_{s0}, for each of the experiments are indicated in Fig. 3.3.1-3. It did seem that lower values of P_{m3}/P_{s0} might have further improved the shortest duct mass flowrate performance, however, this would have been at the sacrifice of the resulting ejector pressure recovery. This matter was not pursued because mixed flow static-to-stagnation pressure ratios in the exit plane, P_{m3}/P_{m0}, below the sonic flow value, .528, were obtained.

During the course of the steady flow experiments, the static pressure profiles observed in all three mixing ducts changed dramatically with the back pressure ratio, P_{m3}/P_{s0}. At back pressures lower than the SR flow break-off value, the static pressure decreased smoothly on the subsonic flow wall and along the primary flow centerline as both secondary and primary flows accelerated after entering the mixing duct. The flow would remain at these low pressure levels to within four duct widths of the exit plane; a rapid pressure rise to the exit plane condition would take place in the remainder of the duct. As P_{m3}/P_{s0} was increased, the

distance downstream in the duct that the flow would remain in a low pressure, high velocity state decreased. The value of P_{m3}/P_{s0} at which the initial pressure decrease and the corresponding acceleration was immediately followed by the onset of the pressure recovery process was approximately the break-off value of P_{m3}/P_{s0}. A decrease in the mass flowrate ratio was always observed to occur as P_{m3}/P_{s0} was further increased for a given value of P_{s0}/P_{p0} in the L/W = 13.0 and L/W = 16.374 mixing ducts. Thus, break-off from SR to MR flow had occurred. As P_{m3}/P_{s0} was further increased the shock structure in the supersonic core became stronger, particularly at lower values of P_{s0}/P_{p0}. Although the primary flow expanded and accelerated to low pressures as it did at lower values of P_{m3}/P_{s0}, the secondary flow was accelerated less as indicated by the smaller pressure drop along the wall downstream of the entrance of the duct, Station 1. As P_{m3}/P_{s0} was increased further, secondary flow wall pressures in the acceleration section of the duct remained constant and equal to P_{s1}. At this value of P_{m3}/P_{s0}, the mass flowrate ratio had probably decreased by approximately 50% from the SR flow value.

The important features of the mixing duct static pressure profile are demonstrated in Fig. 3.3.1-4. Pressure taps along the subsonic secondary flow walls are referred to as being at the wall and pressure taps on the primary flow centerline are referred to as being at the center in all of the following discussions and in all figures. The wall and center tap static pressures along the length of the L/W = 16.374 mixing duct are presented in Fig. 3.3.1-4 for two steady flows with, as near as possible, the same value of P_{s0}/P_{p0}. Although the difference between the two profiles

is significant, the profile for the lower value of P_{m3}/P_{s0} was obtained by increasing the value of P_{p0} above that of the other profile from 71.22 psia to 73.80 psia and adjusting P_{s0} accordingly. With a periodic driver, the reverse case was found, i.e., the value of P_{m3}/P_{s0} is approximately constant while P_{s0}/P_{p0} changes; however, the effects on the mixing duct pressure profile are still the same. At these pressure levels, the oscillator pulses have a total amplitude of 12 to 15.25 psi. Using the theoretical results as a guide, the effective changes in the break-off value of P_{m3}/P_{s0} should be larger than the difference between the two values shown in Fig. 3.3.1-4 at the same value of P_{s0}/P_{p0}.

3.3.2 Periodic Flow Experimental Results

During the experiments with the steady and periodic driver flows, three types of unsteady flow phenomena were observed in the mixing duct flow. The largest disturbances found within the mixing duct appear to be due to changes in and motion of the shock structure in the supersonic core. These shock waves and their location seemed quite unstable, which may have been due to other unsteady disturbances. A low amplitude oscillation of the static pressures within the duct with frequencies up to approximately 1000 Hz was also observed. This oscillation was more noticeable in the mixing duct with L/W = 9.0 than with L/W = 13.0. These oscillations were present in the wall or secondary flow at Station 1 but if observed, were not seen in the center flow until after X/W = 1.0. Oscillation amplitudes usually increased in the acceleration section of the mixing duct; however, low back pressure conditions were found to

inhibit this growth and to diminish the amplitudes at Station 1. The most surprising phenomena found with either steady or periodic driver flows are shown in Fig. 3.3.2-1. Large amplitude pulses, sometimes bursting into periodic groups, were observed in most flows. These pulses originated in the wall flow at approximately the end of the acceleration section of the flow which is near the location of the first shocks embedded in the center flow. The amplitude and frequency of occurrence of these bursts increased as P_{s0}/P_{p0} decreased. In many cases these bursts appear to have been an amplification of the smaller amplitude pulses mentioned above. Neither the origin or amplification of these disturbances is well understood. Changes in operating conditions which adversely increased the secondary flow pressure gradient through the duct and increased the strength of the shocks in the supersonic core are believed to stimulate these pulses. It appears that corner flow separation and reattachments, shear layer instabilities, and disturbances due to the unstable shock structure which propagate into the subsonic wall flow are probable mechanisms for these unsteady phenomena. Investigations of unsteady turbulent boundary layers have found bursts in intensity levels do occur in some cases with periodic freestream flows [44,45]. The turbulence at the edge of the boundary layer can "violently" increase in level and burst into the freestream flow. Oscillations in the shock structure of the supersonic core may be coupled with larger scale turbulence to stimulate such bursts. Figure 3.3.2-2 shows one more feature of all pulses, that is side-to-side symmetry was always found in all flows.

A set of static pressure profile data taken along the length of the mixing duct with L/W = 9.0 and with P_{s0}/P_{p0} = .100 for steady and both periodic driver flows is included in Figs. 3.3.2-3 to 3.3.2-21 to present a clear picture of what occurs within the mixing duct and how some of the many variables affect the flow. All data was taken for steady, 142 Hz, and 250 Hz driver flows with approximately equivalent input and back pressure flow conditions. Figures 3.3.2-3 and 3.3.2-4 are the primary and secondary static pressures at Station 1 versus time for both periodic driver frequencies. The secondary flow pulses are somewhat irregular and the periodicity appears to be much weaker at the lower frequency. These irregular oscillations in the secondary flow were not as large in the mixing duct with L/W = 13.0. The oscillations in the secondary flow have grown by X/W = 0.333 and are prominent with both steady and periodic driver flows; these data are shown in Figs. 3.3.2-5, 3.3.2-6, and 3.3.2-7. Note that the center flow has not been affected by the irregular disturbances observed in the subsonic wall flow. Also, note that the 250 Hz wall flow pulses slightly precede those in flow at the center. This phase shift can be seen in nearly all of the data taken in the first 1/3 of the mixing duct; it was usually more noticeable with the 250 Hz driver flow. Static pressures continue to drop as the flows interact and accelerate until somewhere near X/W = 1.0. Shocks occur in the primary flow where it stops expanding against the secondary and readjusts its flow direction. Disturbances that occur in the wall flow also appear in the center flow at X/W = 1.0, see Figs. 3.3.2-8, 3.3.2-9, and 3.3.2-10. The periodicity of the center flow seems to fade in and out. The pulses at X/W = 1.0 in the

expanded 142 Hz driver ejector flow are larger and steeper than could be produced solely by driver flow pulsations. Figure 3.3.2-11 is an example of how much the driver pulses were diminished by the expansion of the supersonic primary flow. The data in this figure were taken for a back pressure independent SR flow experiment with $P_{s0}/P_{p0} \simeq .070$. The $P_{s0}/P_{p0} = .100$ data under consideration has a back pressure sufficiently high for the mass flowrate ratio to have decreased about 9% from the back pressure independent SR flow value. Shock waves, due to the relatively high back pressure, are present in this MR flow and their unsteady behavior in the periodic flow is believed to be the cause of the larger pulses in the flow at X/W = 1.0. As mentioned earlier, the strength and in most cases the number of shocks in the flow increase when SR flow breaks-off to MR flow due to an increase in P_{n3}/P_{s0}. Note also that the unsteadiness of the shock waves in the steady driver ejector flow is comparable to the periodic driver ejector flows. Shock waves are clearly present at the X/W = 1.333 pressure tap location, as shown in Figs. 3.3.2-12, 3.3.2-13, and 3.3.2-14. The smaller oscillations at the subsonic wall flow pressure taps are similar in appearance to the large oscillations at the center taps and are phase-shifted slightly ahead of the disturbances at the center. The periodic driver moves the shock waves upstream and downstream within the mixing duct; some of these shock waves may disappear or coalesce and then reappear. The shock waves in the steady driver ejector flow are quite unsteady; however, their unsteady action is intermittent and not as vigorous as in the periodic driver flows. The shock wave patterns are the dominant feature within the flow in the mixing duct until

X/W = 6.0; however, at X/W = 4.0, the wall flow appears to be decoupled from the action in the primary flow at the center. These mixing duct flow features are shown in Figs. 3.3.2-15, 3.3.2-16, and 3.3.2-17. The 250 Hz driver flow again appears more pulsatile than the 142 Hz driver flow. The static pressure levels at X/W = 4.0 have not increased significantly since X/W = 1.333 and the flow does not appear to have mixed significantly either. Shock waves are present in the flow downstream of X/W = 6.0 but are not evident at X/W = 8.0. At X/W = 8.0, the center and wall flows have become noticeably more broken and turbulent. The mixing duct flow is significantly more uniform across the duct; the mixing duct flow at this location is essentially the same for all three of the driver flows, see Figs. 3.3.2-18, 3.3.2-19, and 3.3.2-20. The 142 Hz driver ejector flow is weakly periodic at X/W = 8.0 while the 250 Hz driver ejector flow is definitely periodic. The supersonic core flow seems to have finally disintegrated in all three driver flows between X/W = 6.0 and X/W = 8.0, thus initiating a rapid mixing and pressure recovery process. This rapid mixing, which occurred immediately downstream of the disappearance of the supersonic core, was also noticed in water table studies of supersonic-subsonic ejector flow where dye was injected into the wall flow to indicate mixing rates. At the exit plane, all three driver ejector flows are nearly identical. Periodicity was still weakly present at the exit plane of the mixing duct due to the muffler and back pressure valve flow resistance; this is shown in Fig. 3.3.2-21. It should be noted that the mean static pressure levels at most locations in the mixing duct are approximately the same for all three driver flows. As shown in Figs. 3.3.2-22 and 3.3.2-23, the exit

plane stagnation pressures were nearly indistinguishable and periodicity was not a strong feature.

The only notable difference between the steady and periodic driver ejector flows in the mixed regime flows discussed above was the increased activity of the shock waves in the supersonic primary flow. Supersonic regime flows operating at the same P_{s0}/P_{p0} as a mixed regime flow had fewer and weaker shocks than the mixed regime flow. Thus, supersonic regime flows were less susceptible to disturbances due to a periodic driver flow than mixed regime flows.

The primary-to-secondary stagnation pressure ratio had a pronounced effect on mixing duct flow features. Lower values of the stagnation pressure ratio tended to have strong shock waves within the flow for all but the low back pressure SR flows. The experimental data with $P_{s0}/P_{p0} = .100$ that was just discussed is typical.

The opposite case is true for higher values of P_{s0}/P_{p0}. For $P_{s0}/P_{p0} = .160$, the resultant P_{s1}/P_{p1} is roughly .9. In this case the primary flow does not expand as much after entering the mixing duct as it did at the lower values of P_{s0}/P_{p0}; consequently, the resulting shock waves in the supersonic core flow do not have as great an effect on the flow. Static pressure measurements were taken in the L/W = 9.0 mixing duct with $P_{s0}/P_{p0} = .160$ and a back pressure ratio sufficiently high to have caused the mass flowrate ratio to decrease by approximately 8% from the back pressure independent value. The largest disturbances within this flow are shown in Figs. 3.3.2-24, 3.3.2-25, and 3.3.2-26. The pulses in the periodic flow were probably due to a weak shock wave moving and/or

changing in strength. This was the only location where disturbances of any notable size were found. The static pressures at Station 1 for P_{s0}/P_{p0} = .160 and the L/W = 9.0 mixing duct and for P_{s0}/P_{p0} = .070 and the L/W = 13.0 mixing duct are shown in Figs. 3.3.2-27 and 3.3.2-28 respectively. From these figures, the secondary flow pulses are seen to decrease appreciably with P_{s0}/P_{p0}.

Experimental values of P_{s1}/P_{p1} versus time were compared with values determined from the theoretical quasi-steady analysis. Obtaining the P_{s0}/P_{p0} versus time data as required for the theoretical analysis was not as straightforward as was initially expected. Figures 3.3.2-29 and 3.3.2-30 are the simultaneously recorded primary stagnation and static pressures for the 142 Hz and 250 Hz drivers, respectively. The stagnation pressure probe was located immediately upstream of the primary C-D nozzle inlet and the static tap was located at the center of the nozzle exit plane, Station 1. The separation distance between these two locations led to the small phase shift seen in both figures. The 250 Hz driver flow stagnation pressure profile was pressure invariant. The higher frequency components in the 142 Hz driver flow profiles grew slightly in amplitude, relative to that of the base frequency, as the mean pressure level increased. Difficulties were encountered when examining the variation of P_{p1}/P_{p0} with time. The decision was made to phase-shift P_{p1} with respect to P_{p0} such that the relatively sharp valleys of each cycle were in phase before determining P_{p1}/P_{p0} as a function of time. P_{p1}/P_{p0} was found to be oscillatory and to be affected strongly by the higher frequency components of P_{p0} which were not present in P_{p1}; this is shown in

Figs. 3.3.2-31 and 3.3.2-32. Note that for the 250 Hz driver flow, the P_{p1}/P_{p0} curve was determined from a different set of data than was used in Fig. 3.3.2-30; both sets of data were in phase with one another and the pressure difference between the two was not large. The same data was used to determine both 142 Hz plots. The ratio, P_{p1}/P_{p0}, for the 250 Hz driver flow was at a minimum when P_{p0} was at a maximum but the 142 Hz data seems to indicate just the opposite. The mean values of P_{p1}/P_{p0} at both driver frequencies was approximately constant at a value of $P_{p1}/P_{p0} = .140$ as compared to the steady flow value of $P_{p1}/P_{p0} = .136$. The pulsed flow in the resonance chamber of the oscillator adjusts, by wave action, to the area change between the resonance chamber and C-D nozzle throat as well as the choked flow condition at the nozzle throat [46]. This wave action adjustment of the flow apparently has altered the wave form of the pressure pulses between the stagnation probe and Station 1 as indicated in Figs. 3.3.2-29 and 3.3.2-30. In order to obtain P_{s0}/P_{p0} versus time for the theoretical analysis, values of P_{p1} were recorded and divided by the mean value of P_{p1}/P_{p0} at the given pressure conditions to determine P_{p0} versus time. P_{s0} was held constant and P_{s1}, P_{p1}, and P_{p0} were all simultaneously measured. The agreement between experimental and theoretical results is reasonably good; these comparisons are in Fig. 3.3.2-33. The experimental data with a mean value of $P_{s1}/P_{p1} = .504$ was taken for a flow in the mixed regime with the back pressure sufficiently high to have caused an 8% decrease in the mass flowrate ratio from the supersonic regime value. Thus, M_{s1} and w_s/w_p are less than the break-off value while P_{s1}/P_{p1} is greater. The data with a mean value of $P_{s1}/P_{p1} = .656$ was taken for a flow

in the supersonic regime while the data with a mean value of $P_{s1}/P_{p1} = .875$ was taken for a flow in the mixed regime with a mass flowrate 3 to 4% less than the break-off value. The value of the primary nozzle exit Mach number used in the analysis was $M_{p1} = 1.957$, the same value as was used in the steady flow analysis.

The imposed back pressure had other effects on the performance of the ejector than those previously described. Depending on the back pressure, the ejector exit plane stagnation pressures were found to differ between the wall and center probe locations by as much as a factor of two or by very little. Lower back pressures and the shortest mixing duct produced the most non-uniform flow at the ejector exit plane. The periodic driver flow had little effect on the exit plane stagnation pressure uniformity. The mean value of the center and wall stagnation pressures were more nearly equal for some periodic flows that were near the break-off back pressure ratio. However, results were inconsistent. The ratio, P_{s0}/P_{p0}, seemed to have an effect and P_{n3}/P_{s0} itself produced a uniform exit plane flow if it was sufficiently high.

As was mentioned earlier, SR ejector flows at low back pressures remained in a low pressure high velocity state, free of shock waves of noticeable strength, to within four duct widths of the exit plane. It was observed that under these flow conditions the wall and center pressure pulses were shifted completely out of phase downstream of the initial acceleration section of the mixing duct; this is shown in Fig. 3.3.2-34. An expansion of the supersonic primary flow, as indicated by a pressure drop at the center pressure tap, caused a deceleration and pressure rise

in the secondary flow at the wall pressure tap. Thus, it appears that after choking the secondary flow accelerates to a supersonic flow if the primary contracts slightly due to shock waves imbedded in the supersonic core. Nelson [47] found that normal shock waves occurred in the wall flow of a similar two-dimensional constant area supersonic-subsonic ejector.

The way that the mass flowrate ratio declines when an SR flow breaks-off to MR flow due to an increase in P_{m3}/P_{s0} was found to differ for steady, 142 Hz, and 250 Hz driver flows at most values of P_{s0}/P_{p0} which were examined. It was observed that the back pressure independent SR mass flowrate ratios were approximately the same for all three driver flows but that the MR flow mass flowrate ratios at a given back pressure ratio, P_{m3}/P_{s0}, were higher with the periodic drivers than with the steady driver. Figures 3.3.2-35, 3.3.2-36, and 3.3.2-37 show these mass flowrate trends. It appears that the periodic driver ejector flows break-off at higher P_{m3}/P_{s0} than the steady driver ejector flows. The maximum difference between the values of P_{m3}/P_{s0} at a given P_{s0}/P_{p0} and the w_s/w_p occurs between the steady and 250 Hz driver ejector flows at $P_{s0}/P_{p0} = .070$; this difference is less than 5%. The 142 Hz driver did not differ from the steady driver by a significant amount in most cases and all three driver ejector flows followed the same break-off trends at $P_{s0}/P_{p0} = .160$.

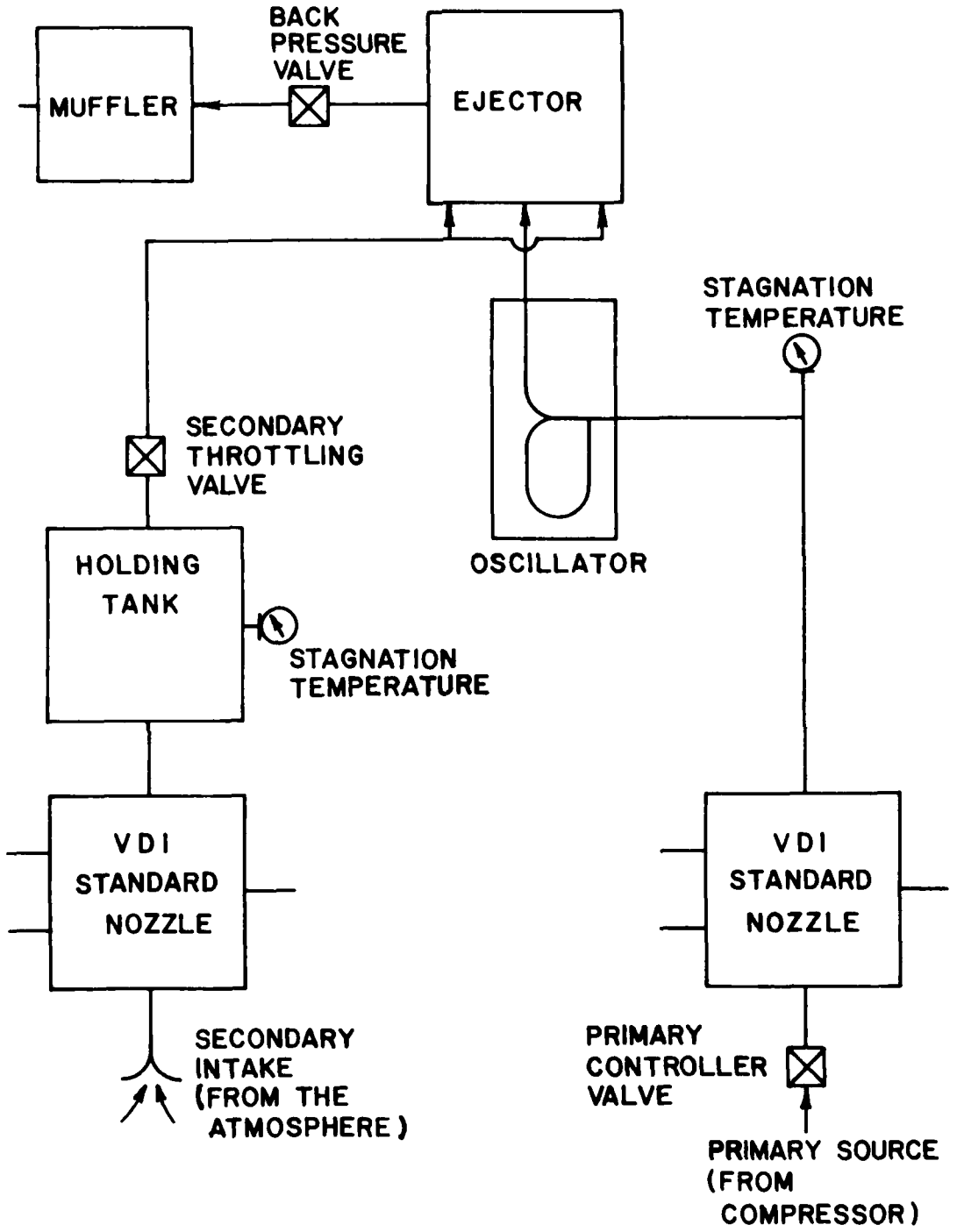

Figure 3.1-1 Flow schematic of the test rig

Figure 3.1-2 The fully assembled ejector unit (L/W = 9.0)

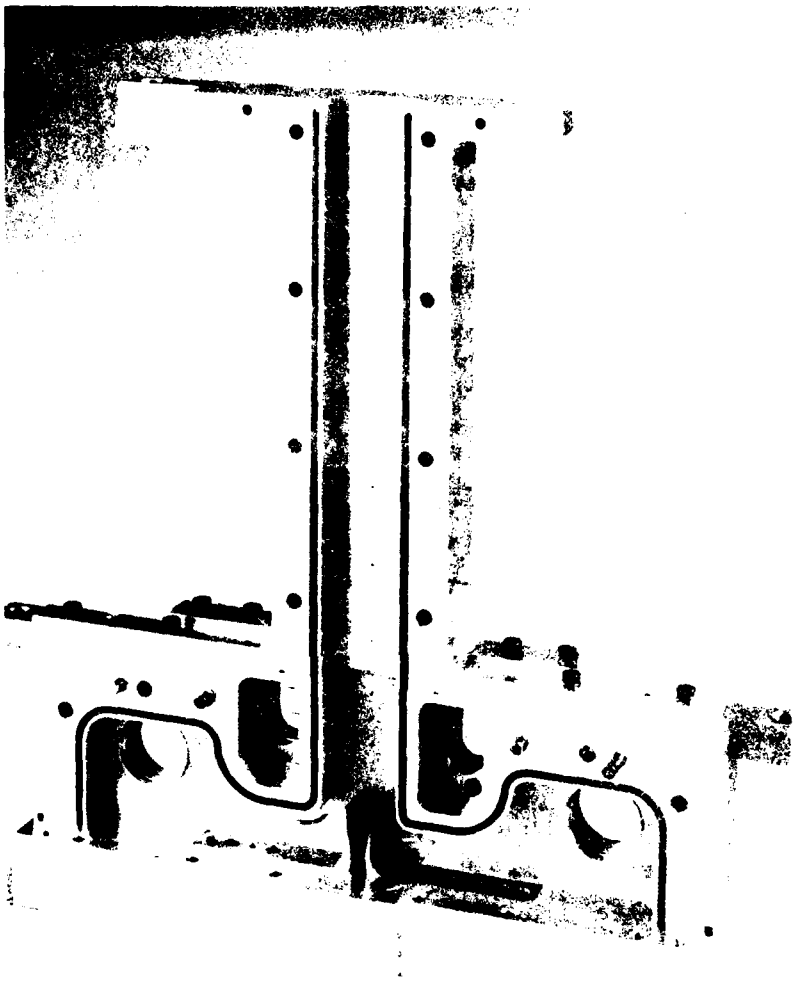

Figure 3.1-3 The partially assembled ejector unit (L/W = 9.0)

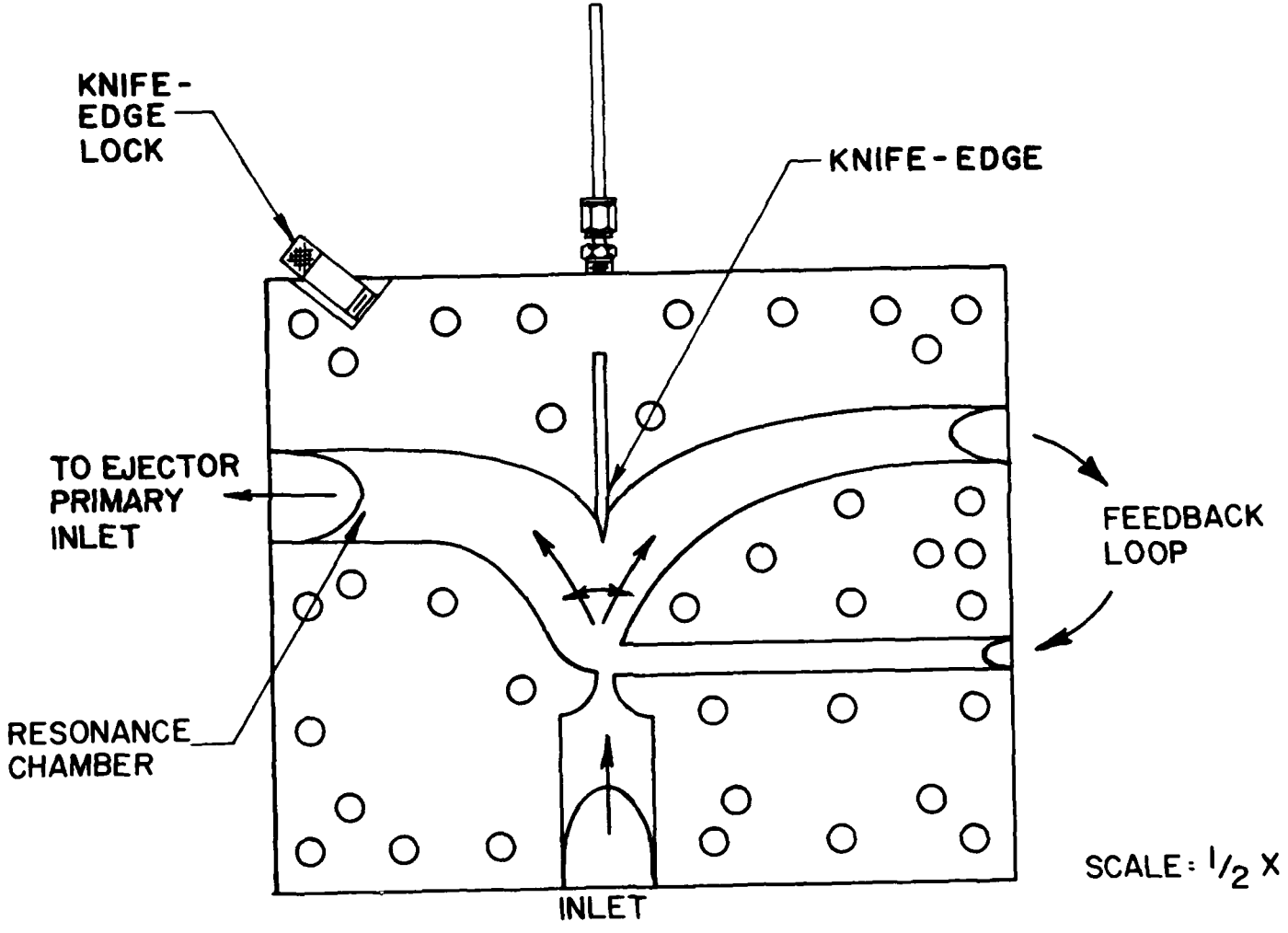

Figure 3.1-4 View of the partially assembled oscillator body

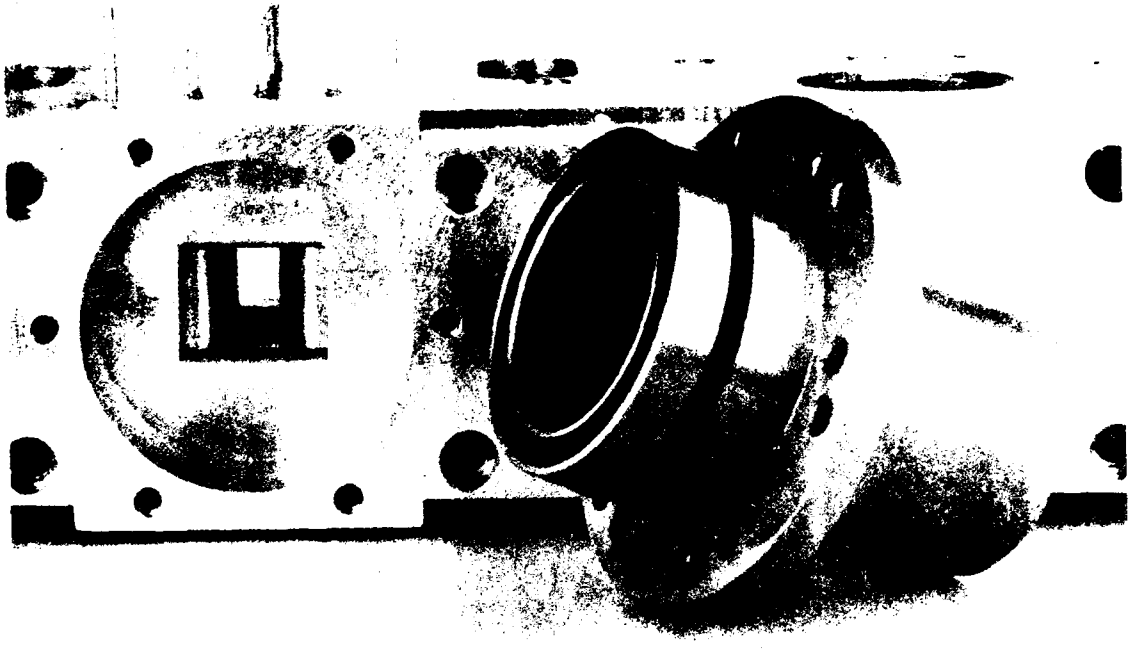

Figure 3.1-5 View of the primary flow inlet to the ejector

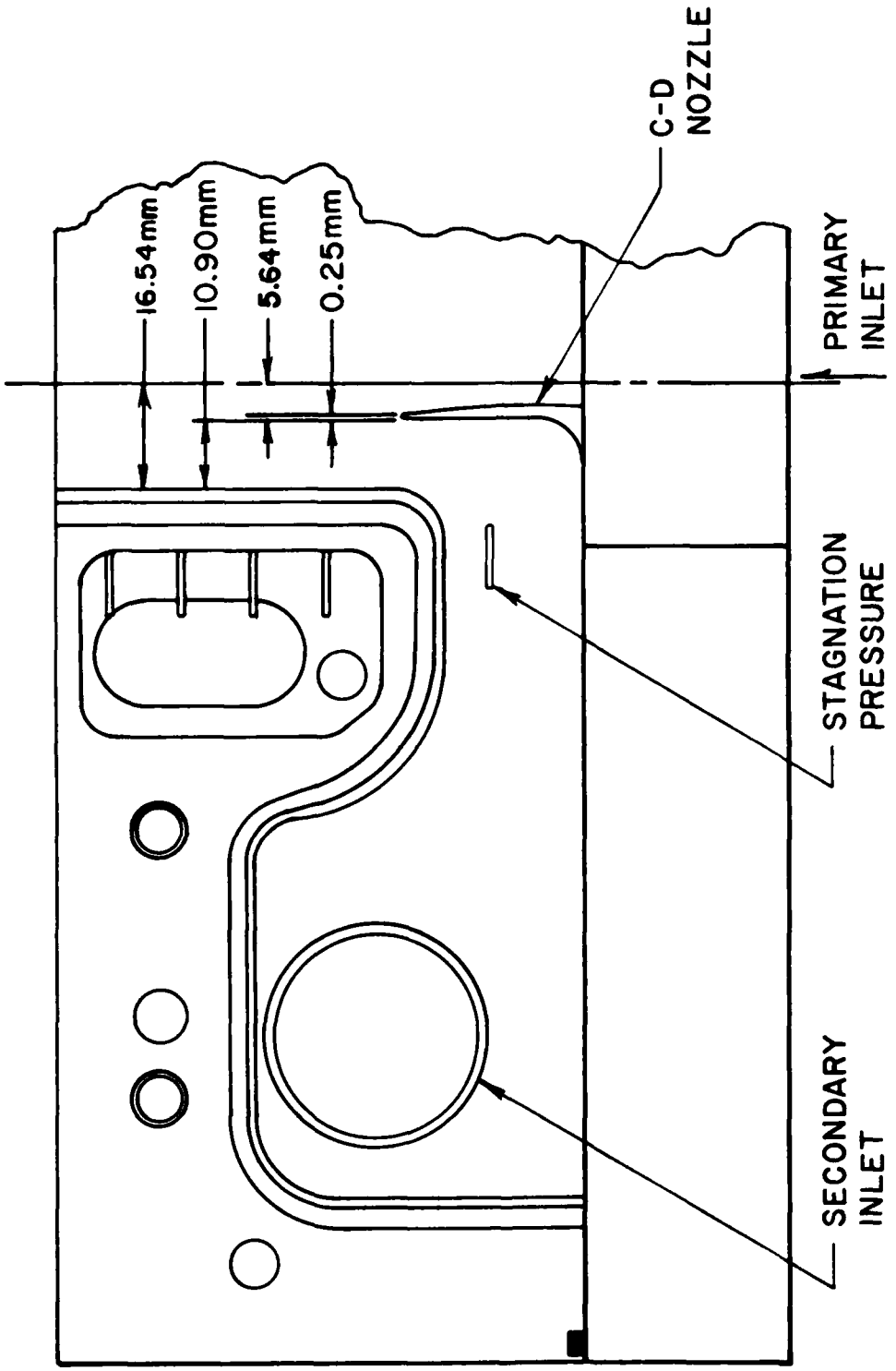

Figure 3.1-6 View of the partially assembled ejector base piece

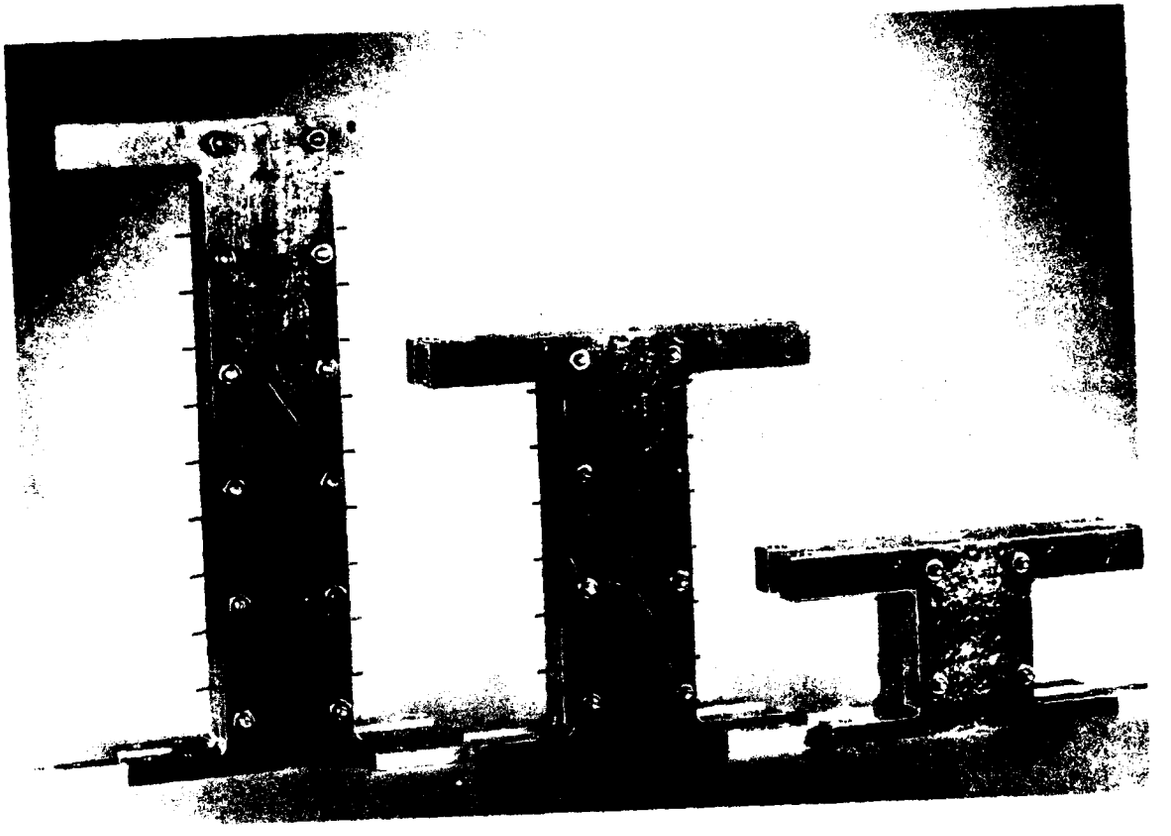

Figure 3.1-7 View of the ejector mixing duct assemblies

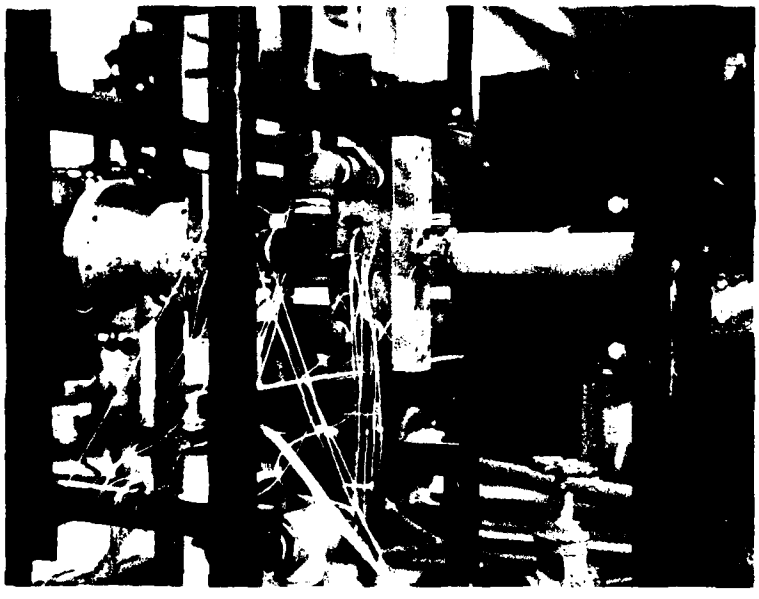

Figure 3.1-8 View of the secondary and primary lines connected to the base assembly

Figure 3.1-9 View of the test rig

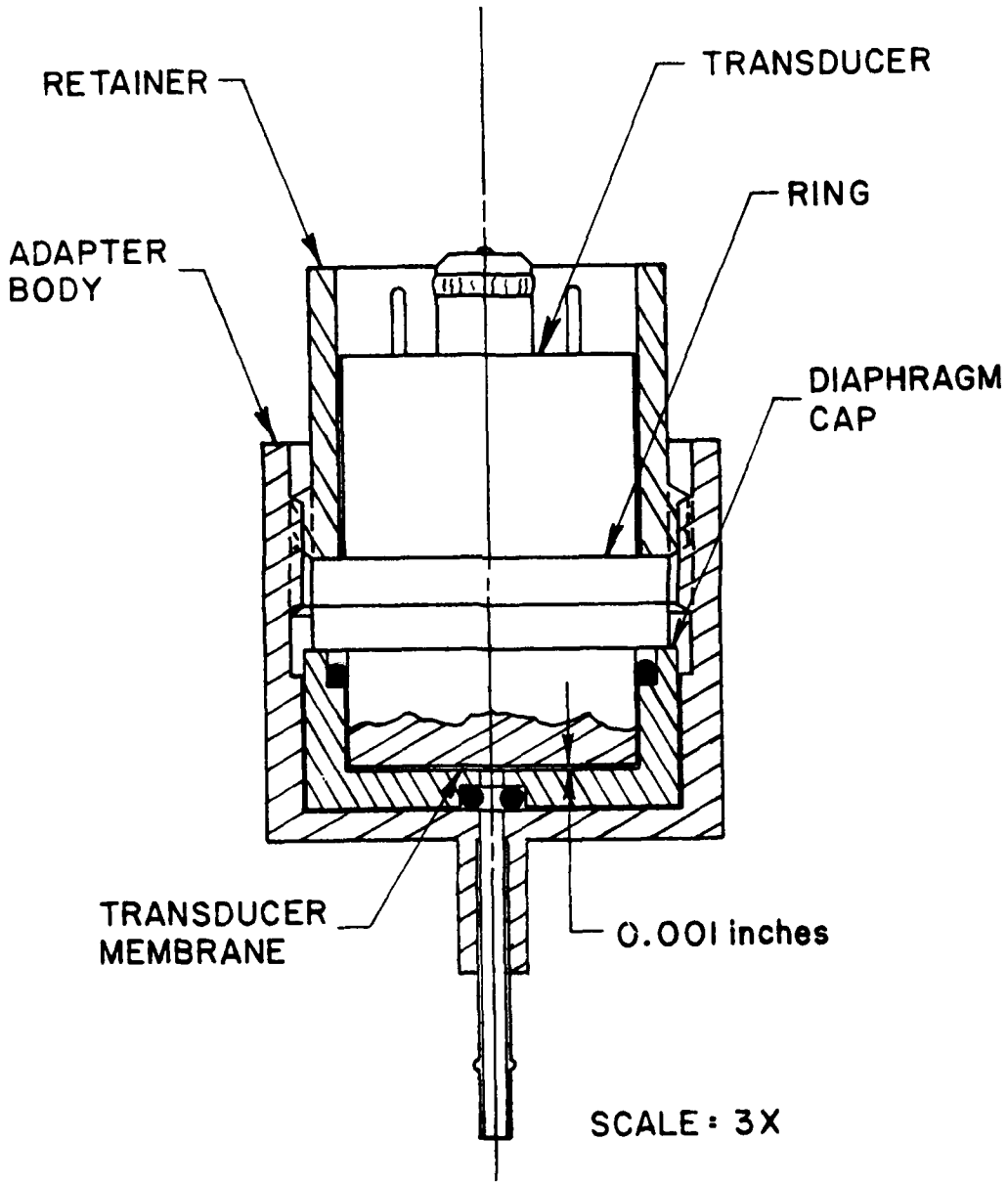

Figure 3.1-10 Cross-sectional view of the Scanivalve "zero" volume line adapter with a CEC type 4-312 pressure transducer in place

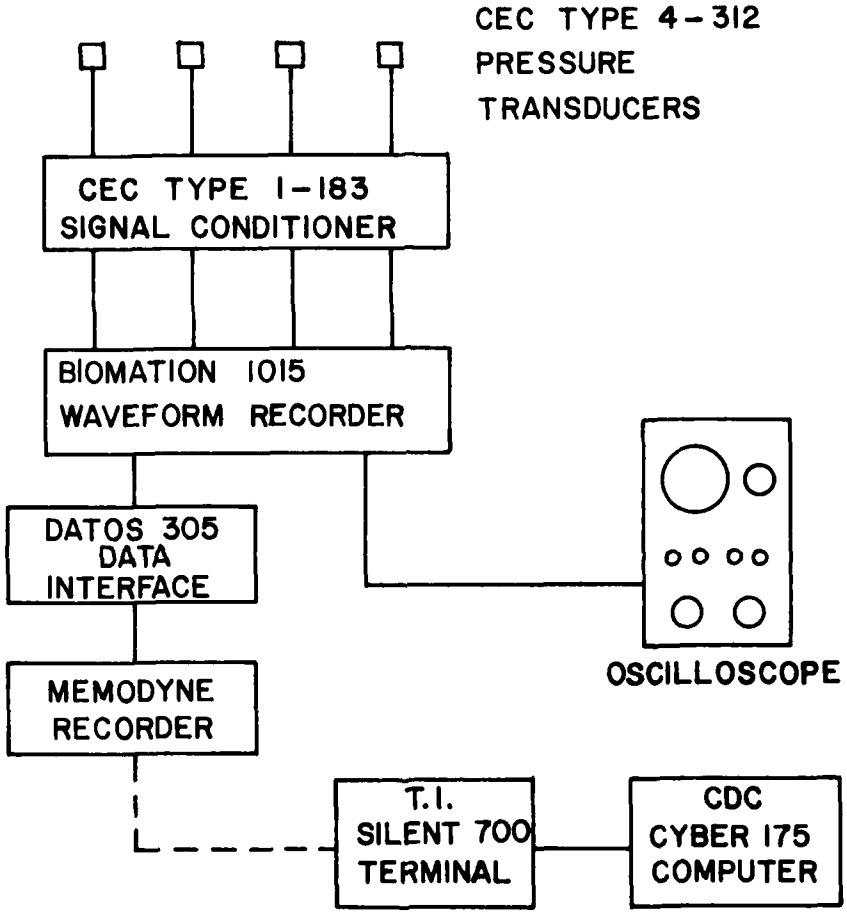

Figure 3.1-11 Schematic detailing the data acquisition system

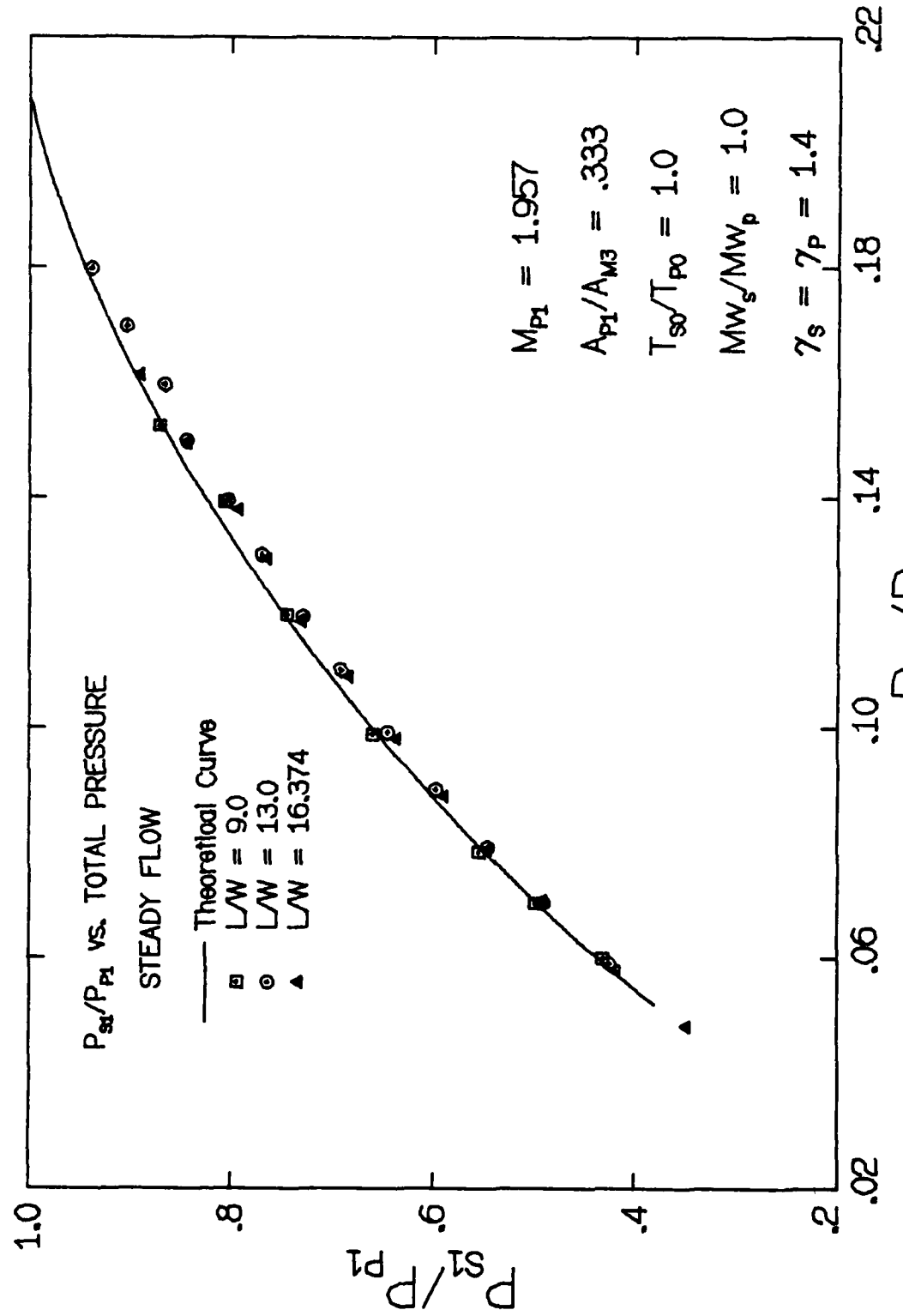

Figure 3.3.1-1 Back pressure independent steady flow values of P_{s1}/P_{p1} versus P_{s0}/P_{p0}

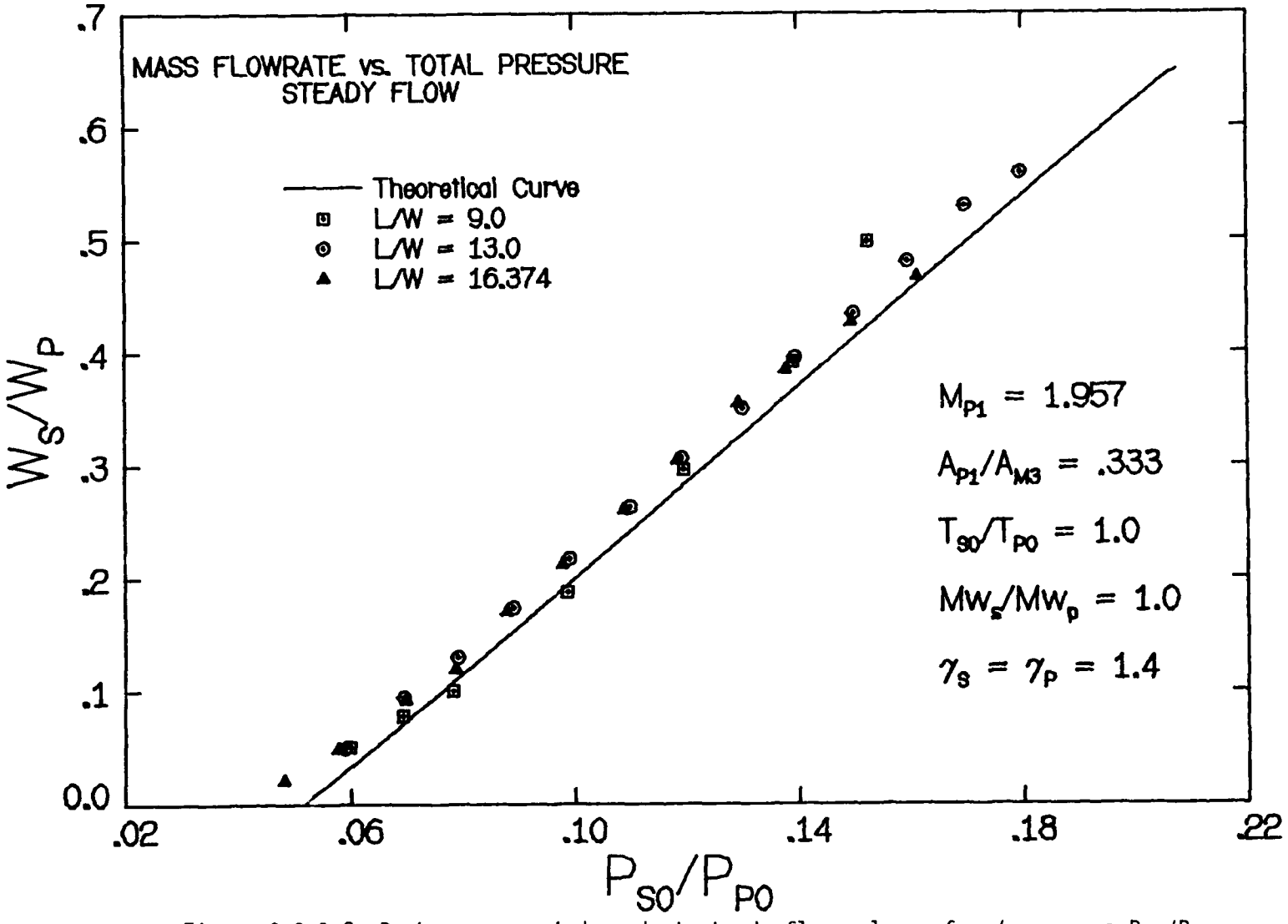

Figure 3.3.1-2 Back pressure independent steady flow values of w_s/w_p versus P_{s0}/P_{p0}

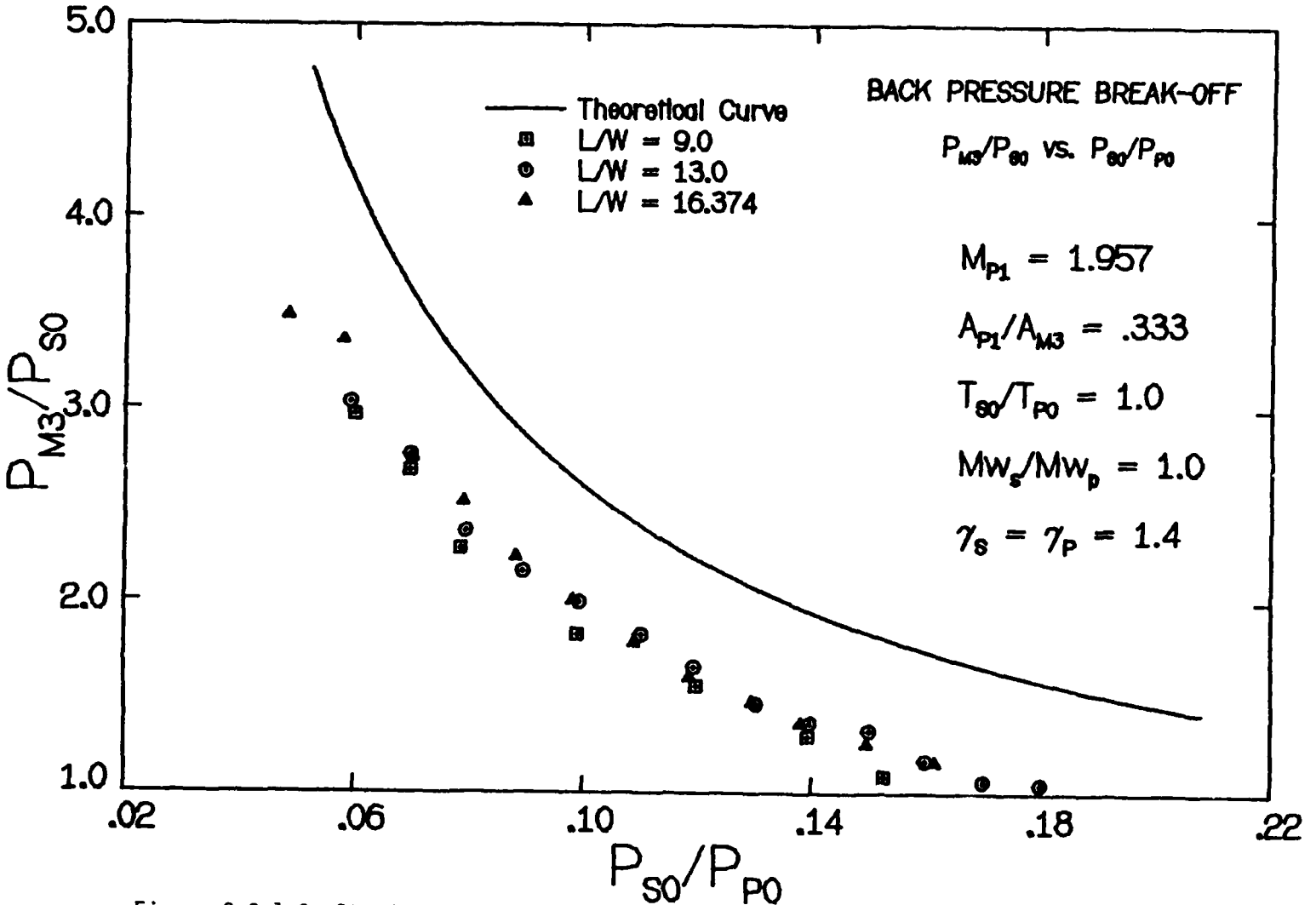

Figure 3.3.1-3 Steady flow values of the back pressure ratio above which SR flow breaks-off to MR flow versus P_{s0}/P_{p0}

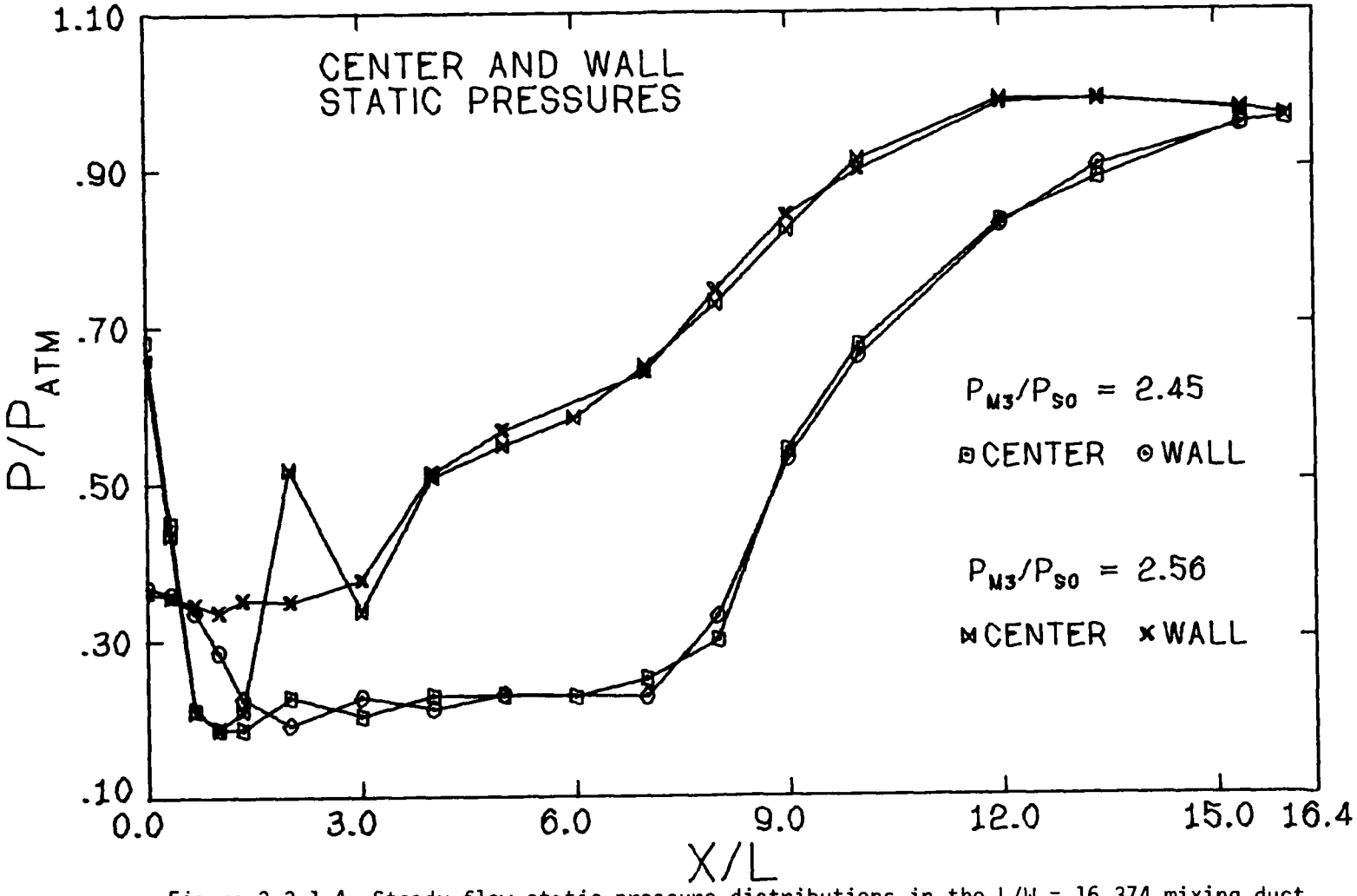

Figure 3.3.1-4 Steady flow static pressure distributions in the L/W = 16.374 mixing duct at P_{m3}/P_{s0} = 2.45 and P_{m3}/P_{s0} = 2.56 ($P_{s0}/P_{p0} \simeq .078$)

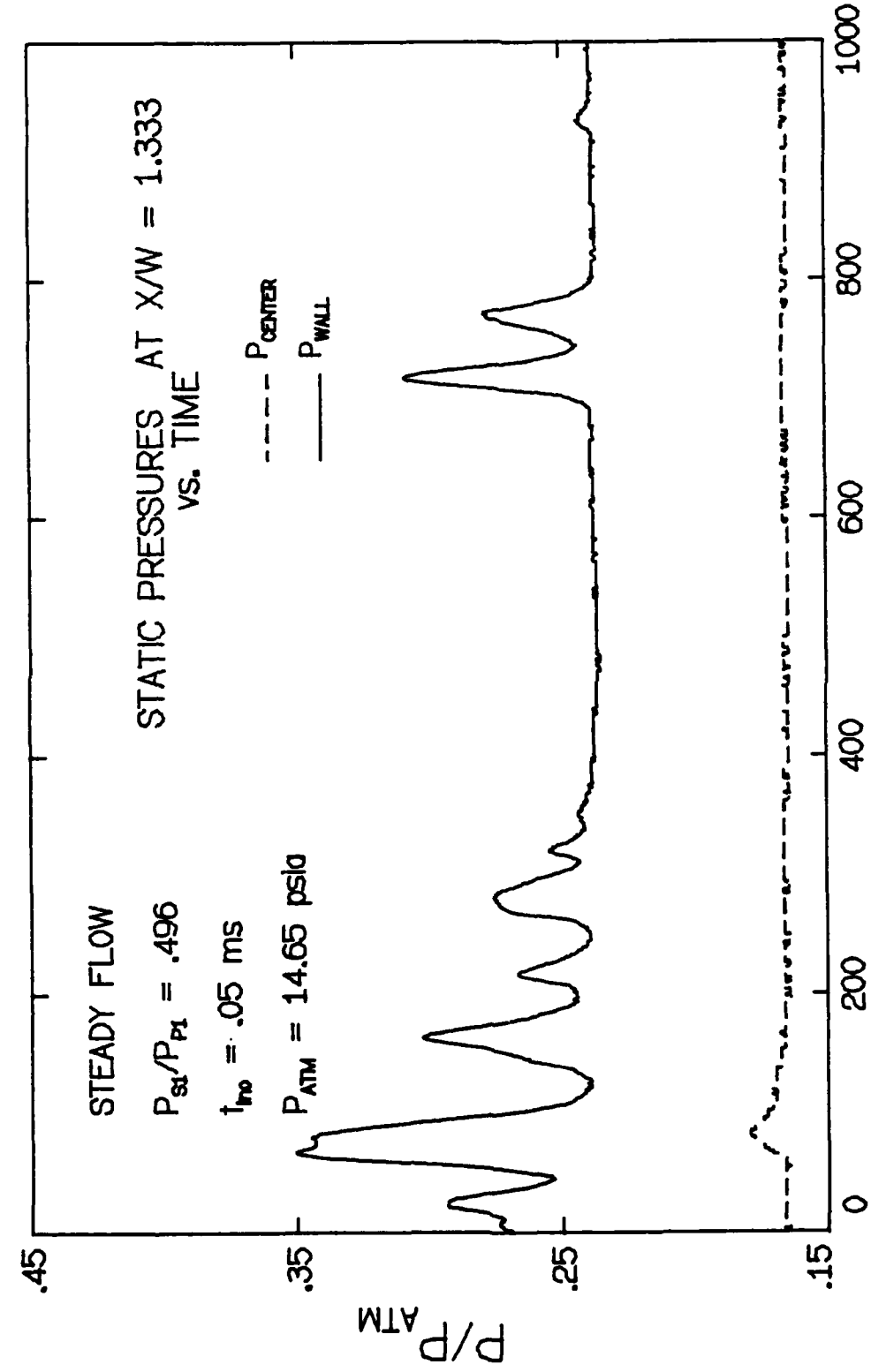

Figure 3.3.2-1 Large amplitude pulses were observed in the subsonic wall flow of both steady and periodic driver experiments ($P_{s0}/P_{p0} \simeq .070$)

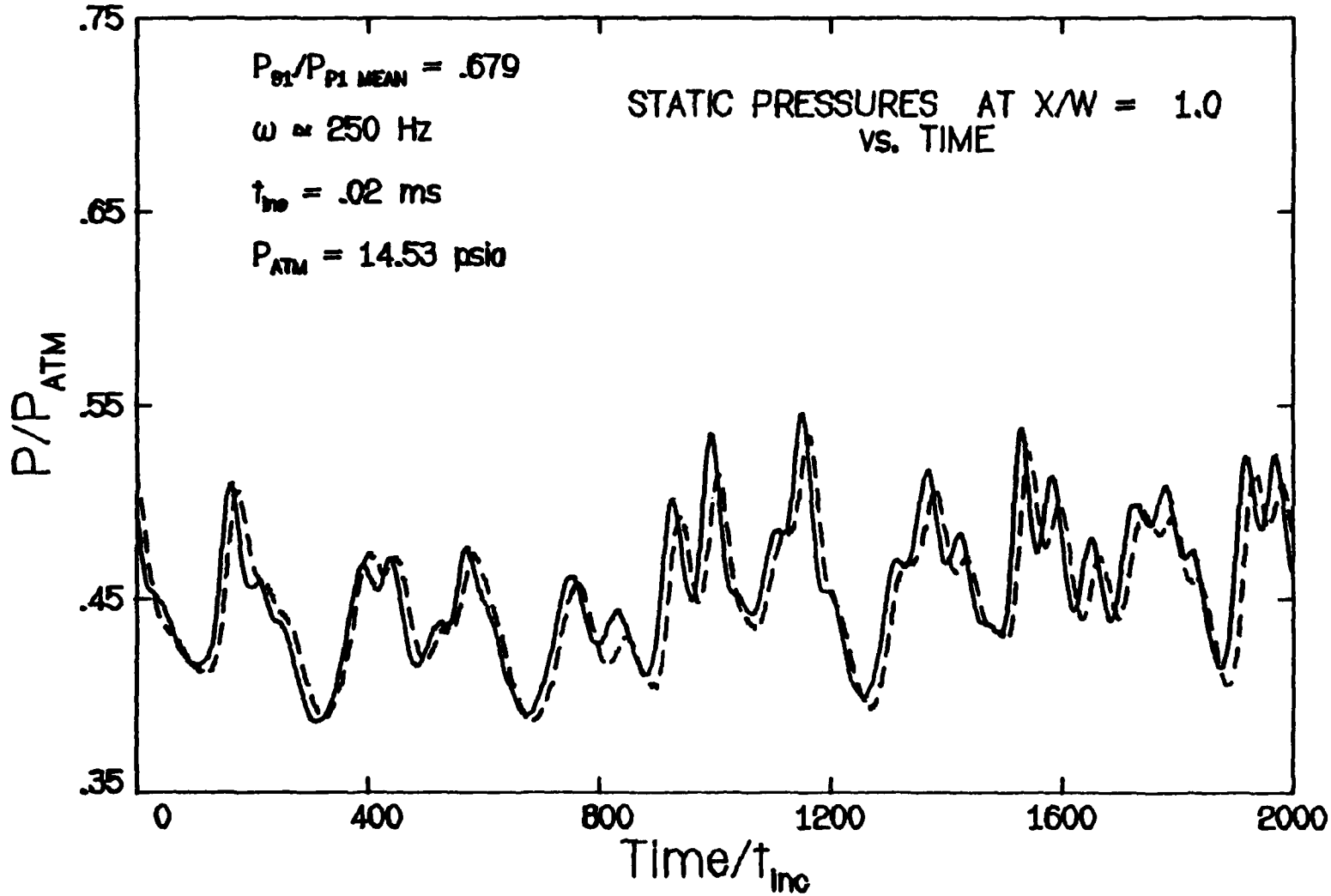

Figure 3.3.2-2 Wall flow static pressures were found to be symmetric about the primary flow centerline ($L/W = 9.0$, $P_{s0}/P_{p0} \simeq .100$)

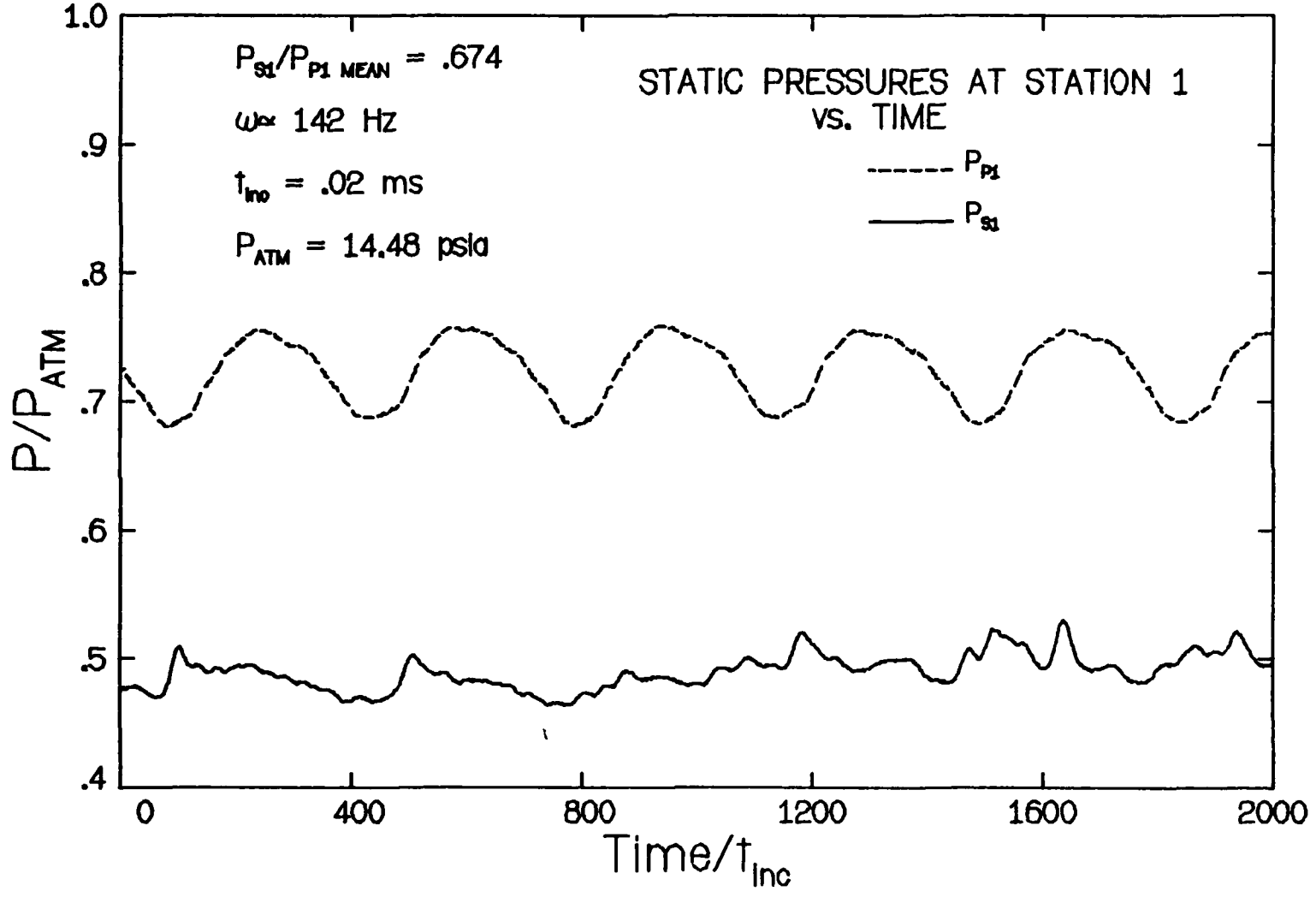

Figure 3.3.2-3 Primary and secondary static pressures at Station 1 for the 142 Hz driver ejector flow versus time (L/W = 9.0, $P_{s0}/P_{p0} \simeq .100$)

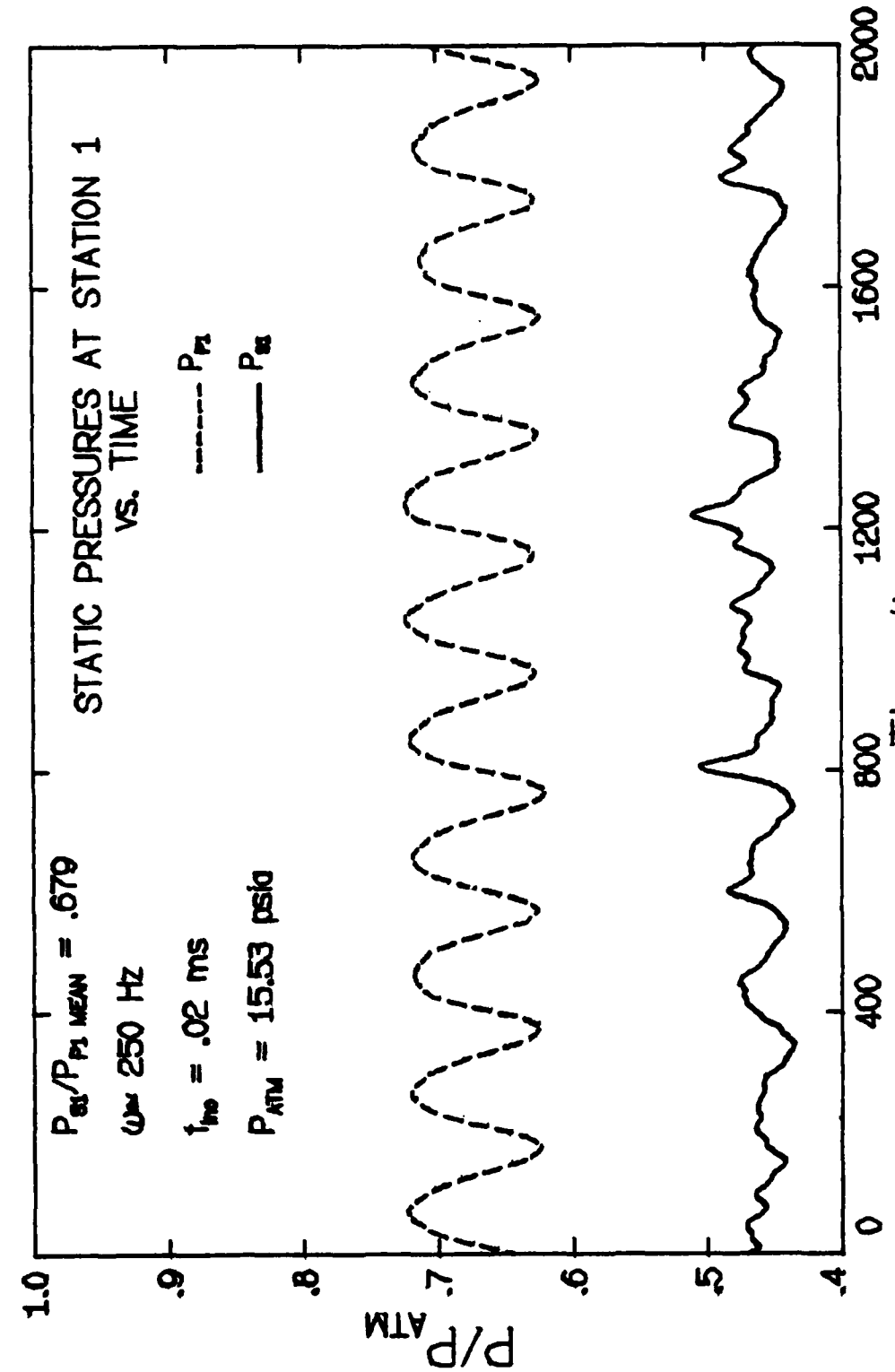

Figure 3.3.2-4 Primary and secondary static pressures at Station 1 for the 250 Hz driver ejector flow versus time (L/W = 9.0, $P_{s,o}/P_{po} \simeq .100$)

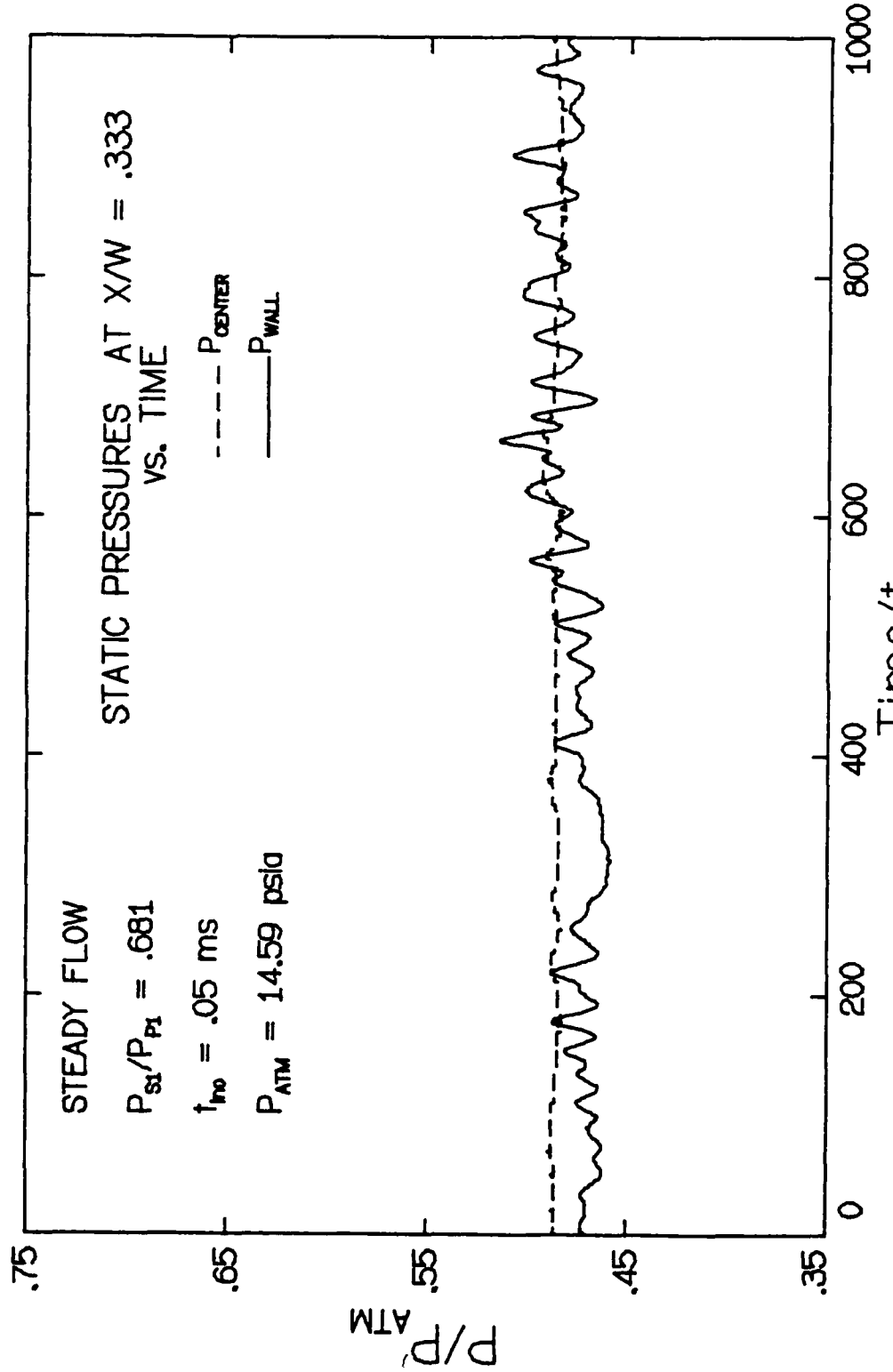

Figure 3.3.2-5 Small disturbances in the subsonic wall flow of the steady driver ejector flow (L/W = 9.0, $P_{s0}/P_{p0} \cong .100$)

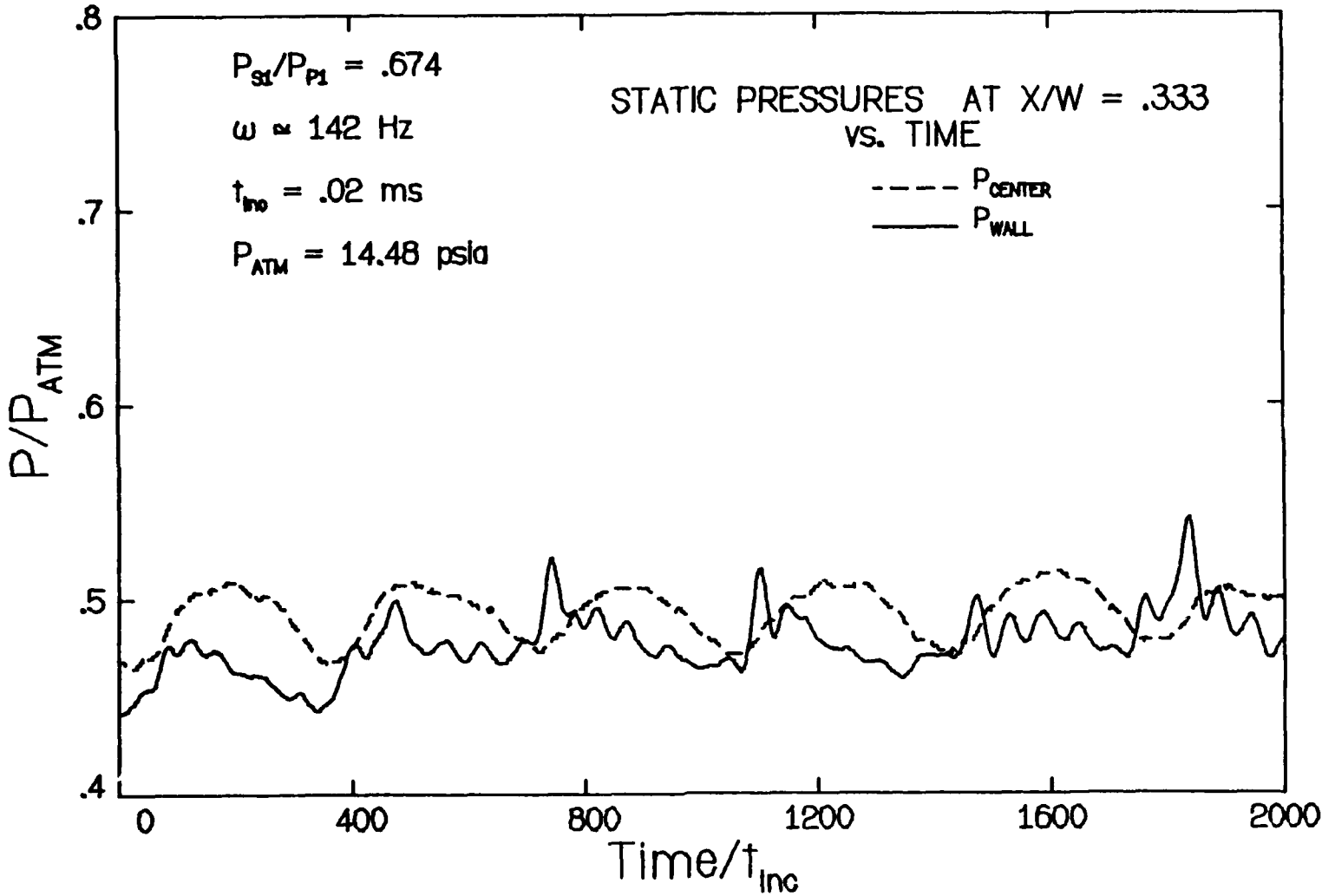

Figure 3.3.2-6 Static pressures versus time in the 142 Hz driver ejector flow at X/W = .333 (L/W = 9.0, $P_{s0}/P_{p0} \simeq .100$)

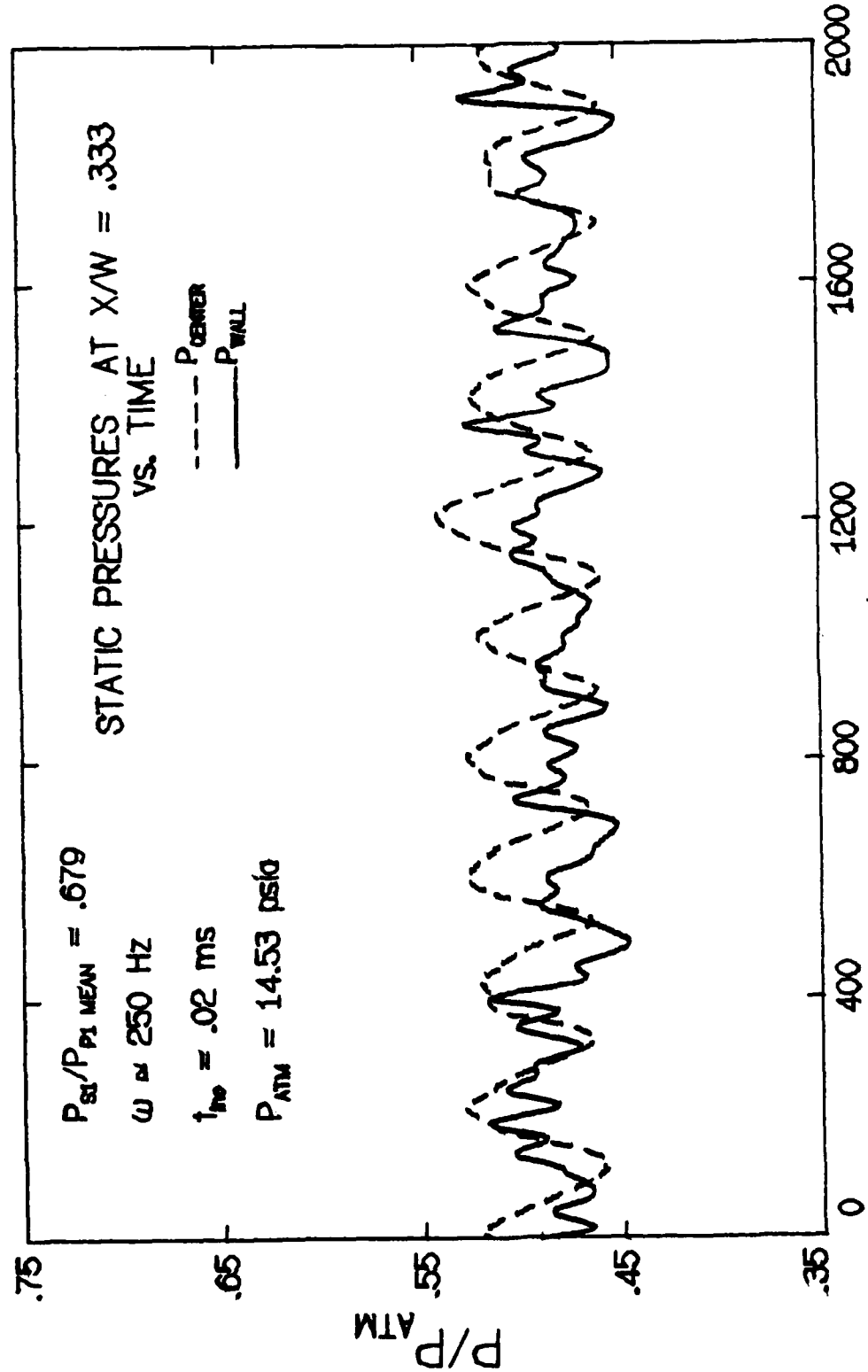

Figure 3.3.2-7 Static pressures versus time in the 250 Hz driver ejector flow at X/W = .333 (L/W = 9.0, $P_{s0}/P_{p0} \simeq .100$)

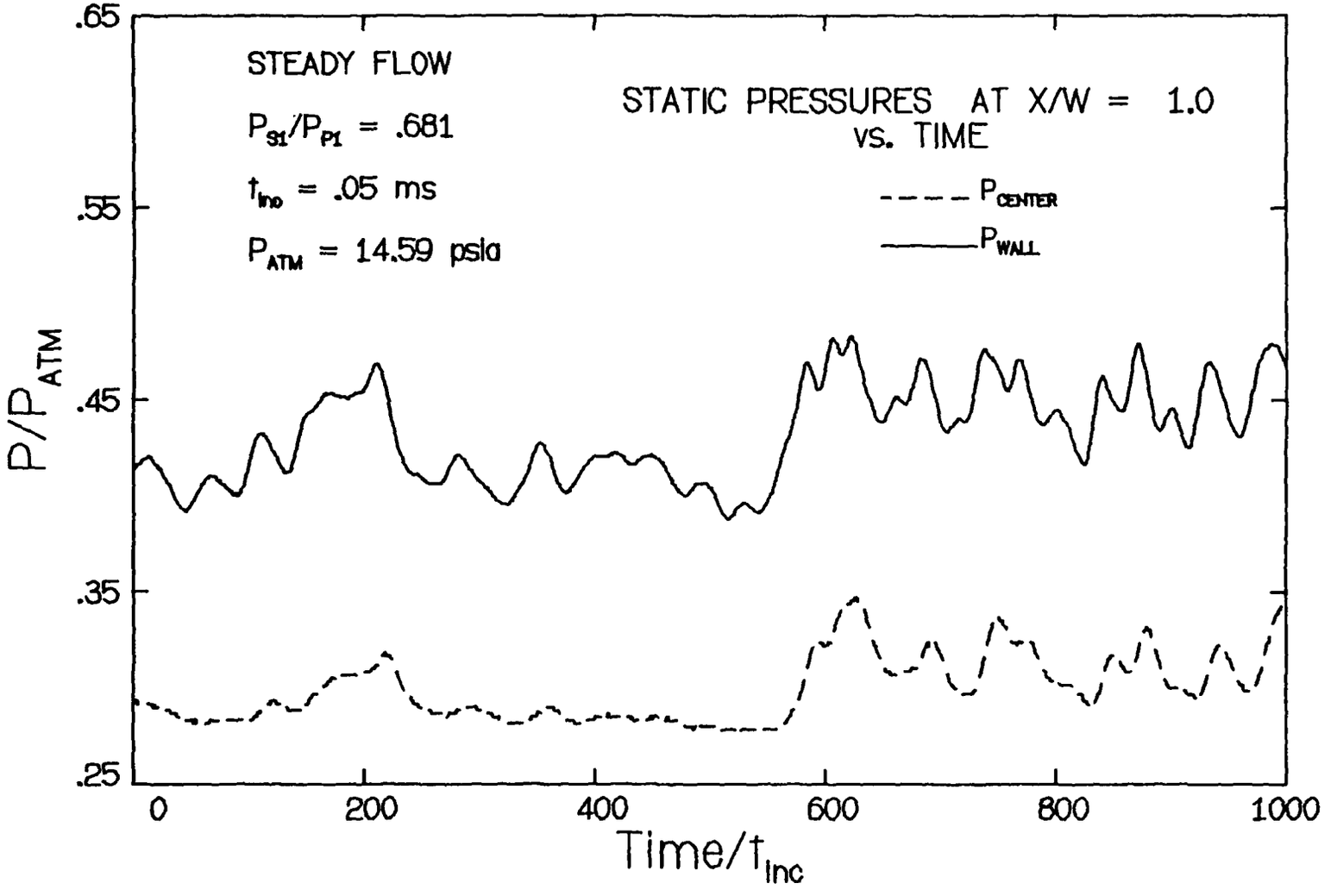

Figure 3.3.2-8 Static pressures versus time in the steady driver ejector flow at X/W = 1.00 (L/W = 9.0, $P_{s0}/P_{p0} \simeq .100$)

AD-A084 786 ILLINOIS UNIV AT URBANA-CHAMPAIGN DEPT OF MECHANICAL --ETC F/G 20/4
AN EXPERIMENTAL AND THEORETICAL INVESTIGATION OF MULTIPLE DUCTE--ETC(U)
JAN 80 H L PETRIE, A L ADDY DAAG29-76-G-0200
UNCLASSIFIED UILU-ENG-80-4002 ARO-13737.2-EX ML

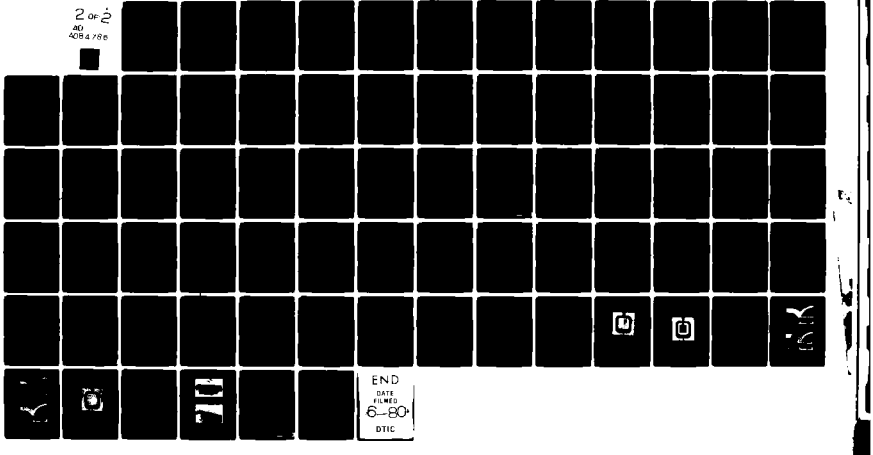

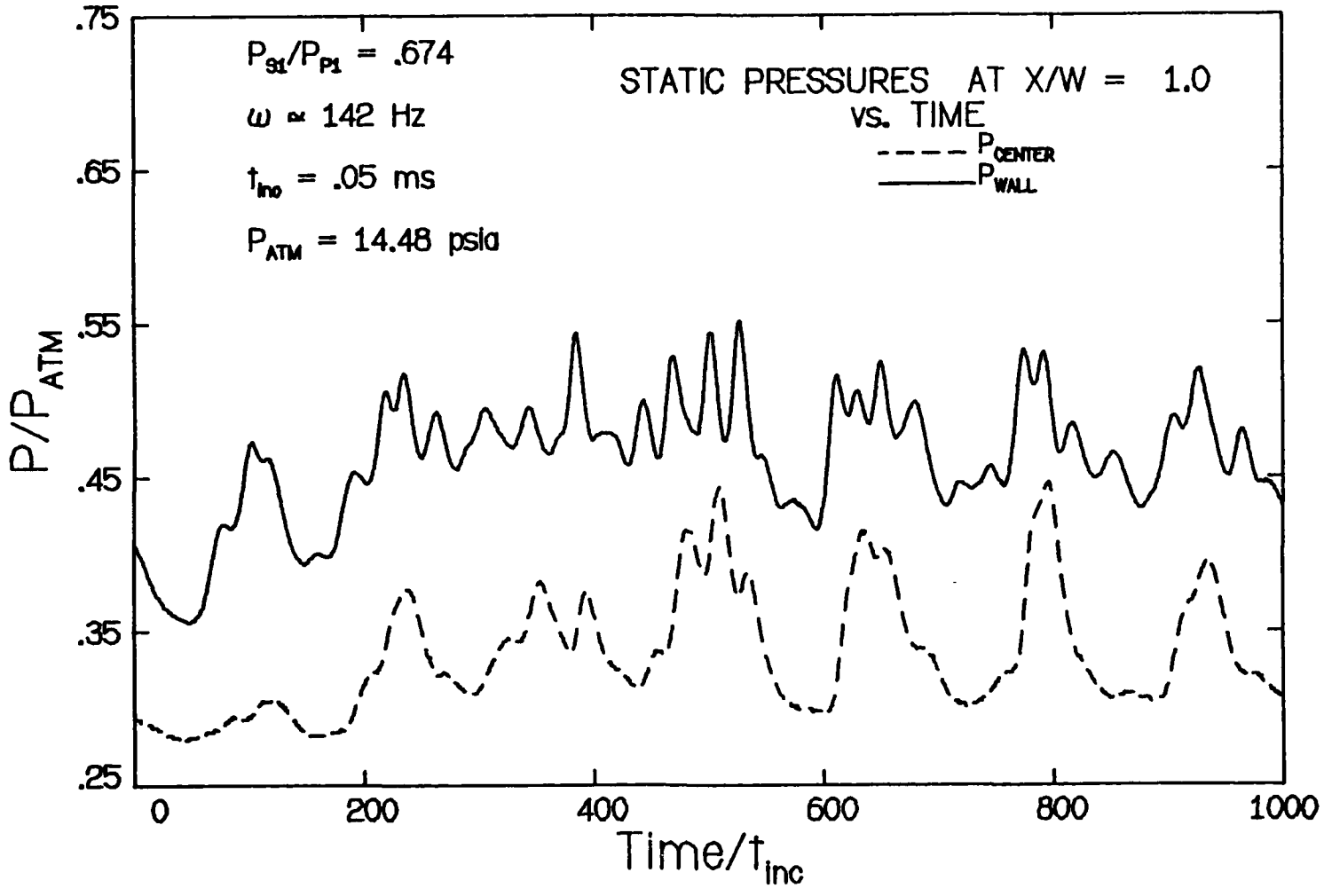

Figure 3.3.2-9 Static pressures versus time in the 142 Hz driver ejector flow at X/W = 1.00 (L/W = 9.0, $P_{s0}/P_{p0} \simeq .100$)

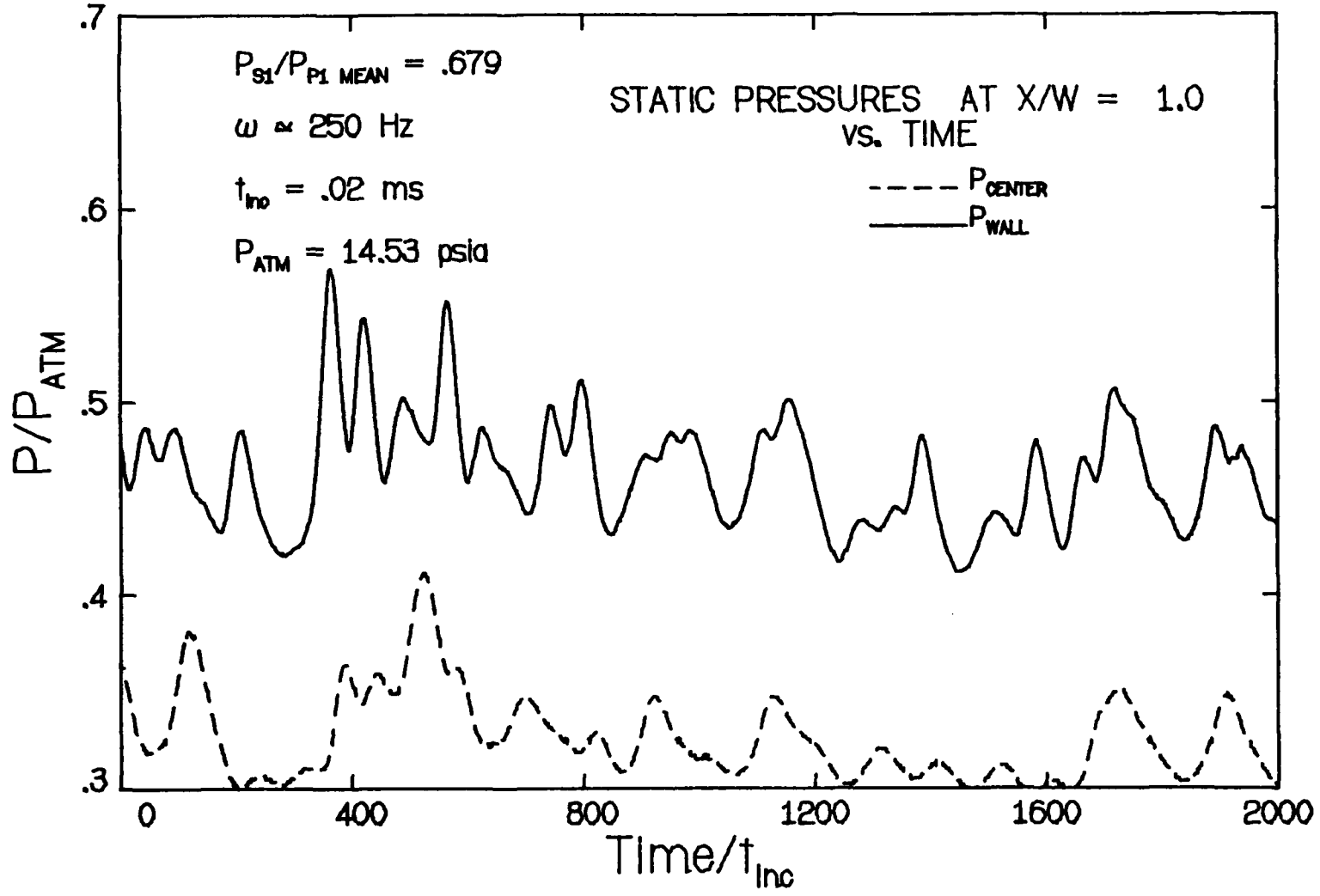

Figure 3.3.2-10 Static pressures versus time in the 250 Hz driver ejector flow at X/W = 1.00 (L/W = 9.0, $P_{s0}/P_{p0} \simeq .100$)

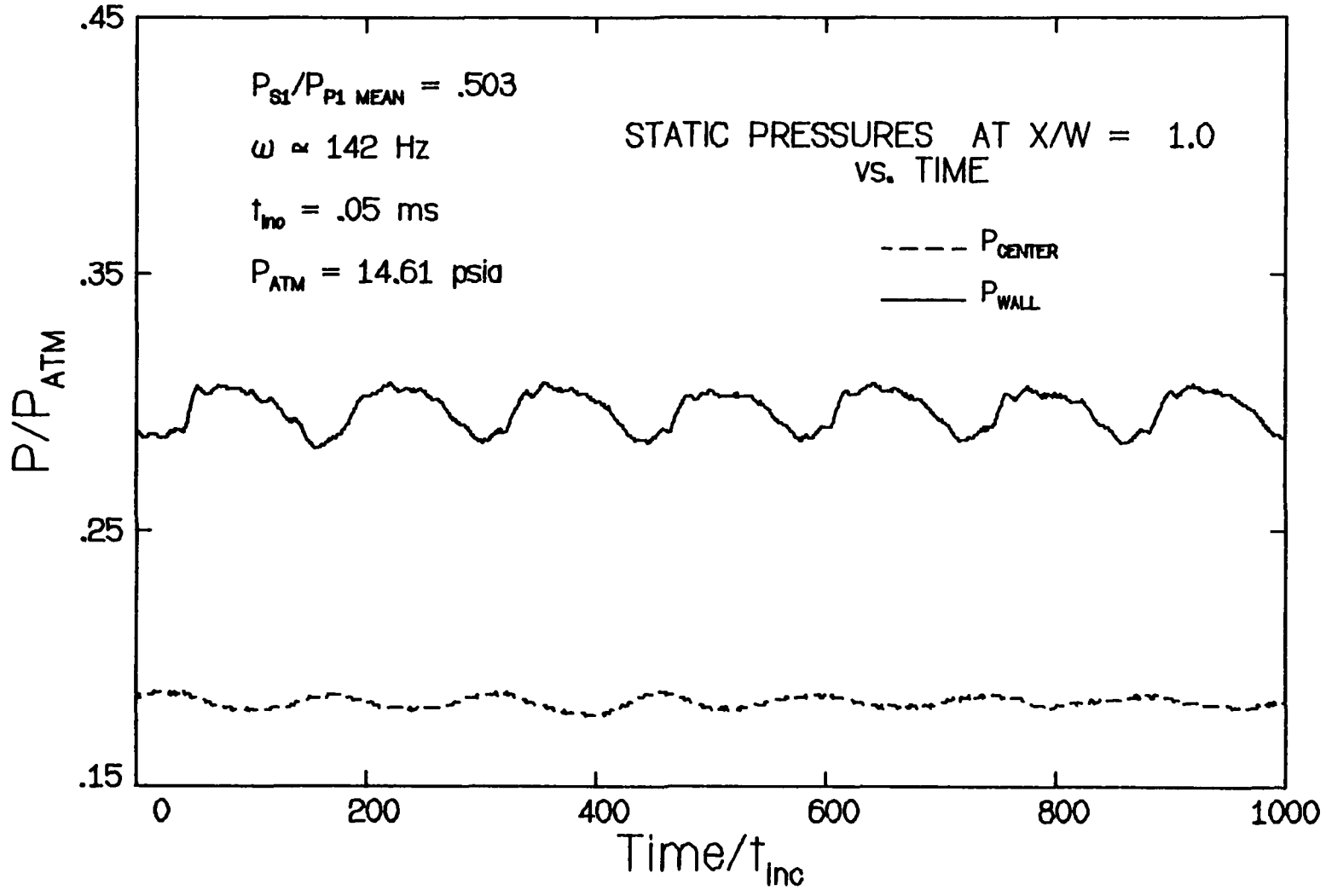

Figure 3.3.2-11 Static pressure pulses in a highly expanded shock free flow. P_{mS}/P_{s0} is relatively low (L/W = 13.0, $P_{s0}/P_{p0} \simeq .070$)

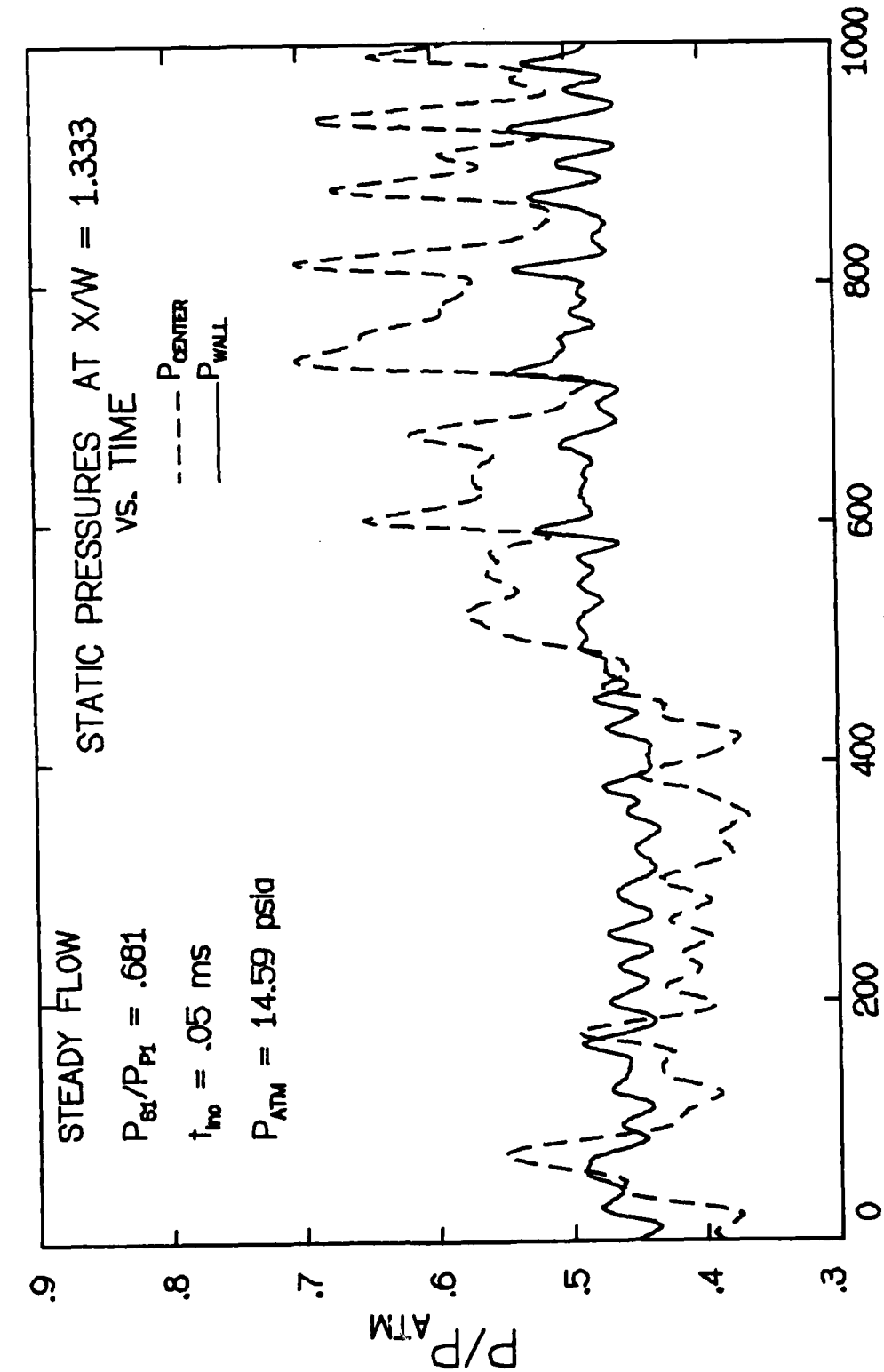

Figure 3.3.2-12 Static pressures versus time in the steady driver ejector flow at X/W = 1.333 (L/W = 9.0, $P_{s0}/P_{p0} \simeq .100$)

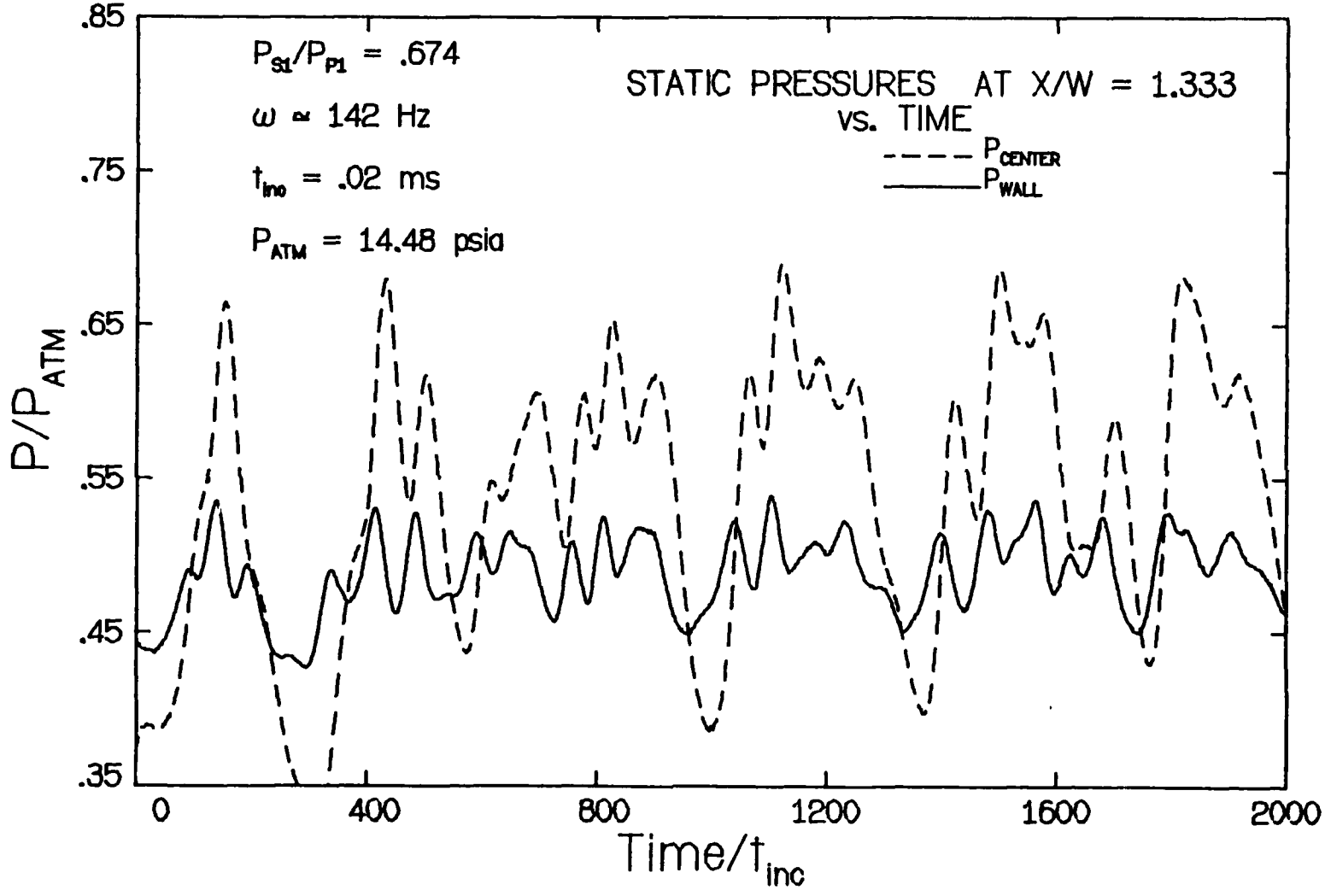

Figure 3.3.2-13 Static pressures versus time in the 142 Hz driver ejector flow at X/W = 1.333 (L/W = 9.0, $P_{s0}/P_{p0} \simeq .100$)

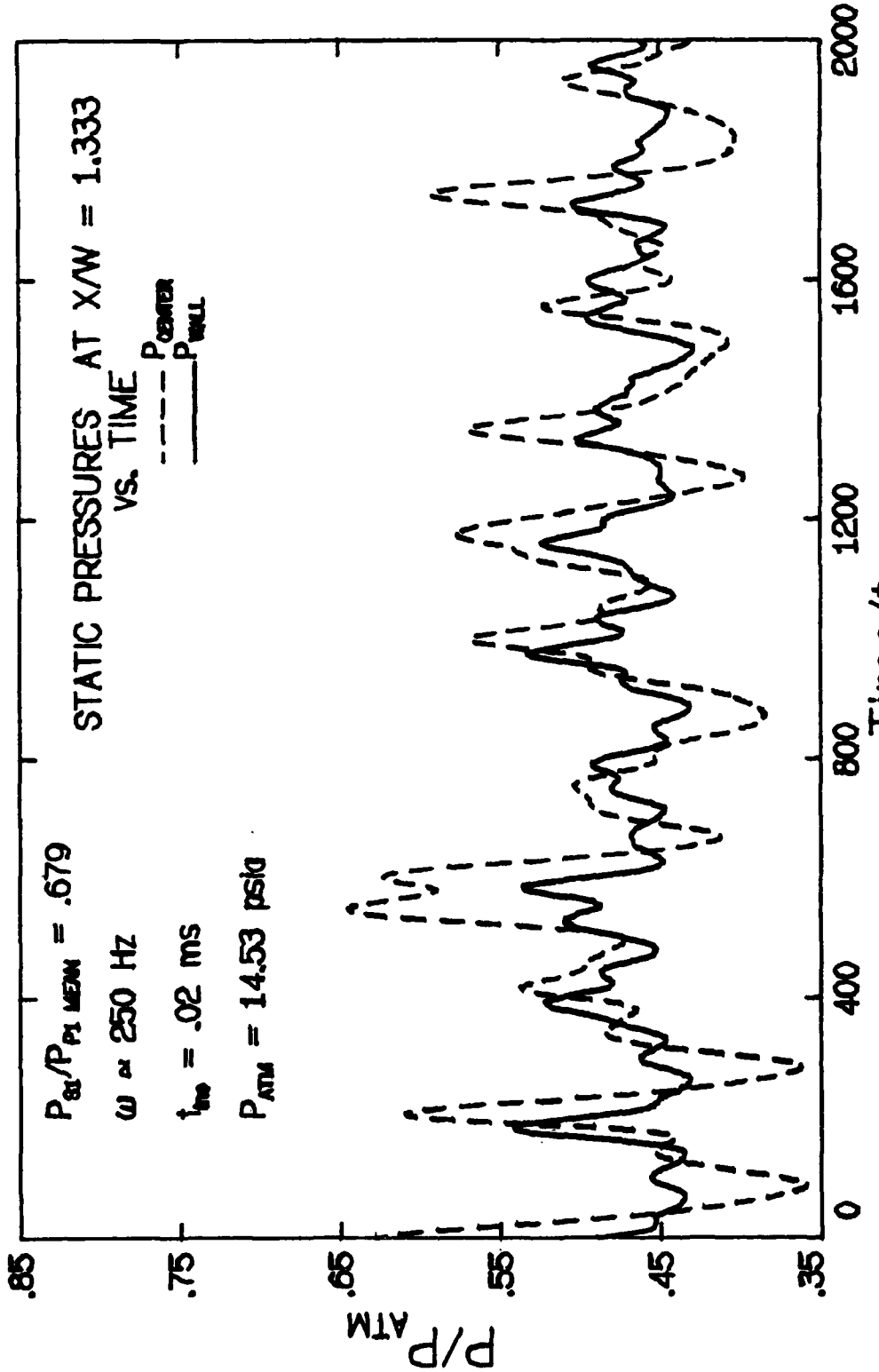

Figure 3.3.2-14 Static pressures versus time in the 250 Hz driver ejector flow at X/W = 1.333 (L/W = 9.0, $P_{s,o}/P_{po} \simeq .100$)

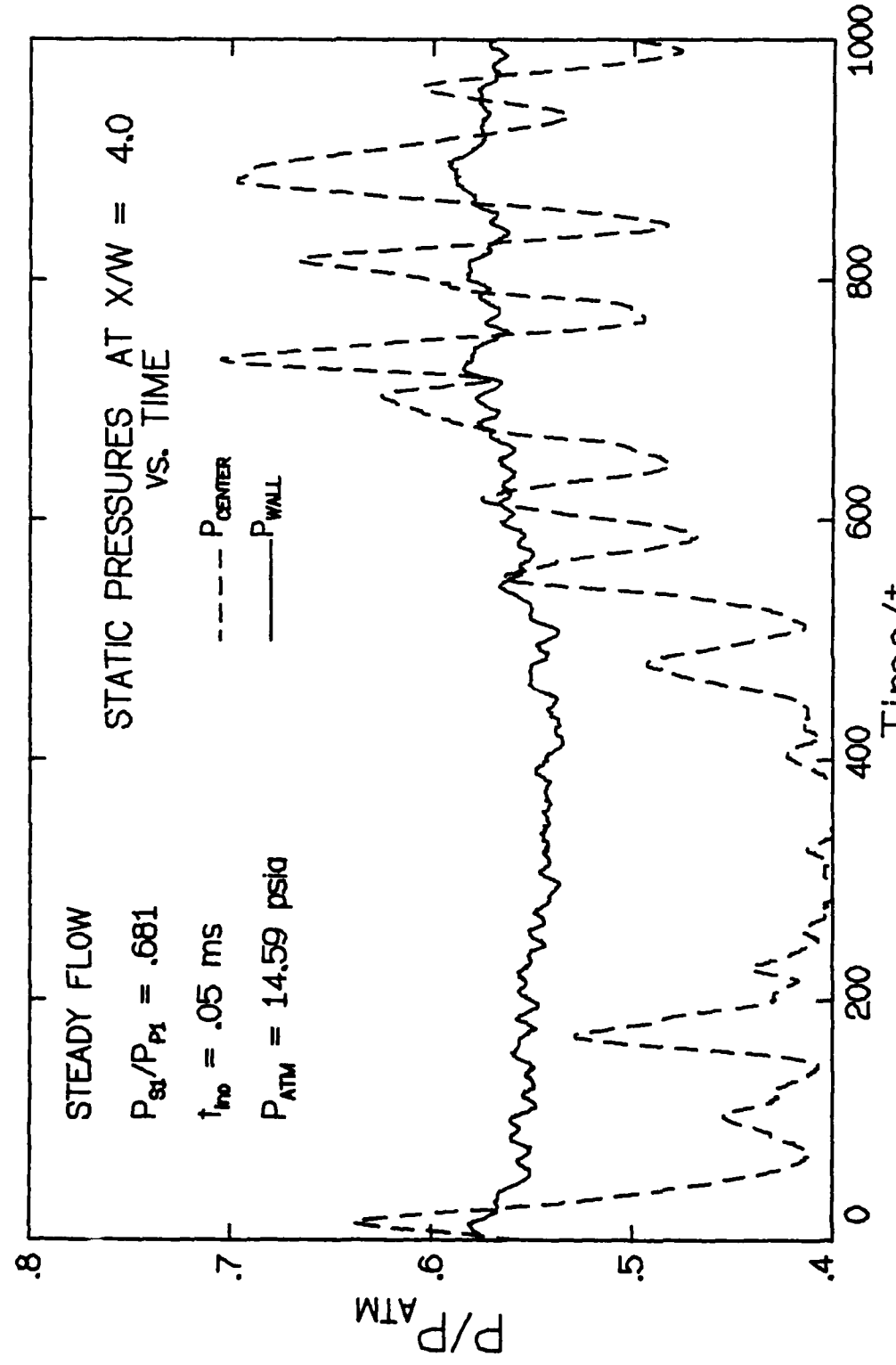

Figure 3.3.2-15 Static pressures versus time in the steady driver ejector flow at X/W = 4.0 (L/W = 9.0, $P_{s0}/P_{p0} \simeq .100$)

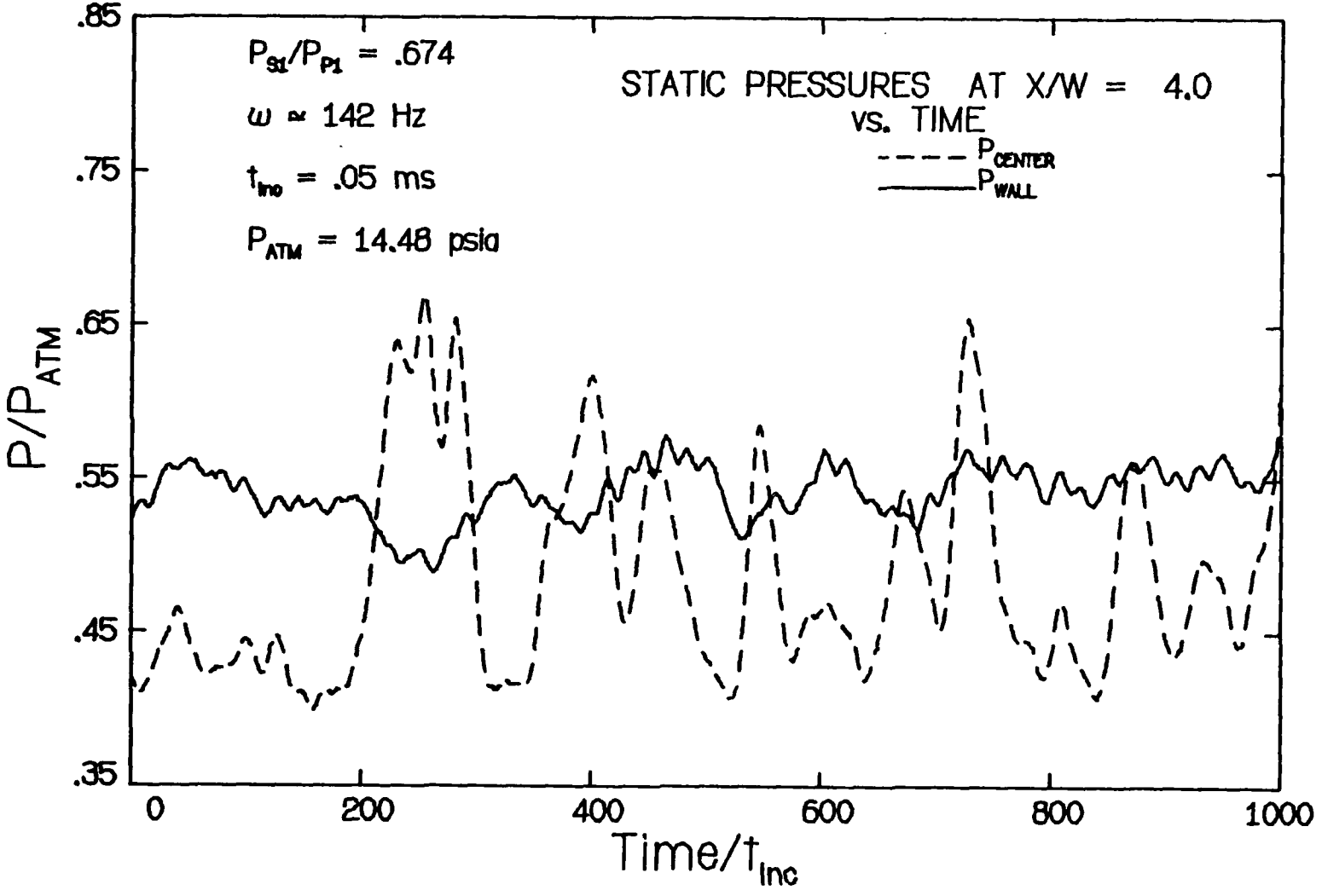

Figure 3.3.2-16 Static pressures versus time in the 142 Hz driver ejector flow at X/W = 4.0 (L/W = 9.0, $P_{s0}/P_{p0} \simeq .100$)

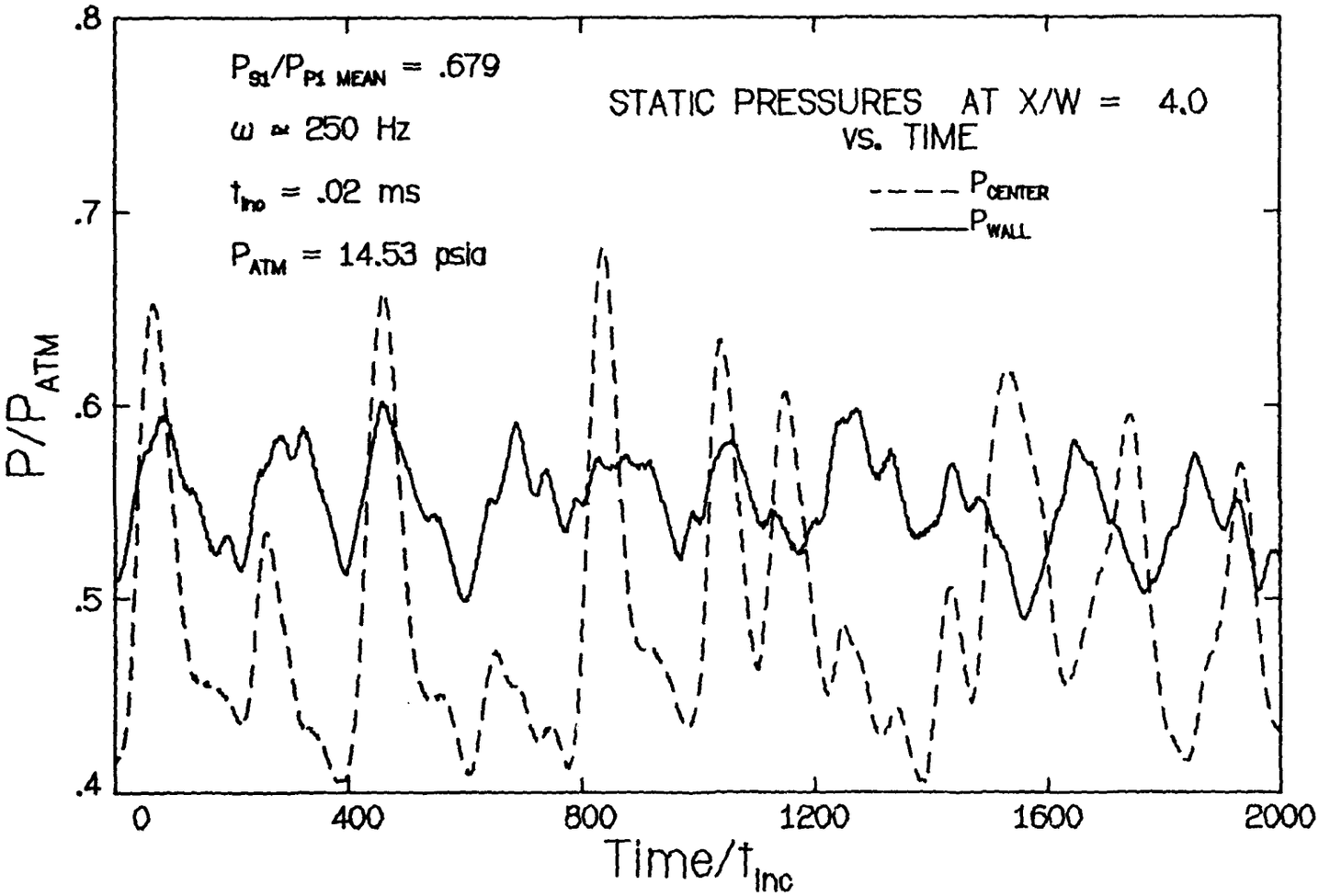

Figure 3.3.2-17 Static pressures versus time in the 250 Hz driver ejector flow at X/W = 4.0 (L/W = 9.0, P_{s0}/P_{p0} ≈ .100)

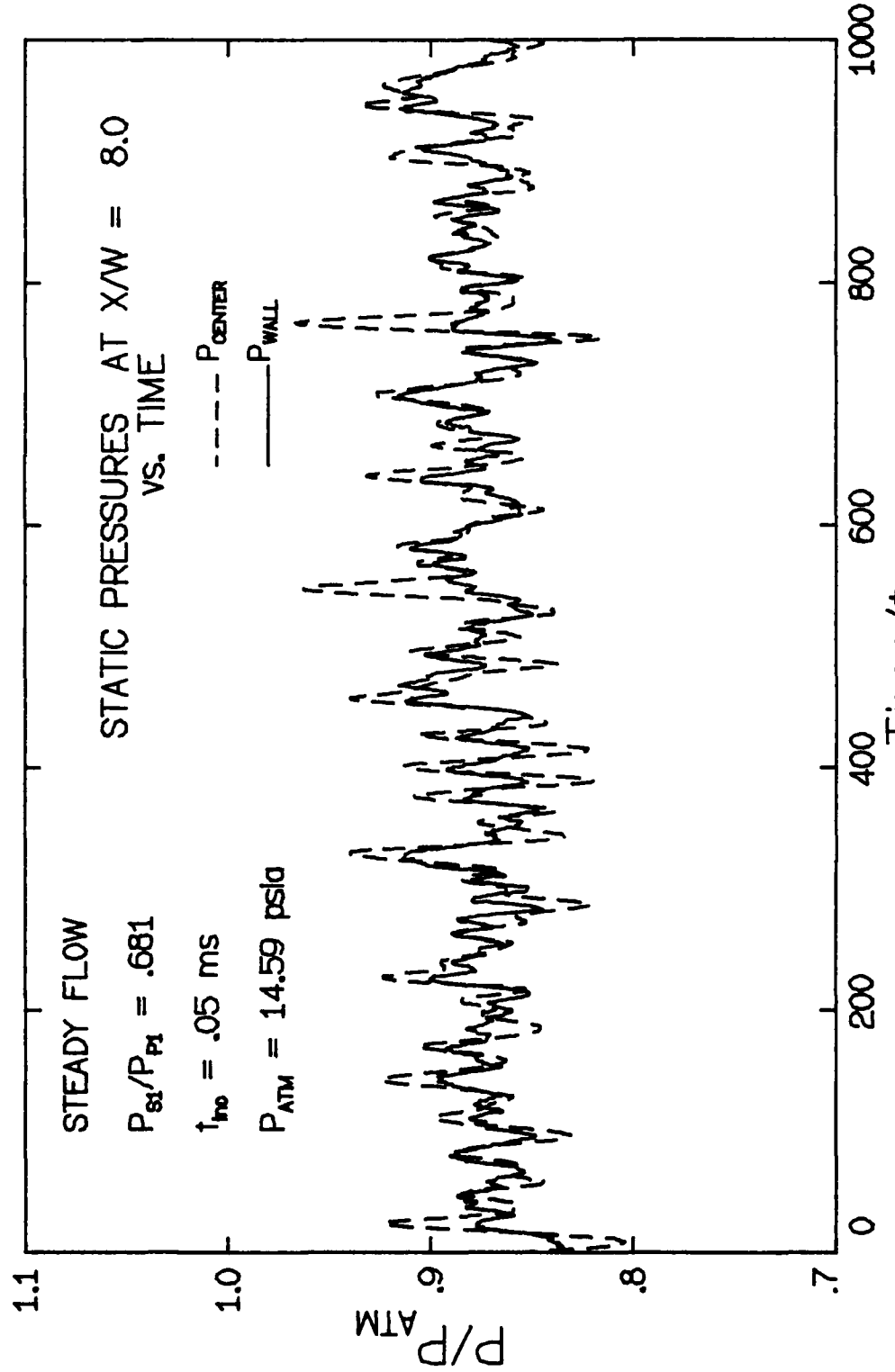

Figure 3.3.2-18 Static pressures versus time in the steady driver ejector flow at X/W = 8.0 (L/W = 9.0, $P_{s0}/P_{p0} \simeq .100$)

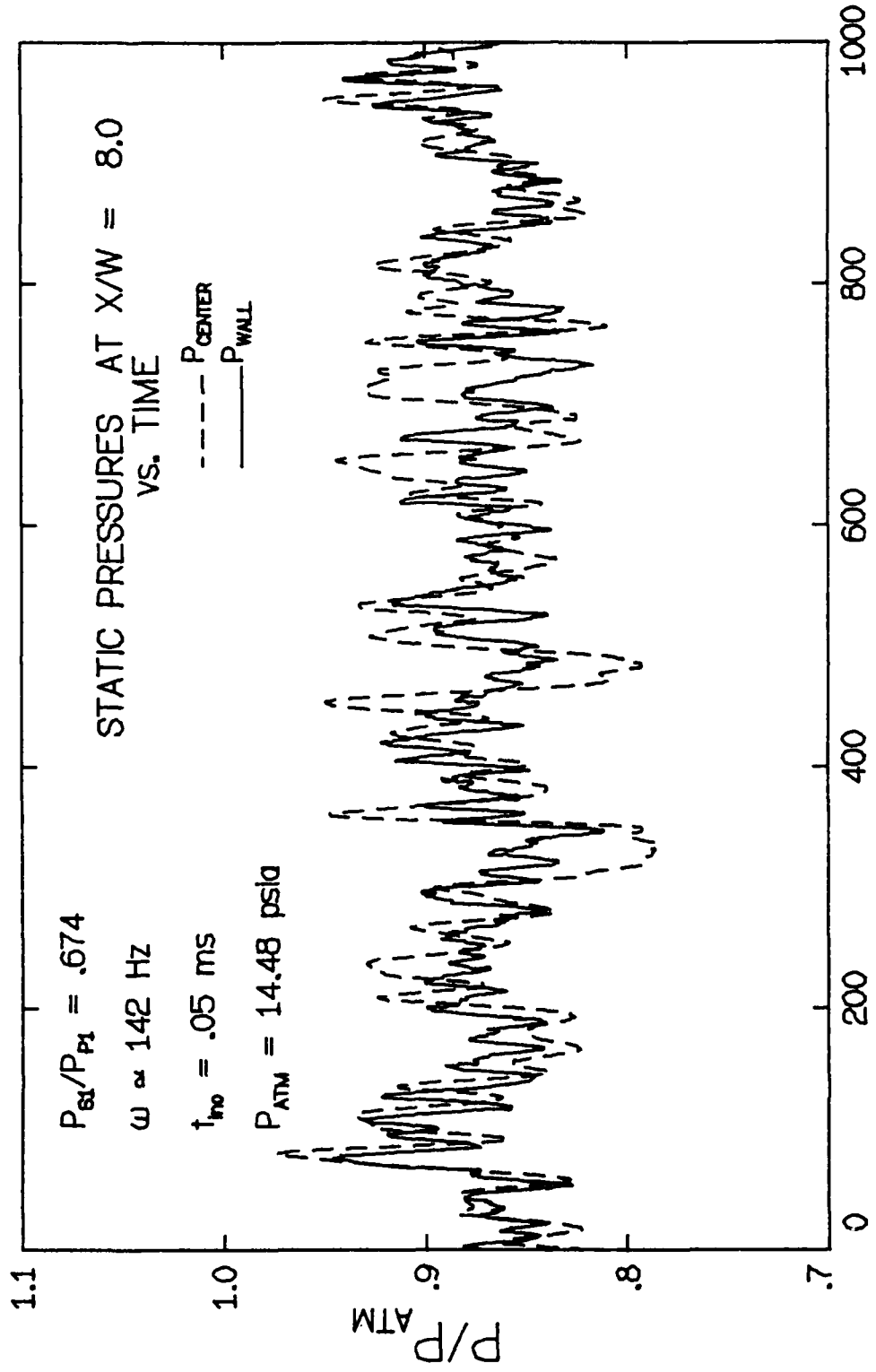

Figure 3.3.2-19 Static pressures versus time in the 142 Hz driver ejector flow at X/W = 8.0 (L/W = 9.0, $P_{s0}/P_{p0} \simeq .100$)

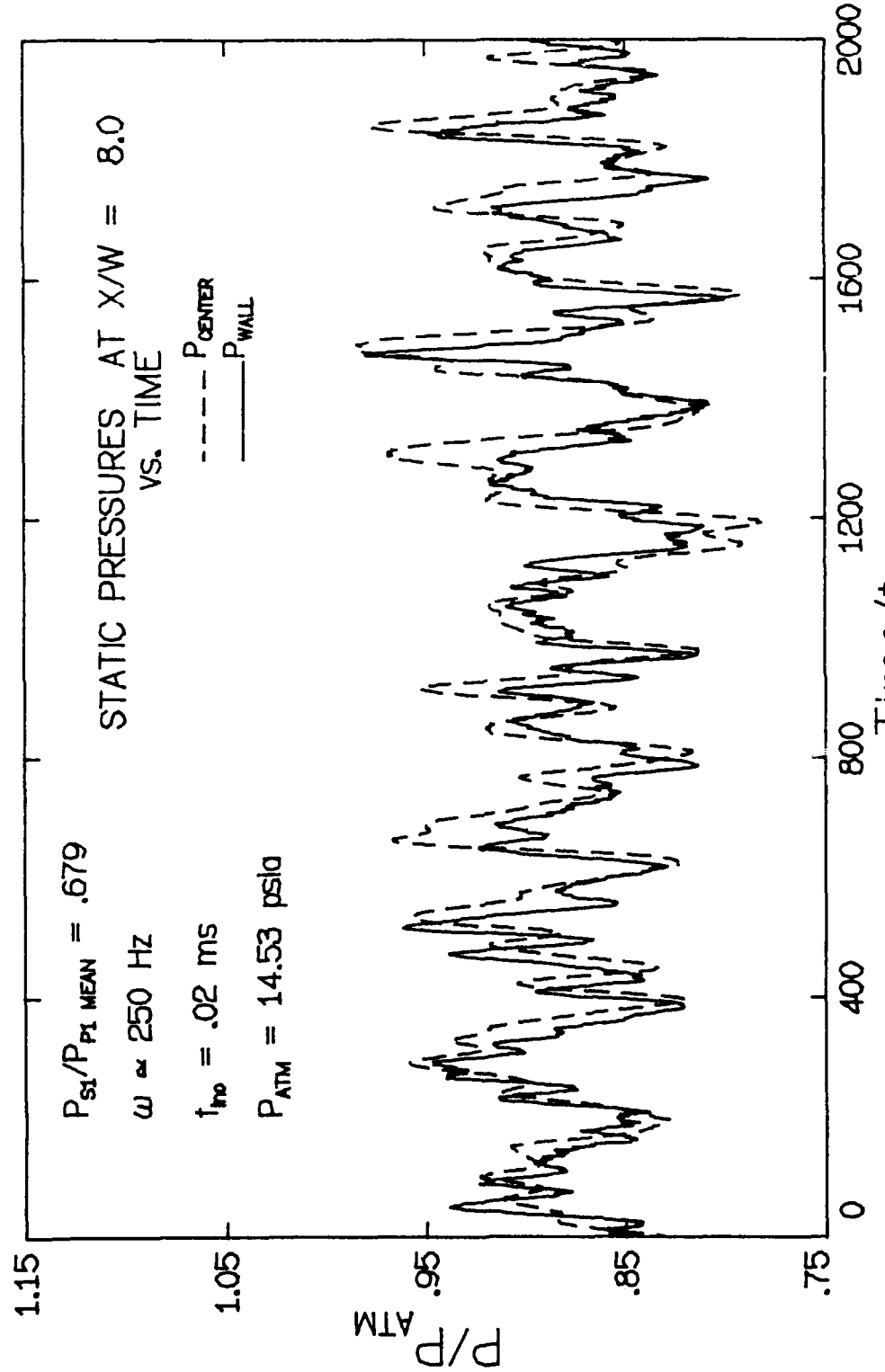

Figure 3.3.2-20 Static pressures versus time in the 250 Hz driver ejector flow at X/W = 8.0 (L/W = 9.0, $P_{s0}/P_{p0} \simeq .100$)

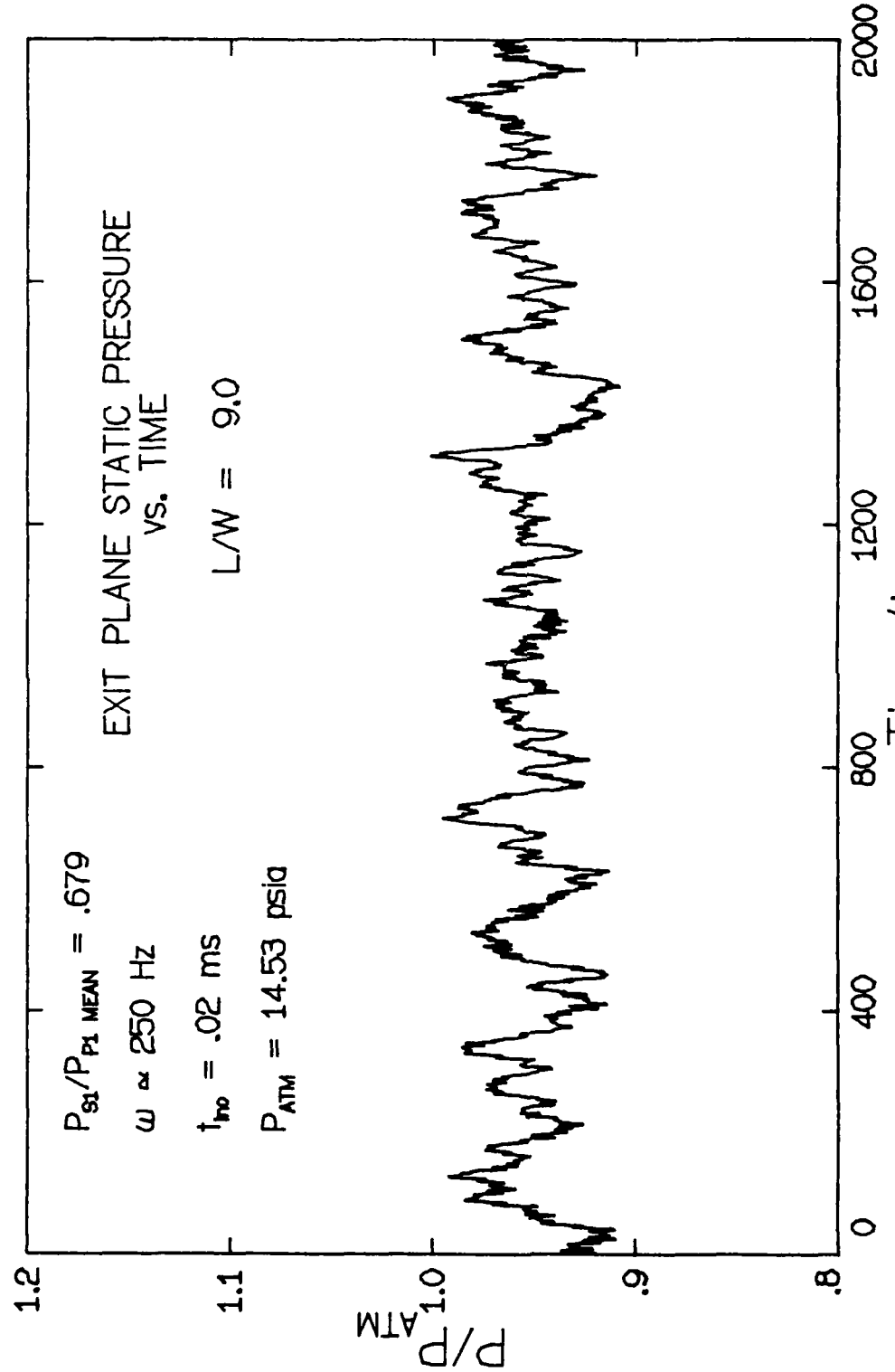

Figure 3.3.2-21 The exit plane static pressure versus time on the primary flow centerline (L/W = 9.0, $P_{s0}/P_{p0} \simeq .100$)

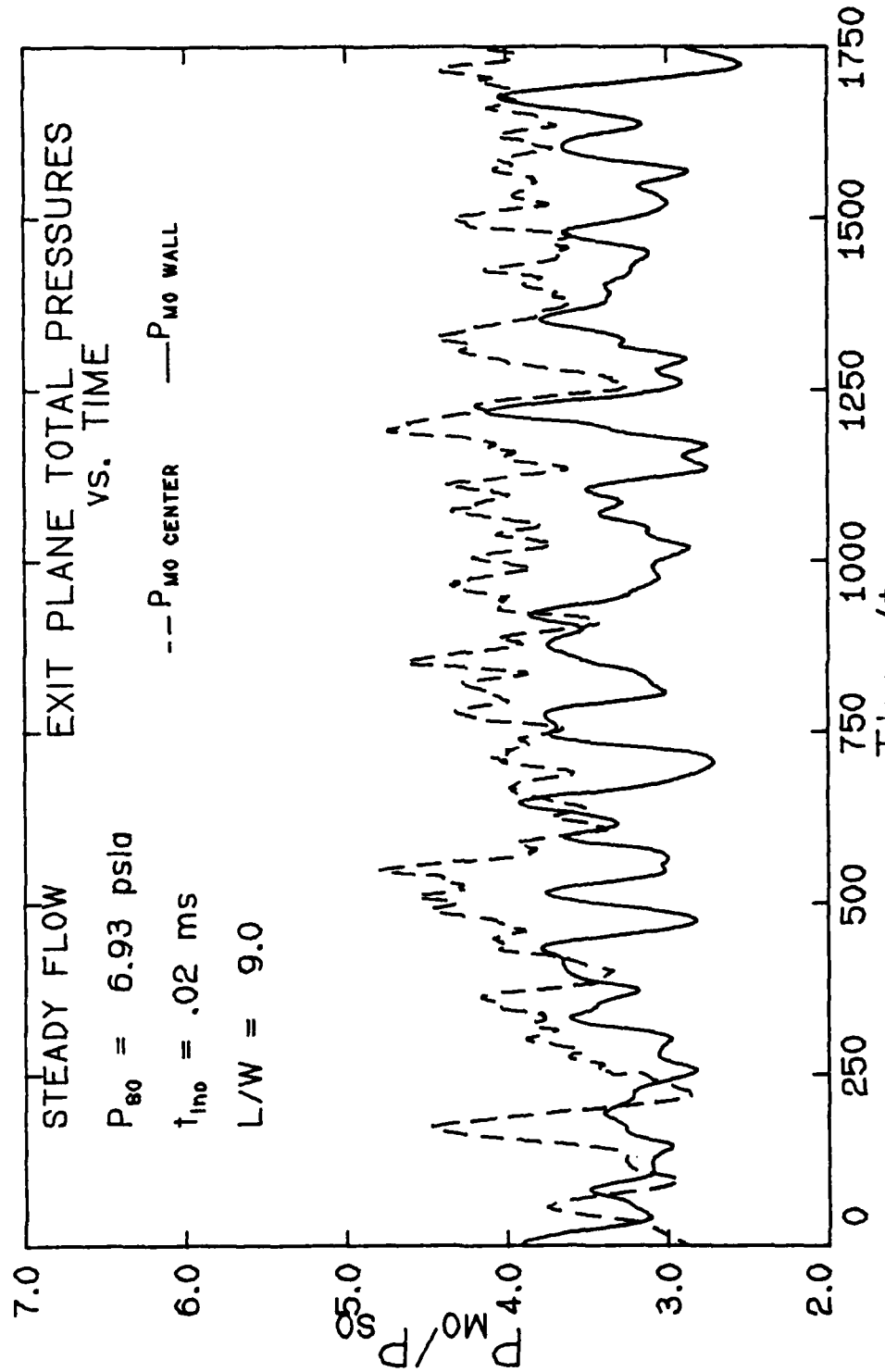

Figure 3.3.2-22 Exit plane stagnation pressures versus time in the steady driver ejector flow (L/W = 9.0, $P_{s0}/P_{p0} \simeq .100$)

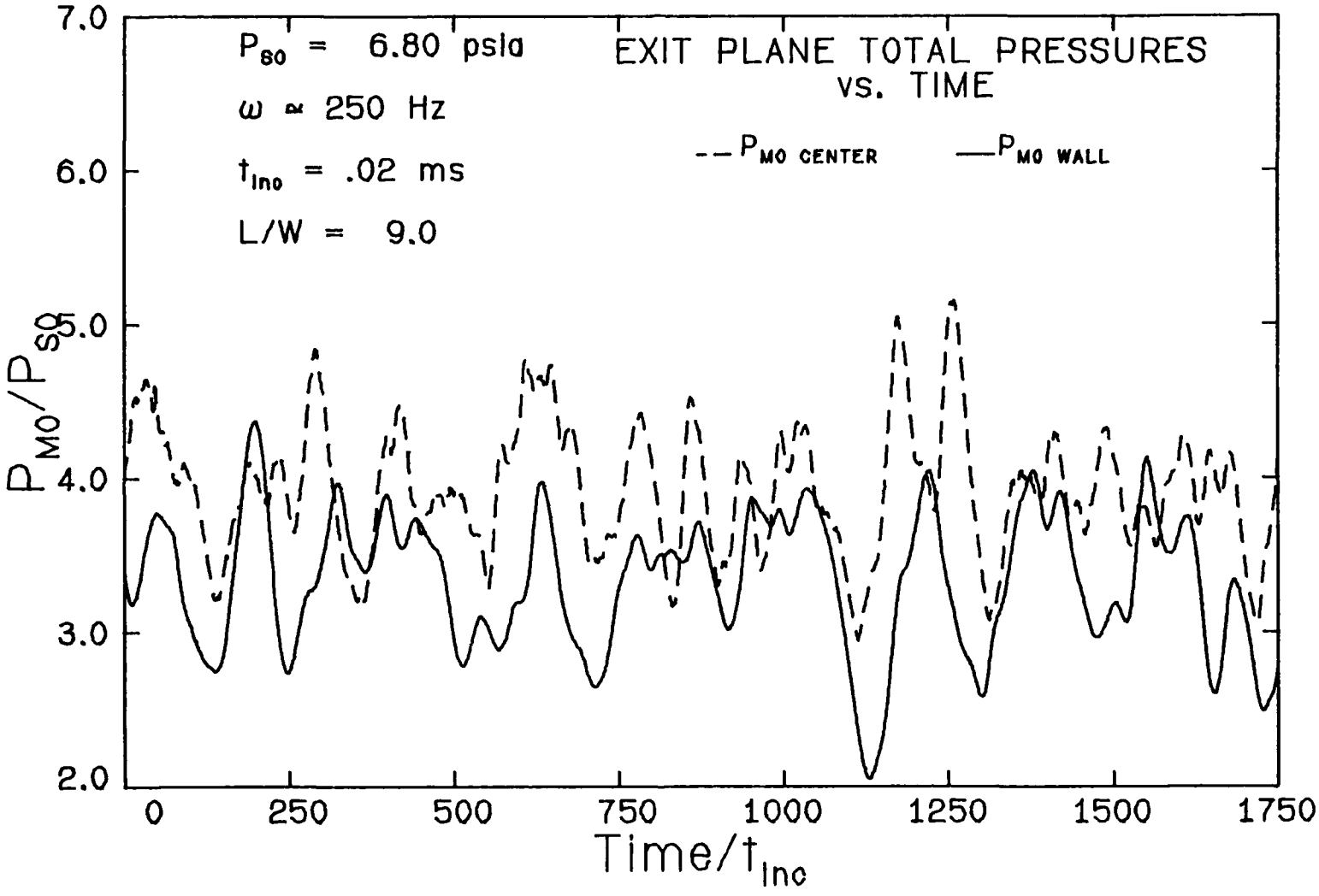

Figure 3.3.2-23 Exit plane stagnation pressures versus time in the 250 Hz driver ejector flow (L/W = 9.0, $P_{s0}/P_{p0} \simeq .100$)

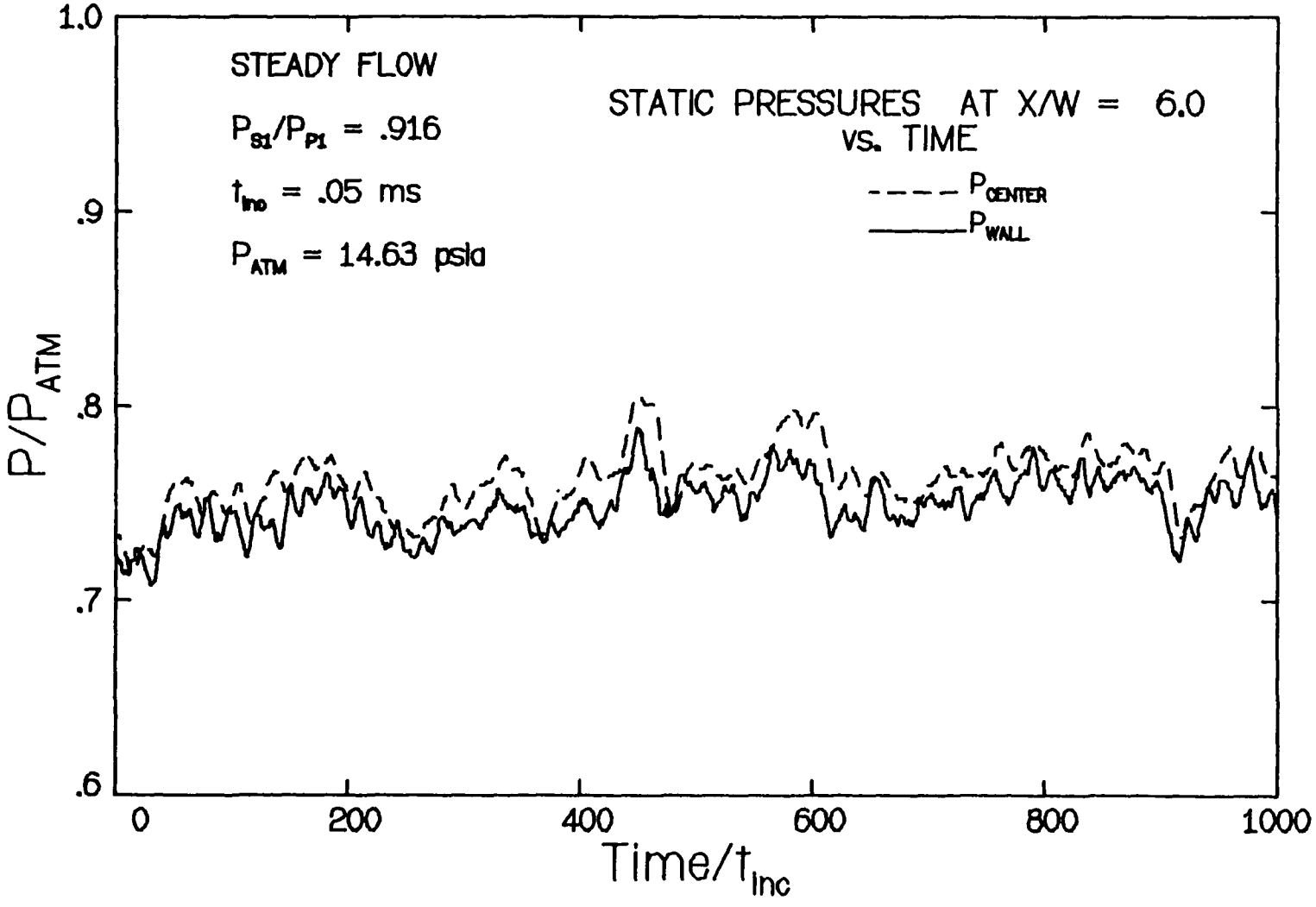

Figure 3.3.2-24 Static pressures versus time in the steady driver ejector flow at X/W = 6.0 (L/W = 9.0, $P_{s0}/P_{p0} \simeq .160$)

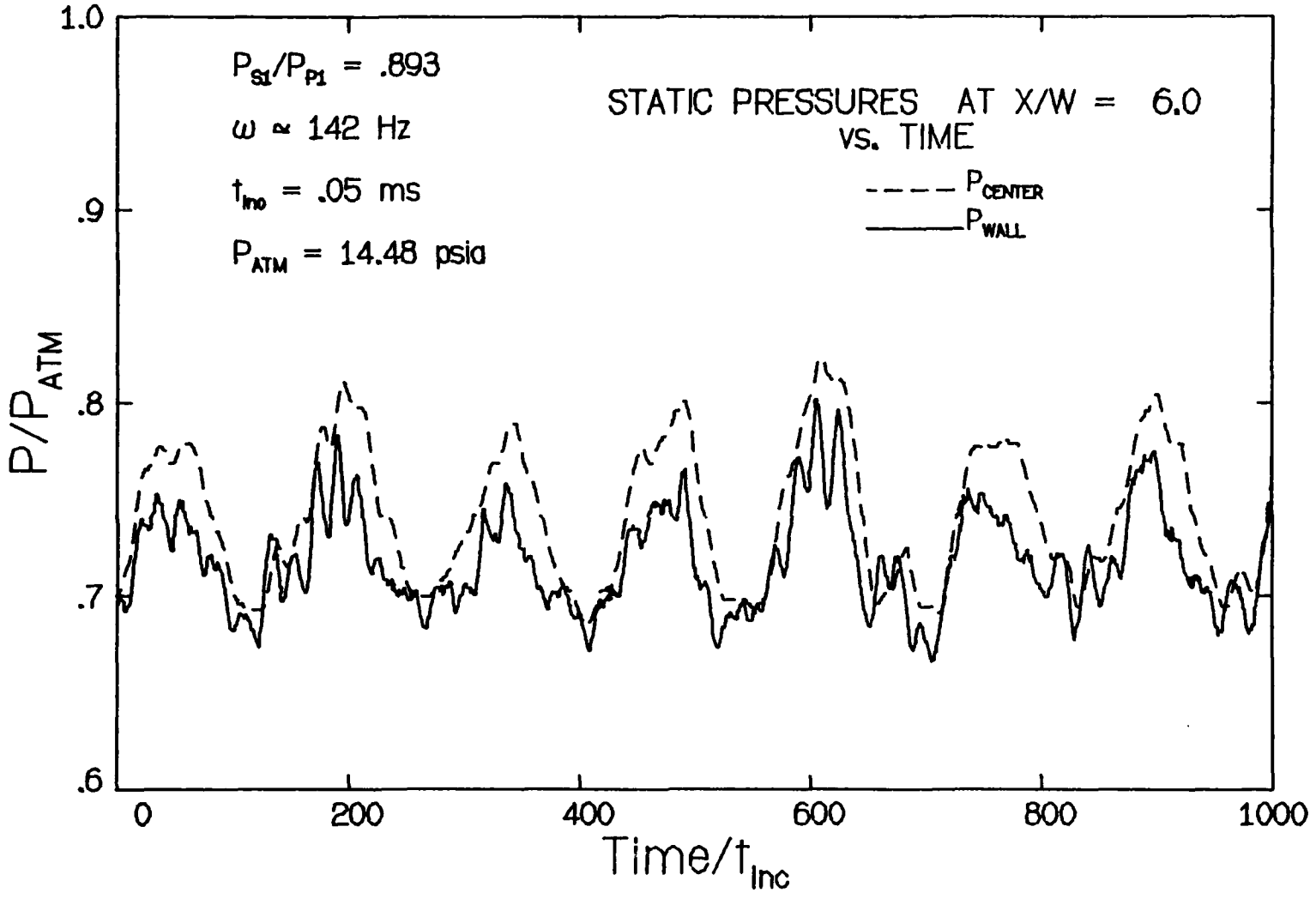

Figure 3.3.2-25 Static pressures versus time in the 142 Hz driver ejector flow at X/W = 6.0 (L/W = 9.0, $P_{s0}/P_{p0} \simeq .160$)

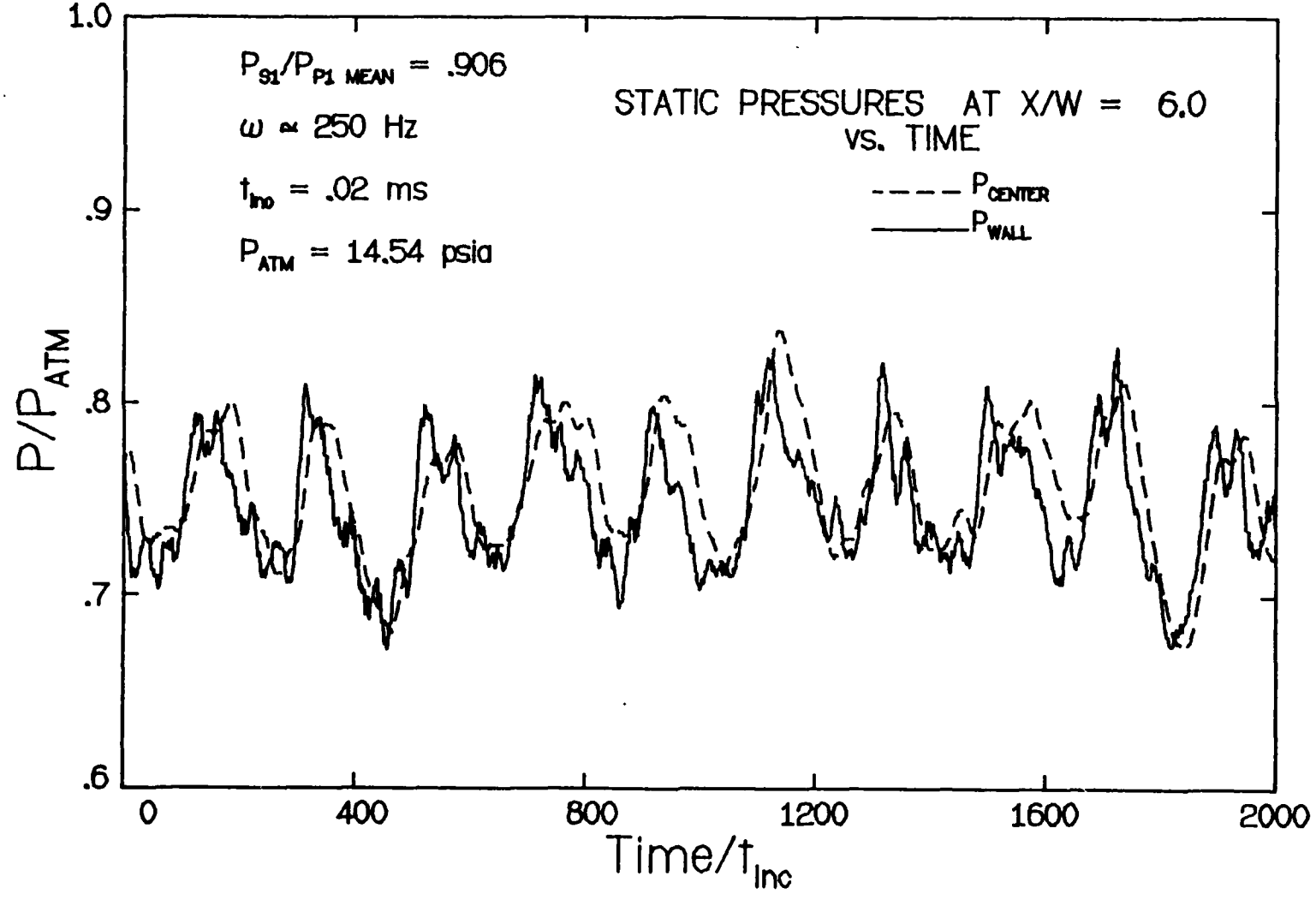

Figure 3.3.2-26 Static pressures versus time in the 250 Hz driver ejector flow at X/W = 6.0 (L/W = 9.0, $P_{s0}/P_{p0} \simeq .160$)

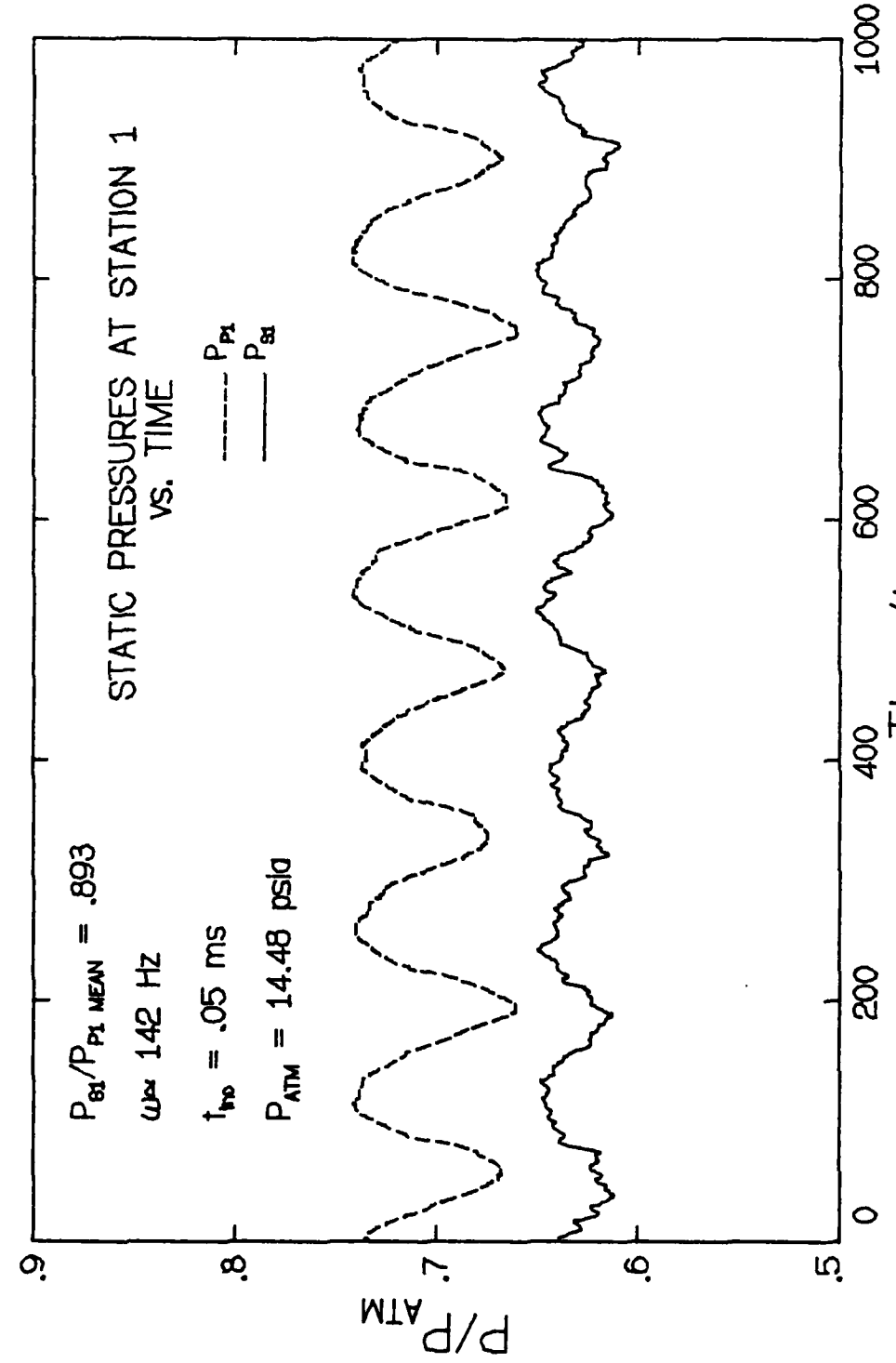

Figure 3.3.2-27 Static pressures at Station 1 versus time ($L/W = 9.0$, $P_{s0}/P_{p0} \simeq .160$)

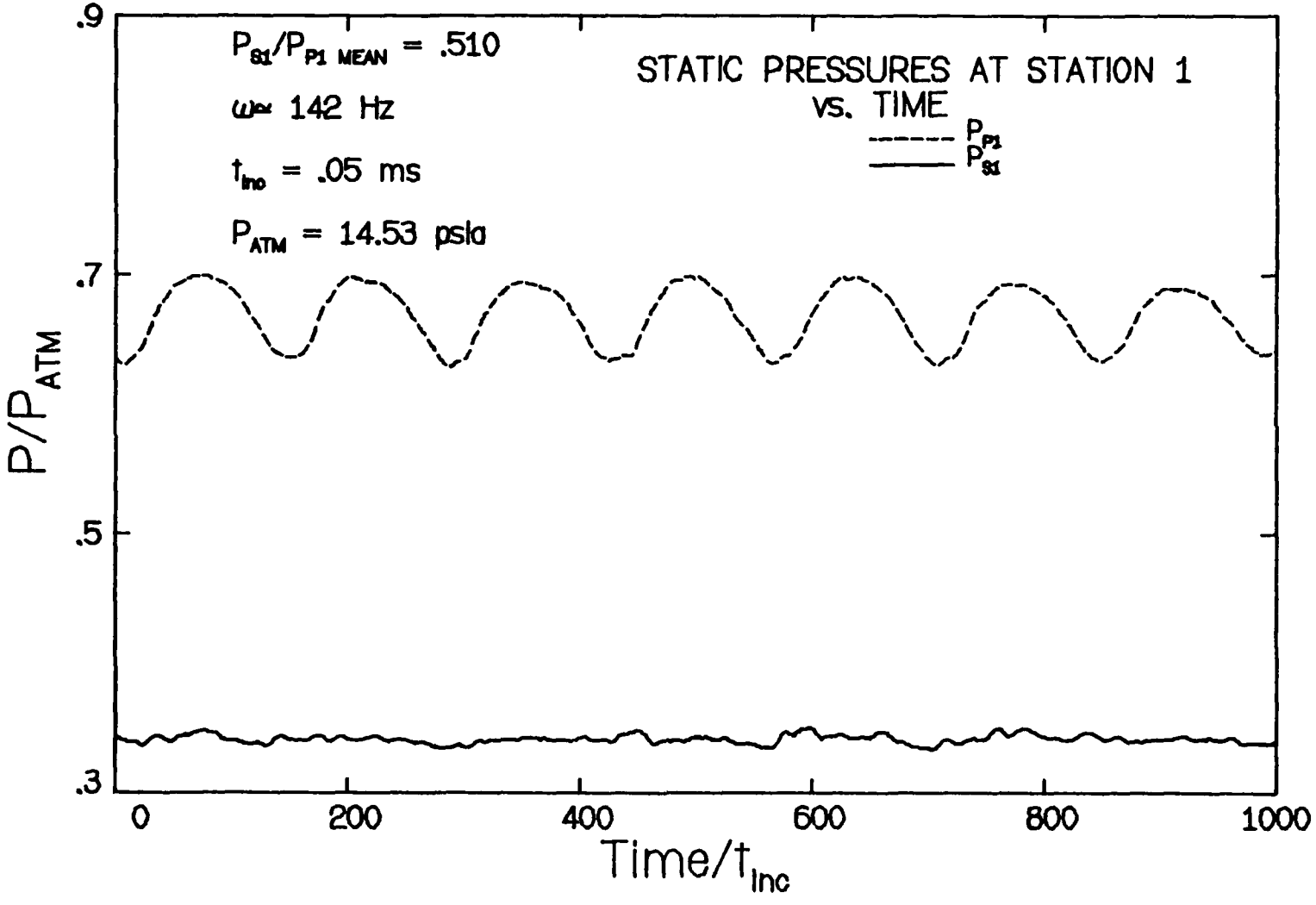

Figure 3.3.2-28 Static pressures at Station 1 versus time
(L/W = 13.0, $P_{s0}/P_{p0} \simeq .070$)

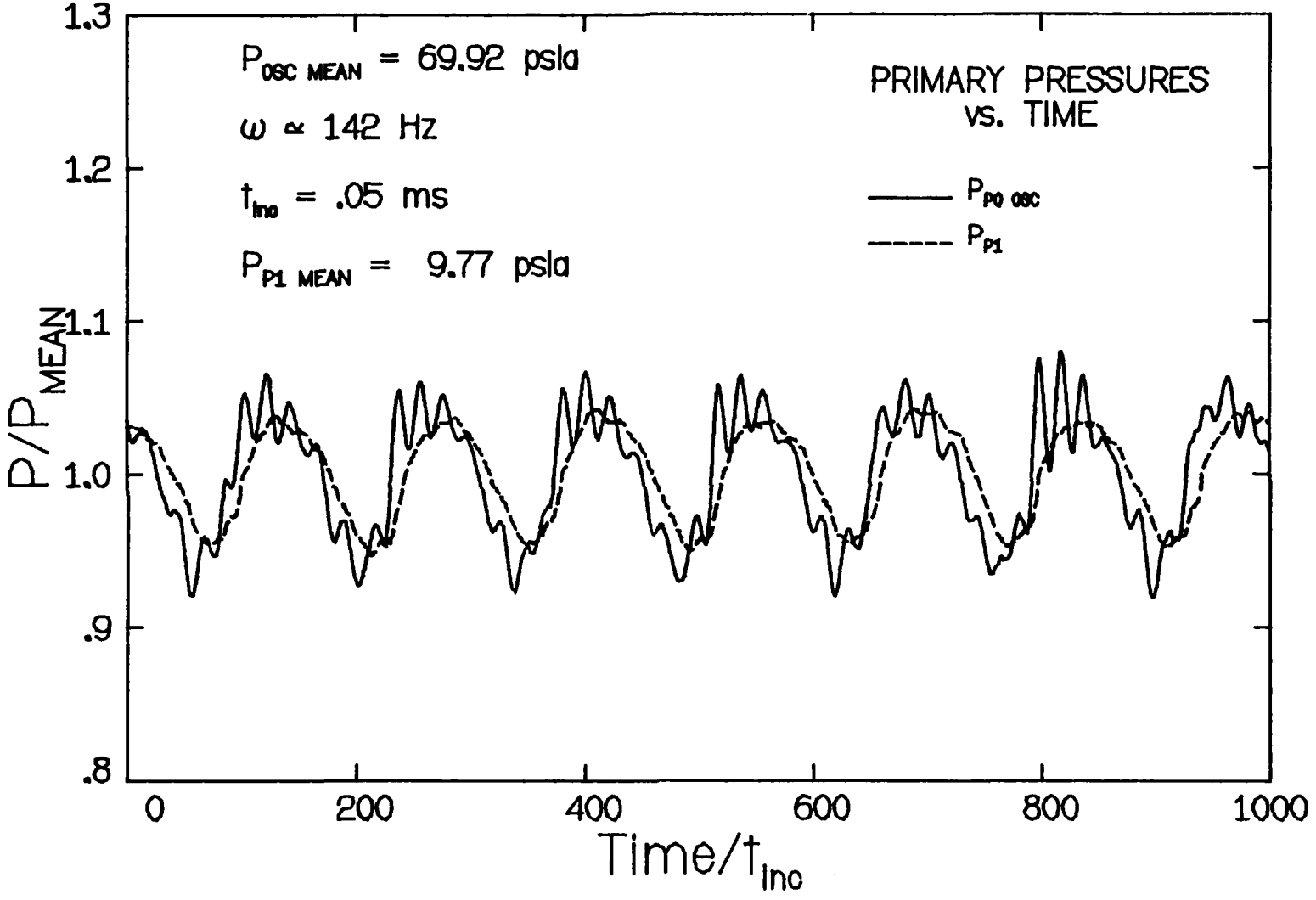

Figure 3.3.2-29 Simultaneously recorded values of P_{p1} and P_{p0} versus time at the 142 Hz driver frequency

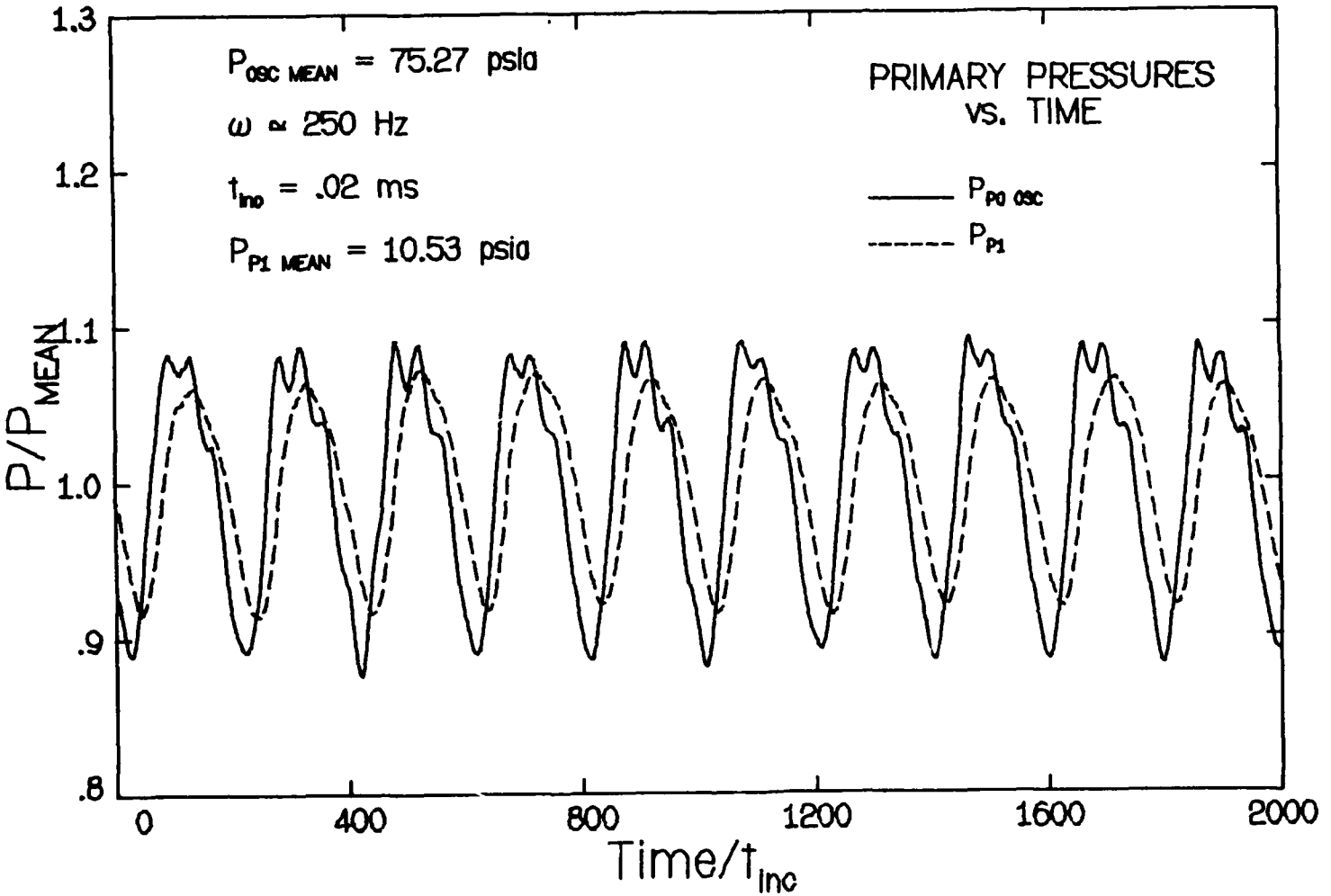

Figure 3.3.2-30 Simultaneously recorded values of P_{p1} and P_{p0} versus time at the 250 Hz driver frequency

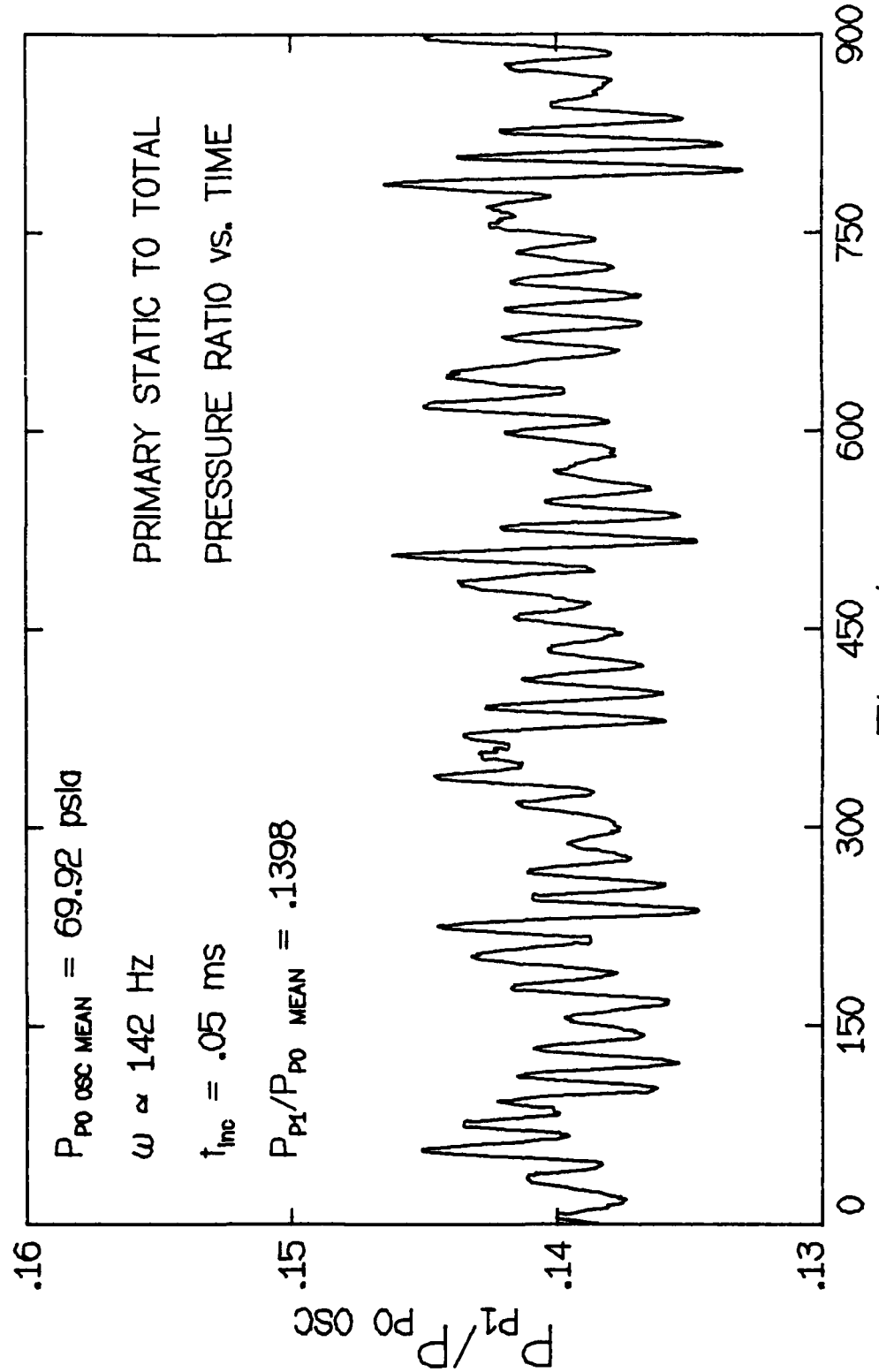

Figure 3.3.2-31 P_{p1}/P_{p0} versus time at the 142 Hz driver frequency

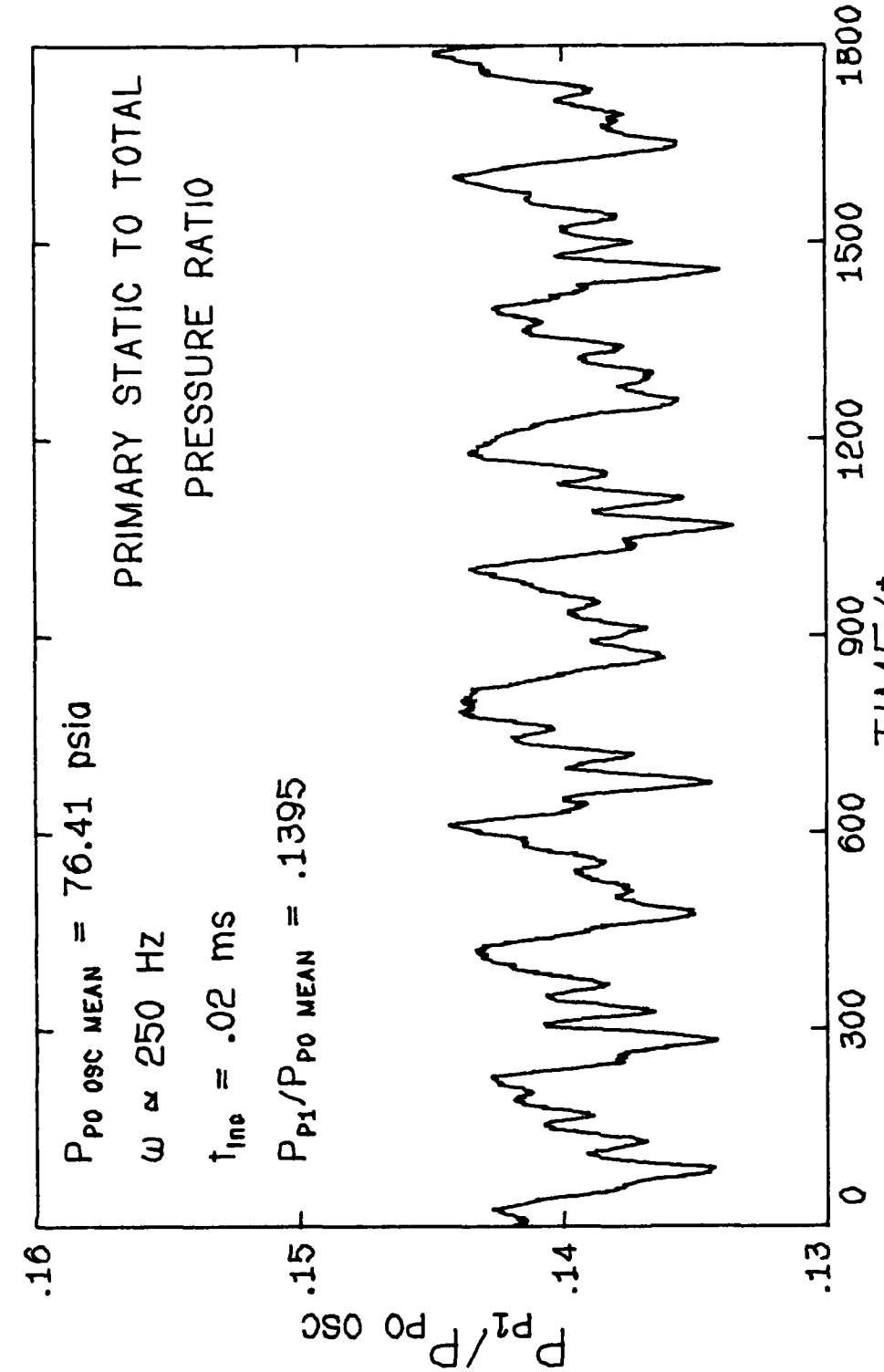

Figure 3.3.2-32 P_{p1}/P_{po} versus time at the 250 Hz driver frequency

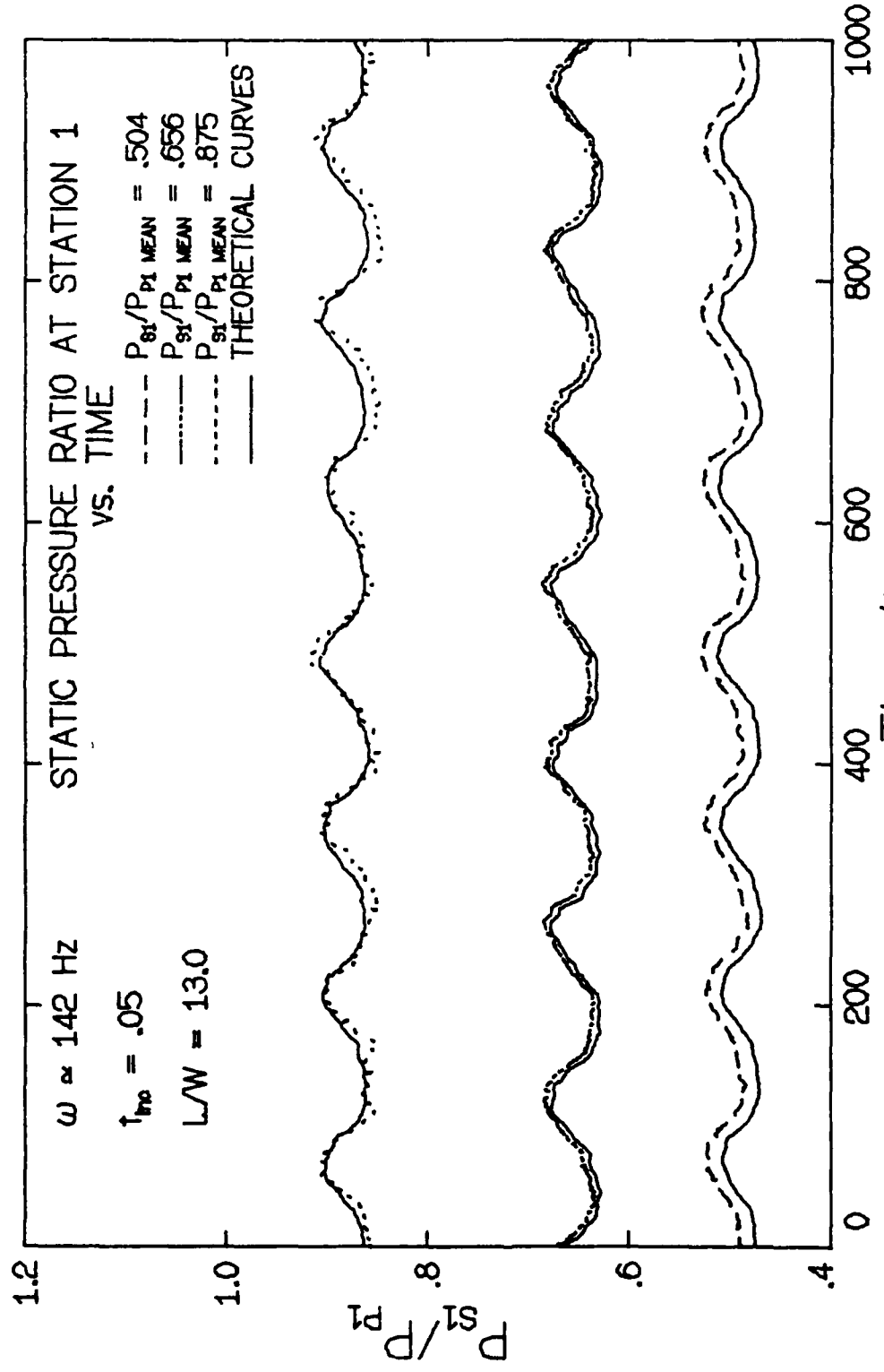

Figure 3.3.2-33 Theoretical and experimental values of P_{s1}/P_{p1} versus time

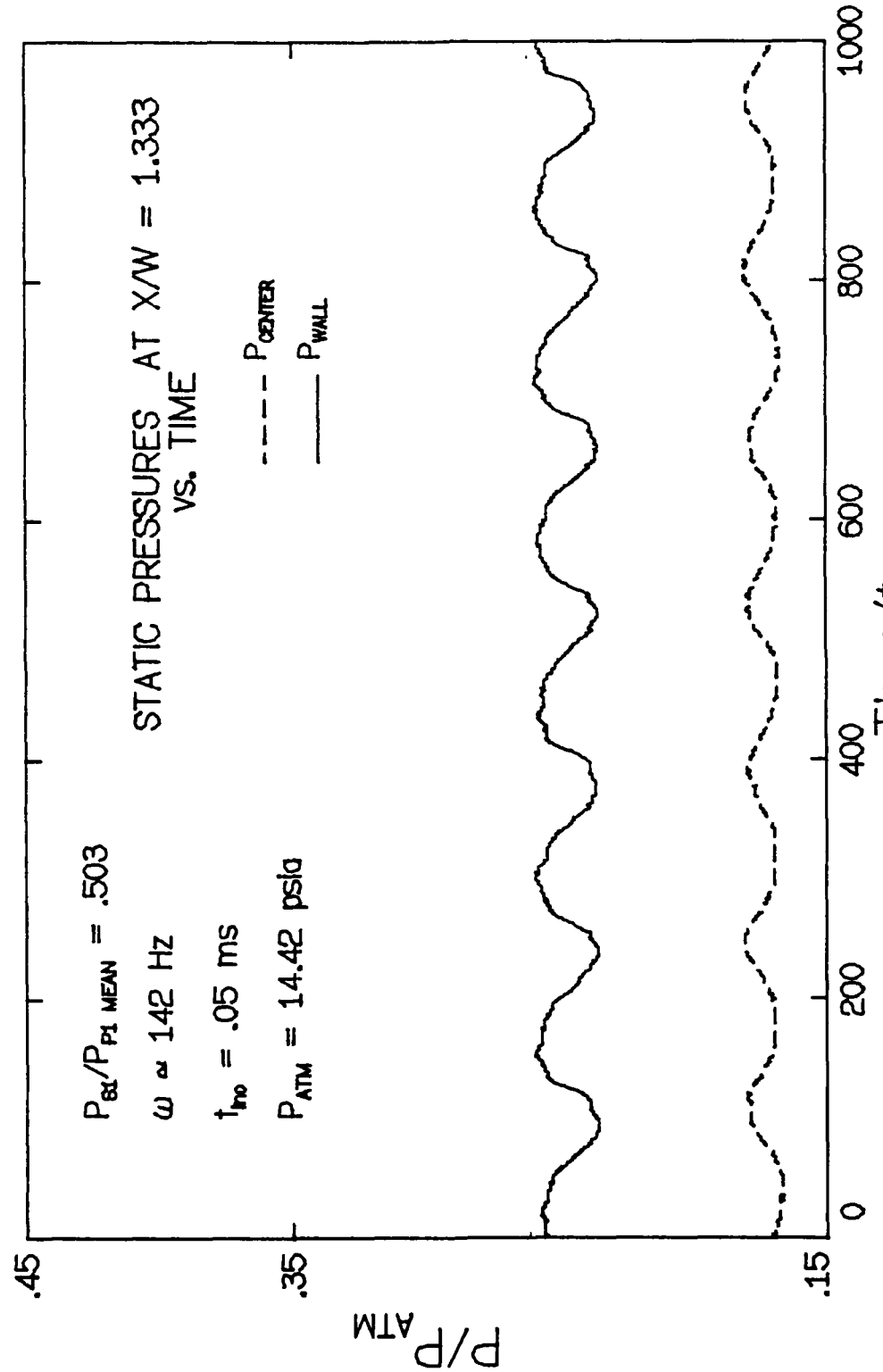

Figure 3.3.2-34 Static pressures versus time at X/W = 1.333 with a relatively low back pressure (L/W = 13.0, $P_{s0}/P_{p0} \simeq .070$)

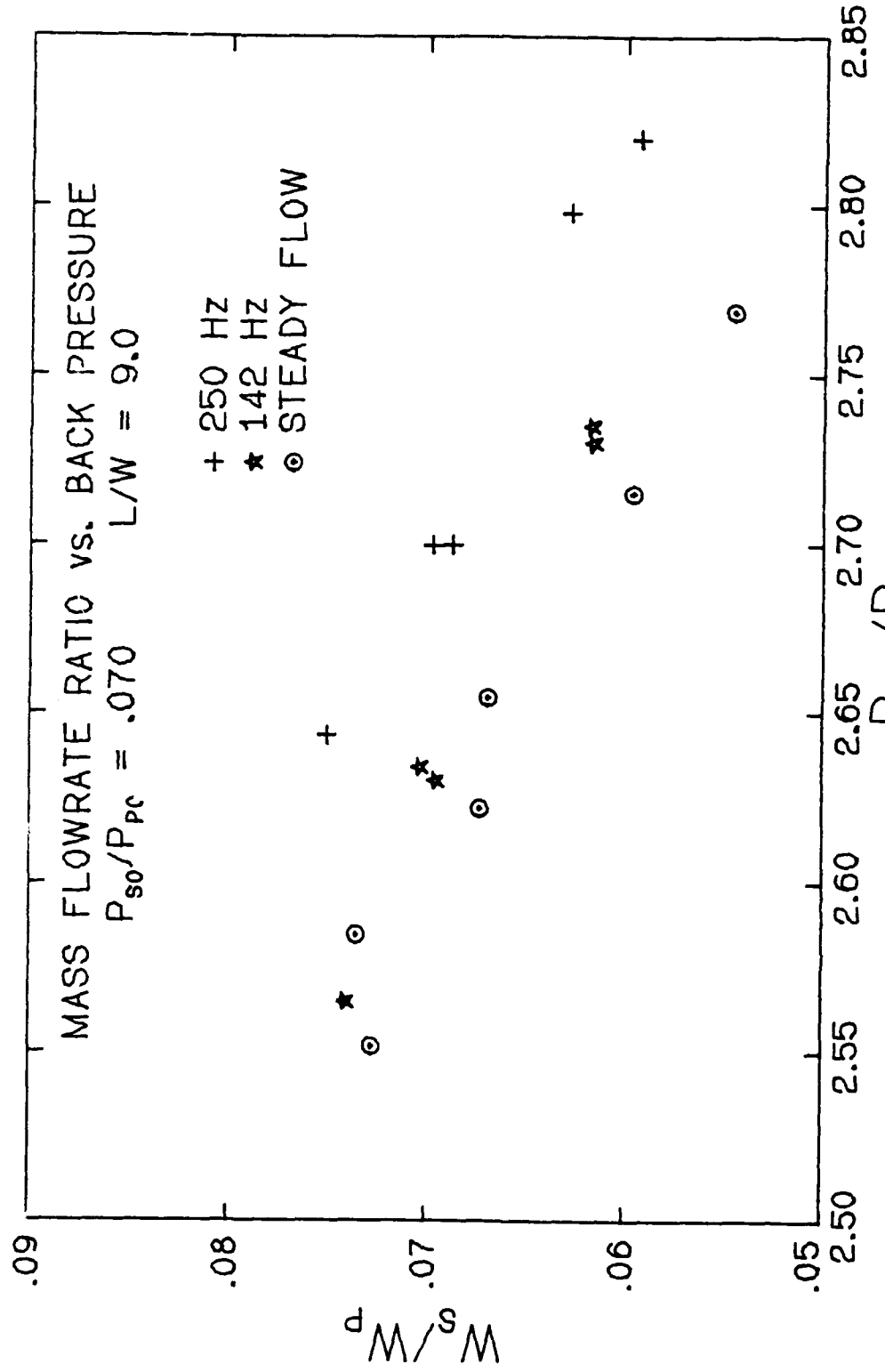

Figure 3.3.2-35 w_s/w_p versus P_{m3}/P_{so} for flows that have passed the break-off point and are in the mixed regime (L/W = 9.0, $P_{so}/P_{po} \simeq .070$)

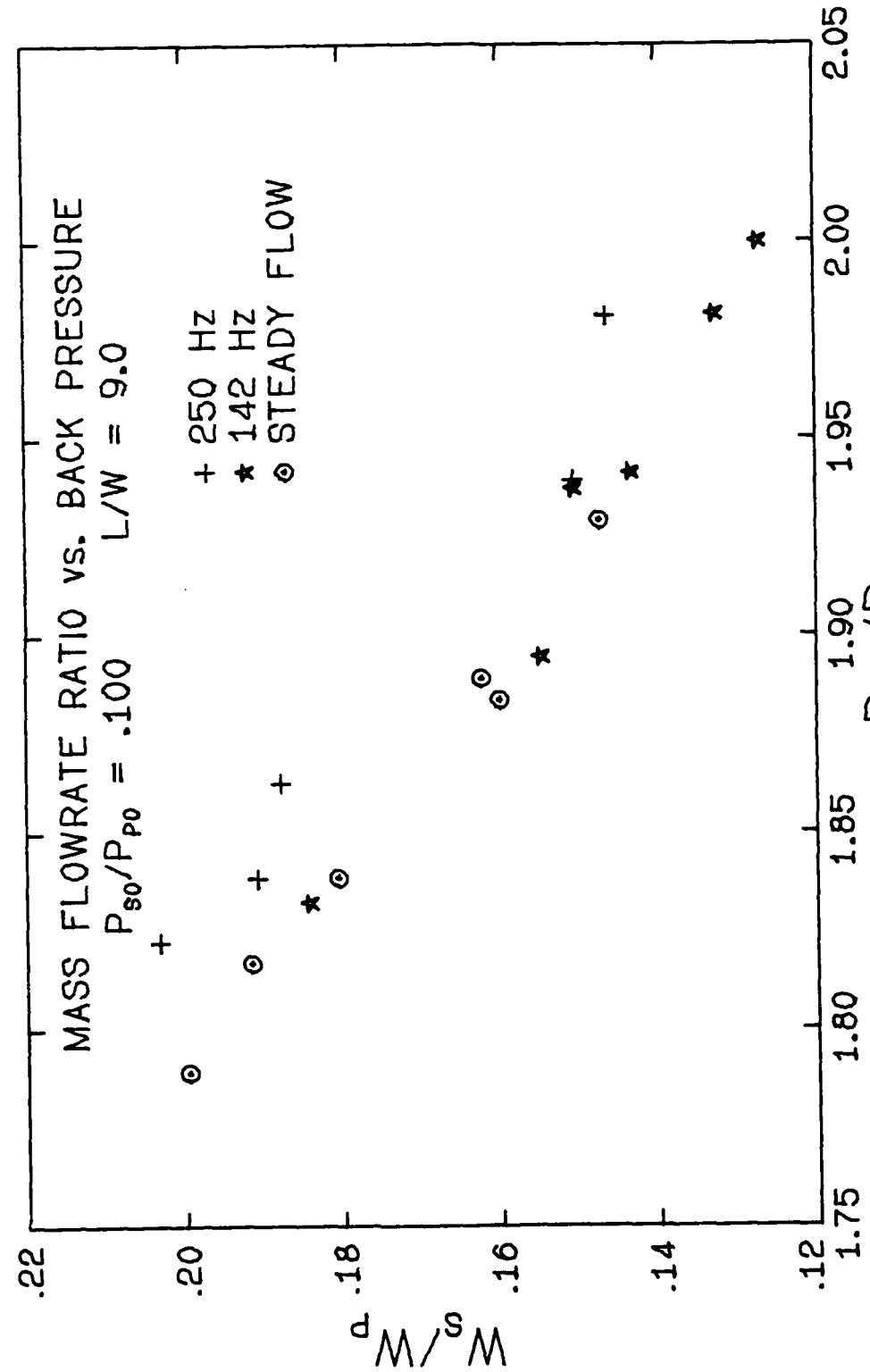

Figure 3.3.2-36 w_s/w_p versus P_{m3}/P_{s0} for flows that have passed the break-off point and are in the mixed regime (L/W = 9.0, $P_{s0}/P_{p0} \simeq .100$)

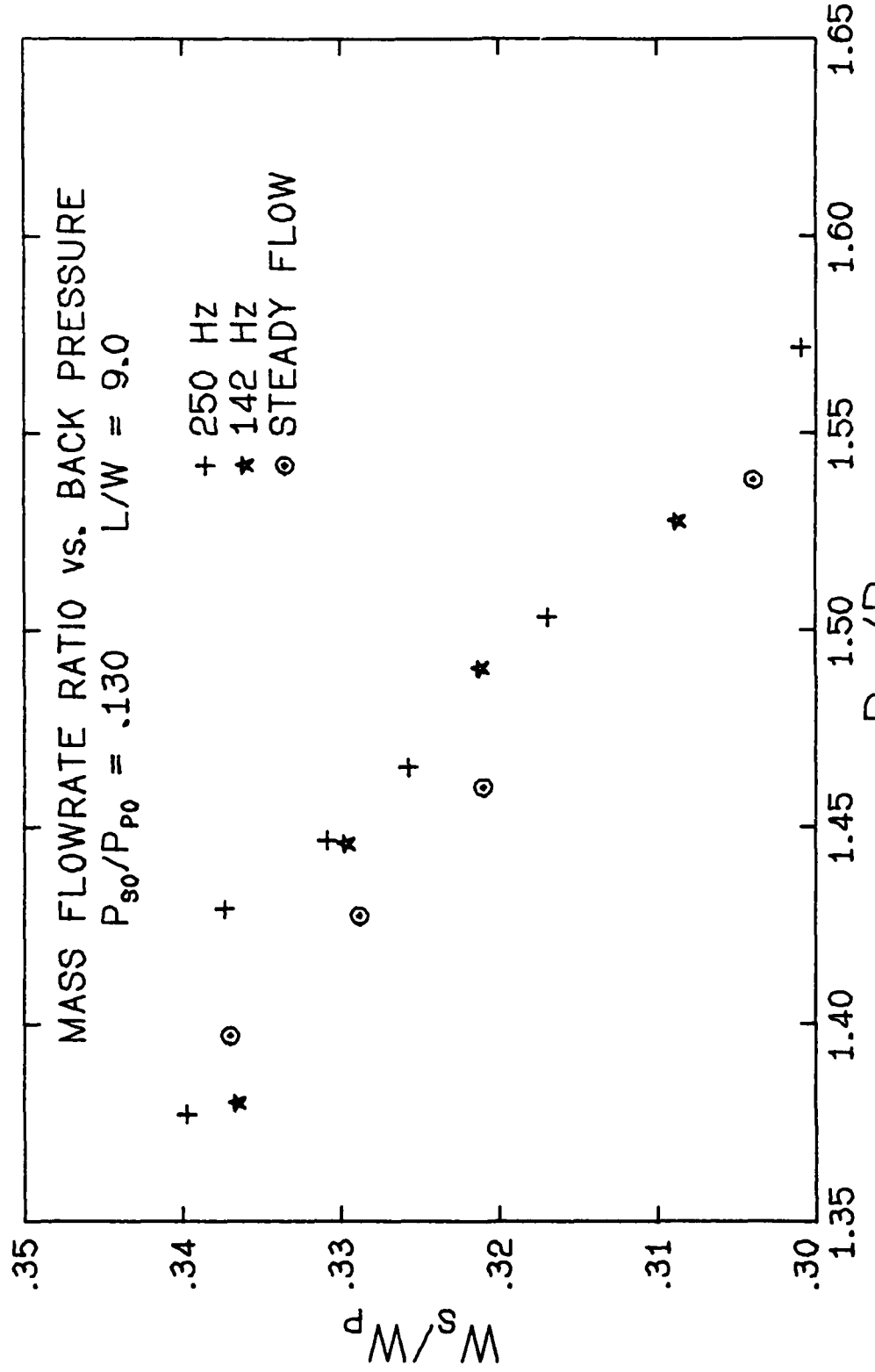

Figure 3.3.2-37 w_s/w_p versus P_{m3}/P_{s0} for flows that have passed the break-off point and are in the mixed regime (L/W = 9.0, $P_{s0}/P_{p0} \simeq .130$)

4.0 CONCLUSIONS

The conclusions that can be drawn as a result of this experimental and theoretical investigation of multiple ducted streams with a steady or a periodic supersonic driver flow are:

1. The one-dimensional analysis predicts the back pressure independent values of w_s/w_p and P_{s1}/P_{p1} for the steady driver ejector flow reasonably well over the range of values of P_{s0}/P_{p0} and mixing duct lengths investigated.
2. The values of the back pressure ratio, P_{m3}/P_{s0}, at which both steady and periodic driver ejector flows began to break-off from back pressure independent SR flow to MR flow were 25 to 35 percent lower than theoretically predicted.
3. Periodic primary ejector flows were found to drive and determine the secondary flow in such a way that the quasi-steady assumption appears to be valid. Theoretical and experimental values of P_{s1}/P_{p1} versus time were in reasonably good agreement. Back pressure independent values of the mass flowrate ratios for the periodic driver ejector flows were in good agreement with the mean values predicted by the quasi-steady analysis. The steady flow values of the mass flowrate ratios at the corresponding mean values of P_{s0}/P_{p0} were nearly the same as the periodic driver flow values.

4. Mass flowrate ratios and pressure recovery capabilities of the ejector were nearly the same for the L/W = 16.374 and L/W = 13.0 mixing ducts. The L/W = 9.0 mixing duct flow broke-off from SR to MR flow at lower values of the back pressure ratio than flow in the longer two mixing ducts. Mass flowrate ratios were less in the shortest mixing duct at given values of P_{s0}/P_{p0} and P_{m3}/P_{s0} than in the two longer mixing ducts.

5. Periodic driver ejector flows subject to back pressures high enough to have caused break-off from SR to MR flow operated at higher P_{m3}/P_{s0}, up to 5 percent higher than the steady flow ejector, at given values of P_{s0}/P_{p0} and w_s/w_p in the L/W = 9.0 mixing duct. Explained another way, one might say that higher mass flowrate ratios were obtained at given values of P_{s0}/P_{p0} and P_{m3}/P_{s0} for ejector flows that had passed the break-off point and were in the mixed regime. However, this is not felt to be the result of increased entrainment due to the periodicity of the driver but rather due to a shift in the position, towards the SR break-off point, that the ejector operates at on the MR solution surface, see Fig. 2.1-2, for a given value of P_{s0}/P_{p0}. The agreement between steady and periodic driver flow back pressure independent mass flowrate ratios, the quasi-steady nature of the periodic ejector flows at Station 1, and the

linearity of the theoretical values of w_s/w_p as a function of P_{s0}/P_{p0}, see Fig. 3.3.1-2, suggests that the entrainment of the secondary flow in the mixed regime near break-off with the supersonic regime is not significantly affected by the periodicity of the driver flow.

6. Static pressure measurements versus time did not indicate that significant differences in the pressure recovery process or flow characteristics within the mixing duct existed between periodic and steady driver ejector flows. Shock waves in the supersonic primary flow were greatly disturbed by a periodic driver but the shock waves in the steady driver ejector flow were also quite transient and unstable. Mean values of static pressures at the same location and under corresponding flow conditions were approximately the same in periodic and steady driver ejector flows.
7. Mixing rates between the primary and secondary flows were not noticeably altered by a periodic driver. The location of the point at which the static pressures became nearly uniform across the mixing duct was approximately the same for periodic and steady driver ejector flows. Exit plane stagnation pressure uniformity was slightly improved in only a few cases by a periodic driver flow. It appears that rapid mixing did not take

place until the primary flow in the center of mixing duct became subsonic. As indicated by the presence of shock waves, the periodicity of the primary flow did not change the average location of the disintegration of the supersonic primary to subsonic flow. The periodic driver had little effect on the character of the flow in the high mixing rate region which lies between the approximate location of the loss of the supersonic primary flow and the exit plane of the mixing duct.

8. The Strouhal number of the periodic driver ejector flows were low in comparison to those in the mixing studies cited in Section 1.2. If based on the velocity of the primary flow at Station 1, the hydraulic diameter of the primary flow C-D nozzle, and the 250 Hz driver frequency, the Strouhal number is St = .0064. The Strouhal number for a subsonic secondary stream at Station 1 with the theoretical flow velocity at P_{s0}/P_{p0} = .100 and with ω = 250 Hz is St = .025. With the theoretical value of M_{m3} for P_{s0}/P_{p0} = .100 and the mixing duct hydraulic diameter, the Strouhal number at the exit plane is St = .029 with ω = 250 Hz. A fluid particle will pass entirely through the mixing duct in only a fraction of a driver cycle. The driver flow frequencies used in this

investigation were too low to significantly effect the dynamics of mixing between high speed compressible streams in a short mixing duct.

9. The large-scale fluidic oscillator was an efficient and reliable method of producing periodic pulses. It is not felt that frequencies higher than approximately 500 Hz could be obtained with a fluidic oscillator configuration similar to one used in this investigation without decreasing the size of the oscillator to such an extent that the mass flowrate through the device must be appreciably decreased.

10. The transient disturbances in the steady driver ejector flows were comparable to disturbances produced by the periodic driver in most cases; thus, the effects of a periodic driver on ejector flow have not been clearly delineated by the "steady" flow comparison. An axisymmetric ejector configuration may prove to be more stable than 2-D planar configuration examined and may therefore provide a more meaningful comparison.

5.0 REFERENCES

1. Ejectors, von Karman Institute, Lecture Series 79, two volumes, 1975, Addy, A. L., "The Analysis of Supersonic Ejector Systems"; Delery, J., "Methods d'étude des éjecteurs Supersonic Application aus tuyéres double-flux;" Olivari, D., "Jets and Mixing Phenomena"; Viets, H., "Thrust Augmenting Ejectors"; Walker, B. J., "Chemical Laser Pumping Systems"; Schmitt, H., "Summary of Possible Applications and Present Status of Various Ejector Techniques."

2. Brown, S. L. and Murphy, R. D., "Design and Testing of Thrust Augmenting Ejectors," V/STOL Aerodynamics, AGARD-CP-143, 1974.

3. DeJoode, A. D. and Pantankar, S. V., "Prediction of Three-Dimensional Turbulent Mixing in an Ejector," AIAA Journal, Vol. 16, February 1978, pp. 145-150.

4. Viets, H., "Thrust Augmenting Ejector Analogy," Journal of Aircraft, Vol. 14, April 1977, pp. 409-411.

5. Gilbert, G. B. and Hill, P. G., "Analysis and Testing of Two-Dimensional Slot Nozzle Ejectors with Variable Area Mixing Sections," NASA CR-2251, May 1975.

6. Hasinger, S. H., "Performance Characteristics of Ejector Devices," former Aerospace Research Laboratories, Wright-Patterson Air Force Base, Technical Report ARL TR 75-205, June 1975.

7. Tai, T. C., "Analysis and Design of Thrust Augmenting Ejectors," Prediction Methods for Jet V/STOL Propulsion Aerodynamics, Vol. 2, M. F. Platzer (editor), Proceedings of a Naval Air Systems Command Research and Technology Group Workshop, Institute for Defense Analysis, Arlington, Virginia, July 28-31, 1975, pp. 702-721.

8. Addy, A. L. and Mikkelsen, C. D., "An Investigation of Gas Dynamic Flow Problems in Chemical Laser Systems," Department of Mechanical and Industrial Engineering, University of Illinois at Urbana, Report No. UILU-ENG-74-4009, 1974.

9. Fabri, J. and Paulon, J., "Theory and Experiments on Supersonic Air-to-Air Ejectors," NACA TM 1410, September 1958.

10. Chow, W. L. and Addy, A. L., "Interaction Between Primary and Secondary Streams of Supersonic Ejector Systems and their Performance Characteristics," AIAA Journal, Vol. 2, April 1964, pp. 686-695.

11. Addy, A. L., "The Analysis of Supersonic Ejector Systems," Supersonic Ejectors, AGARD-CP-163, 1972, pp. 31-101.

12. Chow, W. L. and Yeh, P. S., "Characteristics of Supersonic Ejector Systems with Non-Constant Area Shroud," AIAA Journal, Vol. 3, March 1965, pp. 525-527.

13. Mikkelsen, C. D., Sandberg, M. R., and Addy, A. L., "Theoretical and Experimental Analysis of the Constant Area Supersonic-Supersonic Ejector," Department of Mechanical and Industrial Engineering, University of Illinois at Urbana, Report No. UILU-ENG-76-4003, 1976.

14. Baker, L. R., Jr. and McDermit, J. H., "Survey of Pressure Recovery Methods for Chemical Laser Applications," Chemical Laser Analysis and Development, Vol. VI, Lockheed Missile and Space Co., Technical Report RK-CR-73-2, October 1973.

15. Townsend, A. A., "The Mechanisms of Entrainment in Free Turbulent Flows," Journal of Fluid Mechanics, Vol. 26, Part 4, 1966, pp. 689-716.

16. Kovaszney, L. S. G., "The Structure of Turbulence in Shear Flows," AGARD-CP-93, 1971.

17. Brown G. and Roshko, A., "The Effect of Density Differences on the Turbulent Mixing Layer," Journal of Fluid Mechanics, Vol. 64, Part 4, 1974, pp. 775-816.

18. Roshko, A., "Structure of Turbulent Shear Flows: A New Look," AIAA Journal, Vol. 14, October 1976, pp. 1349-1357.

19. Bradshaw, P., "Interacting Shear Layers in Turbomachines," Turbulence in Internal Flows, Murthy, S. N. B. (editor), A Project SQUID Workshop, Warrenton, Virginia, June 14-15, 1976, pp. 35-65.

20. Dimotakis, P. E. and Brown, G. L., "The Mixing Layer at High Reynolds Numbers: Large Structure Dynamics and Entrainment," Journal of Fluid Mechanics, Vol. 76, Part 3, 1976, pp. 535-560.

21. Bevilaqua, P. M. and Lykoudis, P. S., "Mechanisms of Entrainment in Turbulent Wakes," AIAA Journal, Vol. 9, 1971, pp. 1657-1659.

22. Papailiou, D. D. and Lykoudis, P. S., "Turbulent Vortex Streets and Entrainment," Journal of Fluid Mechanics, Vol. 62, Part 1, 1974, pp. 11-31.

23. Crow, S. C. and Champaign, F. H., "Orderly Structure in Jet Turbulence," Journal of Fluid Mechanics, Vol. 48, Part 3, 1971, pp. 547-591.

24. Becker, H. A. and Massoro, T. A., "Vortex Evolution in a Round Jet," Journal of Fluid Mechanics, Vol. 31, Part 3, 1968, pp. 435-448.

25. Glass, D. R., "Effects of Acoustic Feedback on the Spread and Decay of Supersonic Jets," AIAA Journal, Vol. 6, October 1968, pp. 1890-1897.

26. McCormack, P. D., Cochran, D., and Crane, L., "Periodic Vorticity and Its Effect on Mixing," The Physics of Fluids, Vol. 9, August 1966, pp. 1555-1560.

27. Binder, G. and Favre-Marinet, M., "Mixing Improvement in Pulsating Turbulent Jets," Fluid Mechanics of Mixing, ASME, Symposium Proceedings of the Joint Meeting, Georgia Institute of Technology, June 20-22, 1973, pp. 167-172.

28. Bremhorst, K. and Harch, W. H., "Near Field Velocity Measurements in a Fully Pulsed Subsonic Air Jet," Turbulent Shear Flows, Symposium Proceedings, Pennsylvania State University, April 18-20, 1977, pp. 2.41-2.50.

29. Olivari, D., "Analysis of an Axisymmetrical Turbulent Pulsating Jet," von Karman Institute Technical Note No. 104, November 1974.

30. Viets, H., "Flip-Flop Jet Nozzle," AIAA Journal, Vol. 13, October 1975, pp. 1375-1379.

31. Platzer, M. F., Simmons, J. M., and Bremhorst, K., "Entrainment Characteristics of Unsteady Subsonic Jets," AIAA Journal, Vol. 16, No. 3, March 1978, p. 282.

32. Johnson, J. K., Jr., "An Analytical and Experimental Investigation of Ejector Performance for Nonsteady Flow Conditions," Clemson University, College of Engineering, Engineering Experiment Station Bulletin 107, July 1966.

33. Johnson, W. S. and Yang, T., "A Mathematical Model for the Prediction of the Induced Flow in a Pulsejet Ejector with Experimental Verification," ASME Paper No. 68-WA/FE-33, 1968.

34. Johnson, W. S., "A Performance Comparison of the Wave Energy Exchanger and the Steady Flow Ejector," Ph.D. Thesis, University of Tennessee, Mechanical and Aerospace Engineering Department, 1967.

35. Khare, J. M., "An Analytical and Experimental Investigation of an Unsteady Flow Ejector," University of Calgary, Mechanical Engineering Department, Report No. 53, 1973.

36. Quinn, B., "Interactions Between Screech Tones and Ejector Performance," Journal of Aircraft, Vol. 14, May 1977, p. 467.

37. Zarek, J. M., "The Neglected Parameters in Pulsating Flow Measurement," ASME, Flow Measurement Symposium, K. C. Cotton (editor), Pittsburg, Pennsylvania, September 26-28, 1966.

38. Sparks, C. R., "A Study of Pulsating Effects on Orifice Metering of Compressible Flow," ASME, Flow Measurement Symposium, K. C. Cotton (editor), Pittsburg, Pennsylvania, September 26-28, 1966.

39. Ower, E. and Pankhurst, R. C., The Measurement of Air Flow, Pergomon Press, New York, Oxford, 4th edition, 1966, pp. 323-333.

40. Loh, W. H. T., "Theory of the Hydraulic Analogy for Steady and Unsteady Gas Dynamics," Modern Developments in Gas Dynamics, W. H. T. Loh (editor), Plenum Press, New York, 1969.

41. Halbach, C. R., Otsap, B. A., and Thomas, R. A., "A Pressure Insensitive Fluidic Temperature Sensor," Advances in Fluidics, ASME, Brown, F. T. (editor), 1967, pp. 298-312.

42. Stover, T. R., "Development of a Large-Scale Fluidic Oscillator for Application to an Unsteady Aerodynamic Ejector System Using the Hydraulic Analogy," Masters Thesis, Department of Mechanical and Industrial Engineering, University of Illinois at Urbana, 1978.

43. Shapiro, A. H., The Dynamics and Thermodynamics of Compressible Fluid Flow, Vol. 1, Ronald Press Co., New York, 1953.

44. Telionis, D. P., "Unsteady Boundary Layers, Separated and Attached," Unsteady Aerodynamics, AGARD-CP-227, September 1977.

45. Simpson, R. L., "Features of Unsteady Turbulent Boundary Layers as Revealed from Experiments," Unsteady Aerodynamics, AGARD-CP-227, September 1977.

46. Rudinger, G., Nonsteady Duct Flow: Wave Diagram Analysis, Dover Publications Inc., New York, 1969, pp. 94-106.

47. Nelson, J. R., "Investigation of the Mixing Region Between the Primary and Secondary Streams of a Two-Dimensional Supersonic Air-Air Ejector System," Masters Thesis, Air Force Institute of Technology, Air University, June 1966.

APPENDIX A

UCAE, Unsteady Constant Area Ejector program, was written to perform the quasi-steady, one-dimensional analysis discussed in Section 2.0. The program and a sample input and output are listed in this appendix.

Default values of UCAE assume air-to-air ejector flow with equivalent primary and secondary stagnation temperatures. Variable definitions are given at the beginning of the program. MP1, AP1M3, PM3SOI, and MMAX are not assigned default values and must be assigned values in the first NAMELIST input to the program. An arbitrary sinusoidal curve, PSOPOI(time), as described near the beginning of the program, is available for use as the source of the calculation parameter, PSOPOI. This is the default form of the PSOPOI(time) parameter and is a rough approximation of the experimental periodic flow. The NAMELIST input to the program must include CURVE = .FALSE. if PSOPOI(time) data is to be read from a data file. Input file TAPE5 must include all input data, both the NAMELIST variables and, if CURVE = .FALSE., the PSOPOI data.

The program output, to output file TAPE6, includes input conditions and averages of ejector performance parameters. Output of performance parameter values at each time increment is the default form of the output and can be suppressed by including OUT = .FALSE. in the NAMELIST input. The value of MS1 at which the supersonic regime breaks-off with the approximate regime, MCRIT, and the corresponding stagnation pressure ratio, PCRIT, are written onto the output file TAPE6 for each data set read into the program. PS1P1 is written onto TAPE7 at each time increment. This feature was used to obtain a theoretical PS1P1 versus time curve to compare with experimental results.

Time is normalized by the time increment between successive PSOPOI data points.

A.1 UNSTEADY CONSTANT AREA EJECTOR PROGRAM (UCAE)

UNSTEADY CONSTANT AREA EJECTOR PROGRAM (UCAE)
MAIN PROGRAM

```
      PROGRAM UCAE(INPUT,OUTPUT,TAPE7,TAPE5=INPUT,TAPE6=OUTPUT)          UCA001
C  UNSTEADY CONSTANT AREA EJECTOR INTEGRATION PROGRAM                     UCA002
C                                                                         UCA003
C  THIS PROGRAM CALCULATES THE ONE-DIMENSIONAL THEORETICAL MEAN VALUES    UCA004
C  OF THE EJECTOR/DUCTED MULTIPLE STREAMS PERFORMANCE PARAMETERS FOR THE  UCA005
C  GEOMETRIC AND FLOW BOUNDARY CONDITIONS INPUT.  A PSOPO=PSOPO(TIME)     UCA006
C  CURVE IS TO BE THE SOURCE OF THE CALCULATION PARAMETER, PSOPO. THE     UCA007
C  CURVE IS SUBDIVIDED INTO STEPS OR SLUGS IN TIME AND THE ANALYSIS IS    UCA008
C  PERFORMED ON EACH STEP TO DETERMINE THE AVERAGE VALUES OF THE PER-     UCA009
C  FORMANCE PARAMETERS OF INTEREST.  THE PSOPO(TIME) CURVE CAN BE INPUT   UCA010
C  VIA DATA FILE OR AN ARBITRARY SINUSOIDAL CURVE IS AVAILABLE.  TIME     UCA011
C  IS NORMALIZED BY THE SAMPLING TIME INCREMENT.                          UCA012
C                                                                         UCA013
C     ********************************************************            UCA014
C                                                                         UCA015
C  VARIABLE DEFINITIONS AND THEIR DEFAULT VALUES:                         UCA016
C  SOME VARIABLE DEFINITIONS.                                             UCA017
C                                                                         UCA018
C  GS,GP.... THE RATIO OF SPECIFIC HEATS OF THE SECONDARY AND             UCA019
C             PRIMARY FLUIDS.                                             UCA020
C  MWSP..... THE SECONDARY TO PRIMARY MOLECULAR WEIGHT RATIO.             UCA021
C  TSOPO.... THE SECONDARY TO PRIMARY STAGNATION TEMPERATURE RATIO.       UCA022
C  MP1...... THE PRIMARY FLOW MACH AT STATION 1.                          UCA023
C  MS1...... THE SECONDARY FLOW MACH NUMBER AT STATION 1.                 UCA024
C  M3....... THE MIXED FLOW MACH NUMBER AT STATION 3.                     UCA025
C  MMAX..... THE MAXIMUM MACH NUMBER THAT THE PRIMARY FLOW CAN ATTAIN     UCA026
C             WITHIN THE MIXING SECTION AS A RESULT OF A ONE DIMENSIONAL  UCA027
C             ISENTROPIC EXPANSION.                                       UCA028
C  PM3SOI... INPUT VALUE OF THE BACK PRESSURE CONDITION, RATIO OF THE     UCA029
C             MIXED FLOW EXIT PLANE STATIC TO SECONDARY STAGNATION        UCA030
C             PRESSURE.                                                   UCA031
C  PMOSO.... THE RATIO OF MIXED TO SECONDARY FLOW STAGNATION PRESSURES.   UCA032
C  PS1P1.... THE RATIO OF SECONDARY TO PRIMARY FLOW STATIC PRESSURES AT    UCA033
C             STATION 1.                                                  UCA034
C  PSOPO.... THE SECONDARY TO PRIMARY STAGNATION PRESSURE RATIO.          UCA035
C  AP1M3.... THE RATIO OF THE PRIMARY TO TOTAL FLOW AREAS.                UCA036
C  NCASE.... A DATA SET COUNTER.                                          UCA037
C                                                                         UCA038
C  DEFAULT VALUES OF THE INPUT VARIABLES.                                 UCA039
C                                                                         UCA040
C    GS(1.4),GP(1.4),MWSP(1.0),TSOPO(1.0),MP1(),PM3SOI(),MMAX(),AP1M3()   UCA041
C                                                                         UCA042
C  LOGICAL VARIABLES, THEIR FUNCTIONS AND DEFAULT VALUES.                 UCA043
C                                                                         UCA044
C  NEW...... .TRUE. IS REQUIRED EACH TIME THE DATA SET HAS A DIFFERENT    UCA045
C            MP1, AP1M3, GS, OR GP THAN THE PREVIOUS SET.  TO AVOID       UCA046
C            CALCULATING MCRIT WHEN NO CHANGES OCCUR IN THESE VARIABLES,  UCA047
C            NEW=.FALSE. SHOULD BE INPUT.  .TRUE. IS THE DEFAULT VALUE.   UCA048
C                                                                         UCA049
C  OUT...... CAUSES OUTPUT FOR EACH TIME STEP WHEN .TRUE. IS THE INPUT.   UCA050
C            .FALSE. SHOULD BE USED IF CYCLE AVERAGES AND CASE INPUT      UCA051
C            DATA ARE THE ONLY OUTPUT DESIRED.                            UCA052
C                                                                         UCA053
C  CURVE.... IF AN ARBITRARY SINUSOIDAL PSOPO(T) CURVE IS TO BE USED,     UCA054
C            .TRUE. MUST BE THE INPUT.  THIS IS THE DEFAULT, FOR WHICH:   UCA055
C                                                                         UCA056
C                AMP=.100, THE AMPLITUDE.                                 UCA057
C                PAVG=.100, THE MEAN PSOPO.                               UCA058
C                NCYC=10, THE NUMBER OF TIME STEPS PER CYCLE.              UCA059
C                                                                         UCA060
```

UNSTEADY CONSTANT AREA EJECTOR PROGRAM (UCAE)
MAIN PROGRAM

```
C            ARE THE DEFAULT VALUES.                                          UCA061
C            IF A PSOPO(T) CURVE IS TO BE READ FROM A DATA FILE, .FALSE.      UCA062
C            MUST BE INPUT.                                                   UCA063
C                                                                             UCA064
C  OUTPUT DATA:                                                               UCA065
C                                                                             UCA066
C  ALL DATA INPUT, CYCLE MEAN VALUES OF MS1, PS1P1, MM3, PSOPO, PMOSO,        UCA067
C  AND WSP.  NOTE THAT OUT=.TRUE. WILL CAUSE THE ABOVE TO BE OUTPUT FOR       UCA068
C  EACH TIME STEP IN THE PSOPO(TIME) CYCLE AS WELL AS THE BREAK-OFF           UCA069
C  VALUES OF PM3SO, PMOSO, AND MM3 IN SR, APPM, SSR FLOWS, AND MR             UCA070
C  FLOW SOLUTIONS THAT MEET THE BACK PRESSURE CONDITION.                      UCA071
C                                                                             UCA072
C  ***************************************************************          UCA073
C                                                                             UCA074
C                                                                             UCA075
C  MUCH OF THIS PROGRAM COMES DIRECTLY FROM CAE, CONSTANT AREA EJECTOR        UCA076
C  PROGRAM, USED IN "AN INVESTIGATION OF GAS-DYNAMIC FLOW PROBLEMS IN         UCA077
C  CHEMICAL LASER SYSTEMS", ADDY, A. L. AND NIKKELSON, C  D.,                 UCA078
C  UNIVERSITY OF ILLNOIS REPORT UILU-ENG-74-4009, 1974.                       UCA079
C                                                                             UCA080
C                                                                             UCA081
C  ***************************************************************          UCA082
C                                                                             UCA083
C                                                                             UCA084
      COMMON/BLOCK1/GP,GS,MP1,MWSP,TSOPO,AP1M3,MMIN,MEW,MMAX,                 UCA085
     &PCRIT                                                                   UCA086
      COMMON/BLOCK2/MS1,MM3,PS1P1,PMOSO,WSP,PM3SO                             UCA087
      COMMON/BLOCK3/SMS1,SPMOSO,SMM3,SPSOPO,SPS1P1,SWSP                       UCA088
      LOGICAL CURVE,MEW,OUT                                                   UCA089
      REAL MS1,MP1,MCRIT,MWSP,M,MM3,MMIN,MMAX                                 UCA090
C                                                                             UCA091
C                                                                             UCA092
      NAMELIST/IUCAE/GS,GP,MWSP,TSOPO,AP1M3,MP1,PM3SOI,OUT,NCASE              UCA093
     &,MEW,MMAX,CURVE,AMP,PAVG,NCYC                                           UCA094
C  ASSIGN DEFAULT VALUES.                                                     UCA095
      DATA GS,GP,MWSP,TSOPO,OUT,MEW,NCASE/2*1.4,2*1.,2*.TRUE.,1/              UCA096
      DATA CURVE,AMP,PAVG,NCYC/.TRUE.,0.10,0.10,10/                           UCA097
C  NOTE THAT NCASE IS NOT INCREMENTED BY THE PROGRAM.                         UCA098
C                                                                             UCA099
      PPO(G,M)=(1.0+.5*(G-1.0)*(M*M))**(-G/(G-1.))                            UCA100
  105 IPRESS=0                                                                UCA101
C  THE VARIABLE, IPRESS, IS THE TIME STEP COUNTER IN THE PROGRAM.             UCA102
C  INPUT FLOW AND GEOMETRIC CONDITIONS.                                       UCA103
      READ(5,IUCAE)                                                           UCA104
      IF(EOF(5)) 999,110                                                      UCA105
  110 IF(.NOT.MEW) GO TO 115                                                  UCA106
C  PROGRAM SEEKS THE MAXIMUM MS1 WITH WHICH THE FABRI CHOKING CONDITION       UCA107
C  CAN BE SATISFIED.  THIS IS A FUNCTION OF MP1,AP1M3, AND GP.                UCA108
      CALL CRITH(MCRIT)                                                       UCA109
C  THE PSOPO CORRESPONDING TO MCRIT IS:                                       UCA110
      PCRIT=PPO(GP,MP1)/PPO(GS,MCRIT)                                         UCA111
C  THE INPUT IS NOW OUTPUT                                                    UCA112
  115 WRITE(6,120)NCASE,GS,GP,MWSP,TSOPO,AP1M3,MP1,PM3SOI                     UCA113
  120 FORMAT(5(/),10X,"INPUT DATA FOR CASE NO.",I3,//,10X,"GS=",F7.4,         UCA114
     &8X,"GP=",F7.4,8X,"MWSP=",F7.4,//,10X,"TSOPO=",F7.4,5X,"AP1M3=",         UCA115
     &F7.4,5X,"MP1=",F7.4,//,10X"PM3SOI=",F8.4,//)                            UCA116
      IF(MEW) WRITE(6,125) MCRIT,PCRIT                                        UCA117
  125 FORMAT(//,10X,"FOR THIS CASE, MCRIT=",F7.4,5X,"PCRIT=",F7.4,//)         UCA118
C                                                                             UCA119
C                                                                             UCA120
```

UNSTEADY CONSTANT AREA EJECTOR PROGRAM (UCAE)
MAIN PROGRAM

```
130 CALL PRATIO(AMP,PAVG,NCYC,PSOPOI,IPRESS,CURVE)                    UCA121
    IF(IPRESS.EQ.NCYC.AND..NOT.CURVE) GO TO 145                       UCA122
    IF(.NOT.CURVE.OR.IPRESS.GT.1) GO TO 140                           UCA123
    WRITE(6,135) AMP,PAVG,NCYC                                        UCA124
135 FORMAT(/,10X,"FOR THE SINUSOIDAL PRESSURE RATIO CURVE:",/,10X,    UCA125
   &"AMP=",F7.3,10X,"PAVG=",F7.4,10X,"NCYC=",I5," TIME SLUGS/CYCLE")  UCA126
140 CALL CALCAE(PSOPOI,PM3SOI,OUT,IPRESS,NCYC,NERROR,CURVE,NCRIT)     UCA127
    IF(NERROR.GT.0) GO TO 105                                         UCA128
    IF(IPRESS.LT.NCYC) GO TO 130                                      UCA129
145 WRITE(6,150) NCYC                                                 UCA130
150 FORMAT(//,10X,"THE TOTAL NUMBER OF TIME SLUGS READ WAS",I5,////)  UCA131
    GO TO 105                                                         UCA132
999 CONTINUE                                                          UCA133
    END                                                               UCA134
```

UNSTEADY CONSTANT AREA EJECTOR PROGRAM (UCAE)
SUBROUTINE CALCAE

```
C  ********************************************************************  CAL001
C                                                                        CAL002
C                                                                        CAL003
C                                                                        CAL004
      SUBROUTINE CALCAE(PSOPOI,PM3SOI,OUT,IPRESS,MCYC,NERROR,CURVE,      CAL005
     &MCRIT)                                                             CAL006
C  THIS SUBROUTINE DETERMINES THE FLOW REGIME, CALLS THE PROPER SUB-     CAL007
C  ROUTINES TO DETERMINE THE FLOW CONDITIONS AT STATIONS 1 & 3, AND      CAL008
C  CONTROLS ITERATION PROCEDURES.                                        CAL009
C                                                                        CAL010
C                                                                        CAL011
      COMMON/BLOCK1/GP,GS,MP1,MWSP,TSOPO,AP1M3,MMIN,MMAX,NEW,            CAL012
     &PCRIT                                                              CAL013
      COMMON/BLOCK2/MS1,MM3,PS1P1,PMOSO,WSP,PM3SO                        CAL014
      REAL MS1,MP1,MCRIT,MWSP,M,MX,MM3,MS1B,MR,MMIN,MMAX                CAL015
      LOGICAL NEW,CURVE,OUT                                              CAL016
C                                                                        CAL017
C  W*SQRT(R*TO)/P*A=WM(G,M)                                              CAL018
      WM(G,M)=M*SQRT(G*(1.0+(G-1.0)*(M*M)*.50))                          CAL019
C  THE P/PO FUNCTION.                                                    CAL020
      PPO(G,M)=(1.0+(G-1.0)*(M*M)*.50)**(-G/(G-1.0))                     CAL021
C  THE INVERSE OF THE P/PO FUNCTION                                      CAL022
      PM(G,PR)=SQRT((PR**((1.0-G)/G)-1.0)*2.0/(G-1.0))                   CAL023
C  PY/PX FOR A NORMAL SHOCK WAVE.                                        CAL024
      PYPX(G,MX)=(2.0*G/(G+1.0))*(MX*MX)-((G-1.0)/(G+1.0))               CAL025
C                                                                        CAL026
C                                                                        CAL027
      DATA ERRMS1,ERRORY,NITMAX/2*1.0E-4,35/                             CAL028
      DATA SR/"SP"/,SSR/"SSR"/,MR/"MR"/,APPR/"APPR"/                     CAL029
C  MS1B IS THE LOWEST SECONDARY MACH NUMBER CONSIDERED IN A SEARCH FOR   CAL030
C  A SOLUTION.                                                           CAL031
      NERROR=0    $    NCOUNT=1    $    DMS1B=.100    $    MS1B=.001     CAL032
C  THE MAXIMUM PS1P1 ALLOWED FOR CALCULATIONS TO PROCEDE, PS1P1U,        CAL033
C  IS BASED ON A NORMAL SHOCK STANDING IN THE EXIT PLANE OF THE          CAL034
C  PRIMARY NOZZLE.                                                       CAL035
      PS1P1U=PYPX(GP,MP1)                                                CAL036
      AS1P1=(1.0/AP1M3)-1.0                                              CAL037
      CONST=SQRT(MWSP/TSOPO)*AS1P1/WM(GP,MP1)                            CAL038
C  IF THE REGIME IS SSR PS1P1>= 1.0 AND MS1= 1.0                         CAL039
C                                                                        CAL040
      REGIME=SSR                                                         CAL041
      MS1=1.0                                                            CAL042
      PS1P1=PPO(GS,1.0)*PSOPOI/PPO(GP,MP1)                               CAL043
      IF(PS1P1.LT.1.0.AND.PSOPOI.LT.PCRIT) GO TO 20                      CAL044
      IF(PS1P1.GT.1.0) GO TO 50                                          CAL045
C  THE PRESSURE RATIO LIES BETWEEN SR AND SSR REGIMES.  PS1P1 = 1.0      CAL046
C  IS A GOOD APPROXIMATION                                               CAL047
      REGIME=APPR                                                        CAL048
      PS1P1=1.0                                                          CAL049
      PS1SO=1.0*PPO(GP,MP1)/PSOPOI                                       CAL050
      MS1=PM(GS,PS1SO)                                                   CAL051
      GO TO 50                                                           CAL052
C  IN SR MS1 MUST BE WINDOWED SUCH THAT MS1B < = MS1 <  MCRIT            CAL053
   20 REGIME=SR    $    NIT=1    $    MTYPE=1                            CAL054
      MS1=MS1B                                                           CAL055
   30 CALL FABRI(MS1,PS1P1,NERROR)                                       CAL056
      IF(NERROR.GT.0) GO TO 905                                          CAL057
      PS1P1I=PSOPOI*PPO(GS,MS1)/PPO(GP,MP1)                              CAL058
      IF((NIT.EQ.1).AND.(PS1P1.GT.PS1P1I)) GO TO 909                     CAL059
      Y=(PS1P1-PS1P1I)/PS1P1I                                            CAL060
```

UNSTEADY CONSTANT AREA EJECTOR PROGRAM (UCAE)
SUBROUTINE CALCAE

```
      IF((ABS(Y).GT.ERRORY).AND.(PS1P1.LE.PS1P1I).AND.                  CAL061
     &(ABS(MS1-MCRIT)/MCRIT.LT..0005)) GO TO 40                         CAL062
      IF((MS1+DMS1B).GT.MCRIT) DMS1B=(MCRIT-MS1)/2.0                    CAL063
      CALL ITER(MS1,DMS1B,ERRMS1,+1.0,Y,0.0,ERRORY,NIT,NTYPE,           CAL064
     &XNEG,YNEG,XPOS,YPOS,NSIGN1,NSIGN2)                                CAL065
      IF(NITMAX.LT.NIT.AND.NTYPE.NE.3) GO TO 40                         CAL066
      GO TO (30,30,50),NTYPE                                            CAL067
C  IF NO SOLUTION HAS BEEN FOUND MR WILL BE SEARCHED.                   CAL068
 40   IF(OUT) WRITE(6,908)MS1,PS1P1,PS1P1I                              CAL069
      GO TO 60                                                          CAL070
 50   CALL OCV(NERROR)                                                  CAL071
      IF(NERROR.NE.0) GO TO 902                                         CAL072
C  IF THE VALUE OF PM3SO RETURNED BY OCV IS < PM3SOI THE                CAL073
C  SECONDARY MASS FLOWRATE IS DEPENDENT ON PM3SOI AND THE REGIME        CAL074
C  MUST BE MR.                                                          CAL075
      DELT=PM3SO-PM3SOI                                                 CAL076
      IF(REGIME.NE.MR.AND.PM3SO.GT.PM3SOI) GO TO 70                     CAL077
      IF(ABS(DELT/PM3SOI).LT.ERRMS1.AND.REGIME.EQ.MR.AND.               CAL078
     &DELT.LE.(0.0)) GO TO 70                                           CAL079
C  THE BACK PRESSURE IS TOO HIGH FOR THE SECONDARY TO BE CHOKED.        CAL080
C  MS1 IS LESS THAN THE BREAK-OFF VALUE AND THE REGIME IS MR.  A        CAL081
C  VALUE OF MS1 PRODUCING A PM3SO=PM3SOI IN OCV IS SOUGHT.              CAL082
 60   IF(REGIME.NE.MR)MS1=.500                                          CAL083
      REGIME=MR                                                         CAL084
      IF(NCOUNT.GT.25.OR.MS1.LT.MS1B.OR.MS1.GT..999) GO TO 904          CAL085
      CALL ITMS1(MS1,PM3SO,PM3SOI,NCOUNT,MS1LO,MS1HI)                   CAL086
      PS1P1=PSOPOI*PPO(GS,MS1)/PPO(GP,MP1)                              CAL087
      GO TO 50                                                          CAL088
 70   IF(PS1P1U.LT.PS1P1) GO TO 900                                     CAL089
      WSP=CONST*PS1P1*WR(GS,MS1)                                        CAL090
      IF(.NOT.OUT) GO TO 100                                            CAL091
      IF(IPRESS.EQ.1) WRITE(6,80)                                       CAL092
 80   FORMAT(//,10X,"TIME SLUG DATA",/,3X,"SLUG",2X,"REGIME",4X,       CAL093
     &"PSOPO",6X,"WSP",6X,"MS1",5X,"PS1P1",5X,"MM3",5X,                 CAL094
     &,"PMOSO",7X,"PM3SO",/)                                            CAL095
      WRITE(6,90)IPRESS,REGIME,PSOPOI,WSP,MS1,PS1P1,MM3                 CAL096
     &,PMOSO,PM3SO                                                      CAL097
 90   FORMAT(/,2X,I4,5X,A4,3X,F6.4,4X,F6.4,3(3X,F6.4),                  CAL098
     &3X,F7.4,3X,F8.4)                                                  CAL099
      WRITE(7,95) PS1P1                                                 CAL100
 95   FORMAT(10F10.4)                                                   CAL101
 100  CALL SUMUP(IPRESS,NCYC,PSOPOI,CURVE)                              CAL102
      RETURN                                                            CAL103
C  **********     ERROR MESSAGES     **********                        CAL104
 900  WRITE(6,901) IPRESS,PS1P1,PS1P1U,MS1                              CAL105
 901  FORMAT(/,"* * * * * * * * * * * * * * * * * * * * ",/,"ERROR IN CALCAE  CAL106
     &",/,"* * * * * * * * * * * * * * * * * * * * ",/,5X,"TIME SLUG NO.",I4,5X," CAL107
     &PS1P1=",F8.4,5X,"PS1P1U=",F8.4,5X,"MS1=",F8.4)                    CAL108
      NERROR=1   $   RETURN                                             CAL109
 902  WRITE(6,903) MS1,PS1P1                                            CAL110
 903  FORMAT(//,"* * * * * * * * * * * * * * * * * * ",/,"ERROR IN OCV",/," *  CAL111
     &* * * * * * * * *",/,10X,"MS1=",F8.4,10X,"PS1P1=",F8.4)          CAL112
      RETURN                                                            CAL113
 904  WRITE(6,905) MS1,PM3SO,PM3SOI                                     CAL114
 905  FORMAT(//,"* * * * * * * * * * * * * * * * * *",/,"ERROR IN CALCAE",/," *  CAL115
     & * * * * * * * * ",/,"NON-CONVERGENCE OF MS1 FOR THE INPUT PM3SO,"  CAL116
     &,1X,"MR",/,10X,"MS1=",F8.4,10X,"PM3SO=",F8.4,10X,"PM3SOI=",F8.4)  CAL117
      NERROR=1   $   RETURN                                             CAL118
```

UNSTEADY CONSTANT AREA EJECTOR PROGRAM (UCAE)
SUBROUTINE CALCAE

```
906 WRITE(6,907)                                                        CAL118
907 FORMAT(/," * * * * * * * * * * * * * *",/,"ERROR IN FABRI",/," * * *  CAL119
   & * * * * * * * *")                                                  CAL120
    NERROR=1    $   RETURN                                              CAL121
918 FORMAT(///,10X,"SOLUTION NOT FOUND IN SR BY FABRI WITH ITER",/,     CAL122
   &10X,"MS1=",F8.5,6X,"PS1P1=",F8.5,6X,"PS1P1I=",F8.5)                 CAL123
909 WRITE(6,910)                                                        CAL124
910 FORMAT(3(/,5X,"PSOP0I IS SO LOW THAT MS1<.001 IN SR."))             CAL125
    NERROR=1    $   RETURN                                              CAL126
    END                                                                 CAL127
```

UNSTEADY CONSTANT AREA EJECTOR PROGRAM (UCAE)
SUBROUTINE FABRI

```
C  ************************************************************          FAB001
C                                                                        FAB002
C                                                                        FAB003
      SUBROUTINE FABRI(MS1,PS1P1,NERROR)                                 FAB004
C                                                                        FAB005
C  CONSTANT-AREA EJECTOR, FABRI CRITERION (FABRI) SUBROUTINE.            FAB006
C                                                                        FAB007
C  1-D EJECTOR ANALYSIS WITH SUPERSONIC PRIMARY (MP1>1) AND              FAB008
C  SUBSONIC SECONDARY (MS1<1) WHICH CHOKES IN THE EJECTOR                FAB009
C  SHROUD  (MS2=1).  THIS EJECTOR ANALYSIS IS BASED                      FAB010
C  ON THE CONSTANT-AREA SHROUD EJECTOR ANALYSIS OF FABRI.                FAB011
C  REFERENCE: NACA TN 1410.                                              FAB012
C                                                                        FAB013
      COMMON/BLOCK1/GP,GS,MP1,MWSP,TSOPO,AP1M3,MMIN,NEW,MMAX,           FAB014
     &PCRIT                                                             FAB015
      REAL M,MP1,MS1,MWSP,MMIN,MMAX,MP2                                 FAB016
      LOGICAL NEW                                                       FAB017
C                                                                        FAB018
C  P/P0(G,M) FUNCTION.                                                   FAB019
      PPO(G,M)=(1.+.5*(G-1.)*(M*M))**(-G/(G-1.))                        FAB020
C  A/A*(G,M) FUNCTION.                                                   FAB021
      AASM(G,M)=(1./M)*(((2./(G+1.))*(1.+0.5*(G-1.)*(M*M)))             FAB022
     &   **(0.5*(G+1.)/(G-1.)))                                         FAB023
C                                                                        FAB024
C  FABRI'S CRITERION APPLIES ONLY WHEN (MS1.LE.(1.0)) AND                FAB025
C  (PS1P1.LE.(1.0)).                                                     FAB026
C  CALCULATE THE AREA RATIO FOR STREAM (P) AT STATION (2).               FAB027
      AP2PS=(AASM(GP,MP1)/AP1M3)*(1.-(1.-AP1M3)/AASM(GS,MS1))           FAB028
C  CALCULATE MP2 AT STATION (2) WHERE MS2=1.0.                           FAB029
      CALL ASTAR(GP,AP2PS,MP2,MMIN,MMAX)                                FAB030
C  CALCULATE STATIC PRESSURE RATIO PS1P1 BASED ON                        FAB031
C  FABRI'S CRITERION.                                                    FAB032
      VD=(1.0-AP1M3)*((1.0+GS*(MS1**2))-                                FAB033
     &    (PPO(GS,1.0)/PPO(GS,MS1))*((1.0+GS)/AASM(GS,MS1)))            FAB034
      VN=(PPO(GP,MP2)/PPO(GP,MP1))*AP1M3*(AASM(GP,MP2)/                 FAB035
     &   AASM(GP,MP1))*(1.+GP*(MP2**2))-AP1M3*(1.+GP*(MP1*MP1))         FAB036
      PS1P1=VN/VD                                                       FAB037
      IF(PS1P1.GT.1.0.AND..NOT.NEW) WRITE(6,80)                         FAB038
      IF(PS1P1.LE.(0.0)) WRITE(6,60)                                    FAB039
      IF(MP2.LT.MP1) WRITE(6,40)                                        FAB040
      IF(PS1P1.LE.0.0.OR.MP2.LT.MP1) GO TO 90                           FAB041
      IF(PS1P1.GT.1.0.AND..NOT.NEW) GO TO 90                            FAB042
      RETURN                                                            FAB043
C  ERROR MESSAGES.                                                       FAB044
  40  FORMAT(/,5X,"...ERROR IN FABRI: (MP2.LT.MP1).",//)                FAB045
  60  FORMAT(/,5X,"...ERROR IN FABRI: (PS1P1.LT.(0.0)).",//)            FAB046
  80  FORMAT(/,5X,"...ERROR IN FABRI: PS1P1> 1.0",//)                   FAB047
C  SET ERROR FLAG.                                                       FAB048
  90  NERROR=2                                                          FAB049
      RETURN                                                            FAB050
      END                                                               FAB051
```

UNSTEADY CONSTANT AREA EJECTOR PROGRAM (UCAE)
SUBROUTINE OCV

```
C  ****************************************************************      OCV001
C                                                                        OCV002
C                                                                        OCV003
      SUBROUTINE OCV(NERROR)                                             OCV004
C                                                                        OCV005
C  CONSTANT AREA EJECTOR OVERALL CONTROL VOLUME ANALYSIS(OCV).           OCV006
C  1-D ANALYSIS FROM INLET STATION, 1, TO EXIT STATION, 3.               OCV007
C                                                                        OCV008
      COMMON/BLOCK1/GP,GS,MP1,MWSP,TSOPO,AP1M3,MMIN,NEW,MMAX,            OCV009
     &PCRIT                                                              OCV010
      COMMON/BLOCK2/MS1,MM3,PS1P1,PMOSO,WSP,PM3SO                        OCV011
      REAL M,MP1,MS1,MM3,MM3M,MM3P,MMIN,MWSP,MWMP,MSQD3M,MSQD3P          OCV012
     &,MMAX,MR                                                           OCV013
      LOGICAL NEW                                                        OCV014
      WM(G,M)=M*SQRT(G*(1.0+0.5*(G-1.0)*(M*M)))                          OCV015
      PPO(G,M)=(1.0+.5*(G-1.0)*(M*M))**(-G/(G-1.0))                      OCV016
C  A FORM OF THE 1-D THRUST FUNCTION.                                    OCV017
      T(G,M)=(1.0+G*(M*M))/(M*SQRT(1.0+.5*(G-1.0)*(M*M)))                OCV018
C  REDEFINE MR LOCALLY.                                                  OCV019
      MR="MR"                                                            OCV020
C  CALCULATE CONSTANTS.                                                  OCV021
      C0=SQRT(MWSP/TSOPO)                                                OCV022
C  EJECTOR MASS-FLOW RATIO                                               OCV023
      WSP=PS1P1*((1.-AP1M3)/AP1M3)*C0*(WM(GS,MS1)/WM(GP,MP1))            OCV024
      CPSP=(GS/GP)*((GP-1.)/(GS-1.))/MWSP                                OCV025
C  MIXED FLOW PROPERTIES                                                 OCV026
      MWMP=(1.+WSP)/(1.+(WSP/MWSP))                                      OCV027
      GM=1./(1.-((GP-1.)/GP)*((1.+(WSP/MWSP))/(1.+CPSP*WSP)))            OCV028
C  CALCULATE THE MIXED-TO-PRIMARY STAGNATION TEMPERATURE RATIO.          OCV029
      TMOPO=(1.+WSP*CPSP*TSOPO)/(1.+WSP*CPSP)                            OCV030
C  CALCULATE SOME CONSTANTS.                                             OCV031
      C1=SQRT((TSOPO/MWSP)*(GP/GS))                                      OCV032
      C2=SQRT(TMOPO/MWMP*(GP/GM))                                        OCV033
C  SOLVING FOR MM3.                                                      OCV034
      TM3=(T(GP,MP1)+C1*WSP*T(GS,MS1))/((1.+WSP)*C2)                     OCV035
      TM3MIN=SQRT(2.*(GM+1.))                                            OCV036
      IF(TM3.LT.TM3MIN) GO TO 20                                         OCV037
      C3=(TM3**2-2.*GM)                                                  OCV038
      C4=(((GM-1.)*.5)*(TM3**2)-GM*GM)                                   OCV039
      C5=SQRT(C3*C3+4.*C4)                                               OCV040
      MSQD3M=(-C3-C5)/(2.*C4)                                            OCV041
      MSQD3P=(-C3+C5)/(2.*C4)                                            OCV042
C  DETERMINE  TWO POSSIBLE MIXED-FLOW MACH NO. SOLUTIONS.                OCV043
      IF(MSQD3M.GE.(0.0)) MM3M=SQRT(MSQD3M)                              OCV044
      IF(MSQD3P.GE.(0.0)) MM3P=SQRT(MSQD3P)                              OCV045
C  USE ONLY SUBSONIC RESULT AT (3).                                      OCV046
      MM3=MM3P                                                           OCV047
C  CALCULATE STATIC PRESSURE RATIO, PM3P1, AT (3).                       OCV048
      C6=SQRT(TMOPO/MWMP)                                                OCV049
      PM3P1=C6*AP1M3*(1.+WSP)*(WM(GP,MP1)/WM(GM,MM3))                    OCV050
C  CALCULATE OTHER STATIC AND STAGNATION PRESSURE RATIOS.                OCV051
      PM3SO=(PPO(GS,MS1))*PM3P1/PS1P1                                    OCV052
      PMOSO=PM3SO/PPO(GM,MM3)                                            OCV053
      RETURN                                                             OCV054
C  ERROR MESSAGES.                                                       OCV055
   20 WRITE (6,30)                                                       OCV056
   30 FORMAT(/,57H,"...ERROR IN OCV: NO SOLUTION.",/)                    OCV057
      NERROR=1                                                           OCV058
      RETURN                                                             OCV059
      END                                                                OCV060
```

UNSTEADY CONSTANT AREA EJECTOR PROGRAM (UCAE)
SUBROUTINE PRATIO

```
C  ***************************************************************      PRA001
C                                                                       PRA002
C                                                                       PRA003
      SUBROUTINE PRATIO(AMP,PAVG,NCYC,PSOPOI,IPRESS,CURVE)              PRA004
C  THIS SUBROUTINE INITIALIZES THE INPUT STAGNATION PRESSURE RATIO,     PRA005
C  PSOPOI, FOR EACH TIME SLUG.                                          PRA006
C                                                                       PRA007
      COMMON/BLOCK2/MS1,MM3,PS1P1,PMOSO,MSP,PM3SO                       PRA008
      COMMON/BLOCK3/SMS1,SPMOSO,SMM3,SPSOPO,SPS1P1,SMSP                 PRA009
      LOGICAL CURVE                                                     PRA010
      PI=3.141593                                                       PRA011
      IF(CURVE) GO TO 80                                                PRA012
      READ(5,50) PSOPOI                                                 PRA013
      IF(EOF(5))70,60                                                   PRA014
   50 FORMAT(F10.4)                                                     PRA015
   60 IPRESS=IPRESS+1                                                   PRA016
      NCYC=IPRESS+1                                                     PRA017
      RETURN                                                            PRA018
   70 NCYC=IPRESS                                                       PRA019
      CALL SUMUP(IPRESS,NCYC,PSOPOI,CURVE)                              PRA020
      RETURN                                                            PRA021
   80 IPRESS=IPRESS+1                                                   PRA022
      PRESS=FLOAT(IPRESS)                                               PRA023
      CYC=FLOAT(NCYC)                                                   PRA024
      PSOPOI=PAVG*(1.0+AMP*SIN(2.0*PI*PRESS/CYC))                       PRA025
      RETURN                                                            PRA026
      END                                                               PRA027
```

UNSTEADY CONSTANT AREA EJECTOR PROGRAM (UCAE)
SUBROUTINE CRITM

```
C  ***************************************************************      CRM001
C                                                                       CRM002
C                                                                       CRM003
      SUBROUTINE CRITM(MCRIT)                                           CRM004
C  THIS SUBROUTINE IS USED TO FIND THE SECONDARY MACH NUMBER, MS1,      CRM005
C  AT WHICH  PS1P1 = 1.0 IS ENCOUNTERED IN THE SR  SOLUTION.            CRM006
C                                                                       CRM007
      COMMON/BLOCK1/GP,GS,MP1,MWSP,TSOPO,AP1M3,MMIN,NEW,MMAX,           CRM008
     &PCRIT                                                             CRM009
      REAL MP1,MCRIT,MWSP,MMIN,MMAX,M                                   CRM010
      LOGICAL NEW                                                       CRM011
      M=.001                                                            CRM012
      DM=.010                                                           CRM013
      NTYPE=1                                                           CRM014
      DO 10 I=1,300                                                     CRM015
      MMIN=MP1                                                          CRM016
      CALL PABRI(M,PS1P1,VERROR)                                        CRM017
      IF(PS1P1.GT.1.0) GO TO 9                                          CRM018
      IF(M.GE.(1.0)) GO TO 11                                           CRM019
      OLDM=M                                                            CRM020
      GO TO 10                                                          CRM021
    9 IF(NTYPE.EQ.2) GO TO 11                                           CRM022
      DM=.00005                                                         CRM023
      M=OLDM                                                            CRM024
      NTYPE=2                                                           CRM025
   10 M=M+DM                                                            CRM026
   11 MCRIT=(M+OLDM)/2.0                                                CRM027
      IF(MCRIT.GE.(1.0)) MMIN=MP1                                       CRM028
      RETURN                                                            CRM029
      END                                                               CRM030
```

UNSTEADY CONSTANT AREA EJECTOR PROGRAM (UCAE)
SUBROUTINE ASTAR

```
C  ****************************************************************      AST001
C                                                                        AST002
C                                                                        AST003
      SUBROUTINE ASTAR(G,ARATIO,MP2,MMIN,MMAX)                           AST004
C  THIS SUBROUTINE SOLVES FOR MP2 GIVEN AP2/AP* FROM FABRI.              AST005
      REAL MP2,MHI,MMIN,M,MLO,MMAX                                       AST006
C  THE A/A* FUNCTION                                                     AST007
      AASM(G,M)=(1.0/M)*(2.0*(1.0+.5*(G-1.0)*(M*M))/(G+1.0))             AST008
     &**((G+1.0)/(2.0*(G-1.0)))                                          AST009
C  MAKE SURE THAT MMAX IS BIG ENOUGH FOR THE DATA SET INPUT.             AST010
      MHI=MMAX                                                           AST011
      MLO=MMIN                                                           AST012
      NIT=1                                                              AST013
   10 AHI=AASM(G,MHI)                                                    AST014
      ALO=AASM(G,MLO)                                                    AST015
      MP2=MLO+(ARATIO-ALO)*(MHI-MLO)/(AHI-ALO)                           AST016
      IF(NIT.GT.30) RETURN                                               AST017
      DIFF=ARATIO-AASM(G,MP2)                                            AST018
      IF(ABS(DIFF)/ARATIO.LE..00001)RETURN                               AST019
      IF(DIFF.GT.0.0)GO TO 20                                            AST020
      MHI=MP2                                                            AST021
      GO TO 30                                                           AST022
   20 MLO=MP2                                                            AST023
   30 NIT=NIT+1                                                          AST024
      GO TO 10                                                           AST025
      END                                                                AST026
```

UNSTEADY CONSTANT AREA EJECTOR PROGRAM (UCAE)
SUBROUTINE ITER

```
C  ********************************************************************** ITR001
C                                                                         ITR002
C                                                                         ITR003
      SUBROUTINE ITER(X,DX,ERRORX,SIGN,Y,YGIVEN,ERRORY,NIT,NTYPE,         ITR004
     &XNEG,YNEG,XPOS,YPOS,NSIGN1,NSIGN2)                                  ITR005
C  SUBROUTINE PERFORMS AN ITERATION TO FIND X SUCH THAT THE               ITR006
C  ABSOLUTE VALUE OF (Y-YGIVEN) IS .LE. TO ERRORY OR THE                  ITR007
C  ABSOLUTE VALUE OF (X(I+1)-X(I)) IS .LE. TO ERRORX.                     ITR008
C  VARIABLES:                                                             ITR009
C  X       = INDEPENDENT VARIABLE                                         ITR010
C  DX      = INCREMENT IN INDEPENDENT VARIABLE                            ITR011
C  ERRORX  = MAXIMUM VALUE OF ABS(X(I+1)-X(I)) FOR SOLN                   ITR012
C  SIGN    = +1.0 OR -1.0, +/- INCREMENTING FROM INITIAL X                ITR013
C  Y       = DEPENDENT VARIABLE                                           ITR014
C  ERRORY  = MAXIMUM VALUE OF ABS(Y-YGIVEN)                               ITR015
C  YGIVEN  = GIVEN VALUE OF DEPENDENT VARIABLE                            ITR016
C  NIT     = INCREMENT NUMBER                                             ITR017
C  NTYPE   = 1--INCREMENT, 2--INTERPOLATION, 3--SOLUTION                  ITR018
C                                                                         ITR019
      DY=Y-YGIVEN                                                        ITR020
      IF((ABS(DY)-ERRORY).LE.0.0) GO TO 90                               ITR021
      IF(DY.GT.0.0) GO TO 20                                             ITR022
      NSIGN2=-1                                                          ITR023
      XNEG=X                                                             ITR024
      YNEG=Y                                                             ITR025
      GO TO 40                                                           ITR026
   20 NSIGN2=+1                                                          ITR027
      XPOS=X                                                             ITR028
      YPOS=Y                                                             ITR029
   40 IF(NTYPE.EQ.2) GO TO 80                                            ITR030
   50 IF((NIT-1).LE.0) GO TO 60                                          ITR031
      NSIGN=NSIGN1*NSIGN2                                                ITR032
      IF(NSIGN.LE.0) GO TO 80                                            ITR033
   60 NSIGN1=NSIGN2                                                      ITR034
      NIT=NIT+1                                                          ITR035
C  INCREMENT TO FIND SOLUTION INTERVAL                                    ITR036
      X=X+SIGN*DX                                                        ITR037
      GO TO 100                                                          ITR038
C  INTERPOLATION FOR SOLUTION                                             ITR039
   80 NTYPE=2                                                            ITR040
      NIT=NIT+1                                                          ITR041
      XSAVE=X                                                            ITR042
      RATIO=(XPOS-XNEG)/(YPOS-YNEG)                                      ITR043
      X=XNEG+RATIO*(YGIVEN-YNEG)                                         ITR044
      IF(ABS(X-XSAVE) - ERRORX) 90,90,100                                ITR045
   90 NTYPE=3                                                            ITR046
  100 RETURN                                                             ITR047
      END                                                                ITR048
```

UNSTEADY CONSTANT AREA EJECTOR PROGRAM (UCAE)
SUBROUTINE ITMS1

```
C  ********************************************************************  IMS001
C                                                                        IMS002
C                                                                        IMS003
      SUBROUTINE ITMS1(MS1,PM3SO,PM3SOI,NCOUNT,MS1LO,MS1HI)              IMS004
C                                                                        IMS005
C  THIS SUBROUTINE SEARCHES FOR AN MS1 MEETING THE EXIT PLANE            IMS006
C  PRESSURE CONDITION IN CONJUNCTION WITH OCV.  RELEASE=MR.              IMS007
C                                                                        IMS008
      REAL MS1,MS1LO,MS1HI                                               IMS009
      IF(NCOUNT.GT.1) GO TO 20                                           IMS010
      MS1=.500                                                           IMS011
      MS1LO=0.0                                                          IMS012
      MS1HI=1.00                                                         IMS013
      NCOUNT=2                                                           IMS014
      RETURN                                                             IMS015
C  INCREASING MS1 DECREASES PM3SO SO:                                    IMS016
 20   IF(PM3SO.GT.PM3SOI) GO TO 40                                       IMS017
      MS1HI=MS1                                                          IMS018
      GO TO 60                                                           IMS019
 40   MS1LO=MS1                                                          IMS020
 60   MS1=(MS1HI+MS1LO)/2.0                                              IMS021
      NCOUNT=NCOUNT+1                                                    IMS022
      RETURN                                                             IMS023
      END                                                                IMS024
```

UNSTEADY CONSTANT AREA EJECTOR PROGRAM (UCAE)
SUBROUTINE SUMUP

```
C  ****************************************************************      SUM001
C                                                                         SUM002
C                                                                         SUM003
      SUBROUTINE SUMUP(IPRESS,NCYC,PSOPOI,CURVE)                          SUM004
C  THIS SUBROUTINE CALCULATES THE MEAN VALUES OF MS1, PS1P1, WSP,         SUM005
C  PMOSO, PSOPO, AND MM3.  IF A DATA FILE IS TO BE READ IT SHOULD         SUM006
C  CONTAIN AN INTEGER NUMBER OF PRESSURE CYCLES.                          SUM007
C                                                                         SUM008
      COMMON/BLOCK2/MS1,MM3,PS1P1,PMOSO,WSP,PM3SO                         SUM009
      COMMON/BLOCK3/SMS1,SPMOSO,SMM3,SPSOPO,SPS1P1,SWSP                   SUM010
      REAL MS1,MM3                                                        SUM011
      LOGICAL CURVE                                                       SUM012
      IF(IPRESS.GT.1) GO TO 10                                            SUM013
      SMS1=0.0                                                            SUM014
      SPMOSO=0.0                                                          SUM015
      SMM3=0.0                                                            SUM016
      SPSOPO=0.0                                                          SUM017
      SPS1P1=0.0                                                          SUM018
      SWSP=0.0                                                            SUM019
   10 IF(NCYC.EQ.IPRESS.AND..NOT.CURVE) GO TO 20                          SUM020
      SMS1=MS1+SMS1                                                       SUM021
      SMM3=MM3+SMM3                                                       SUM022
      SPSOPO=PSOPOI+SPSOPO                                                SUM023
      SPS1P1=PS1P1+SPS1P1                                                 SUM024
      SPMOSO=PMOSO+SPMOSO                                                 SUM025
      SWSP=WSP+SWSP                                                       SUM026
      IF(IPRESS.NE.NCYC) RETURN                                           SUM027
   20 TOT=FLOAT(NCYC)                                                     SUM028
      SMS1=SMS1/TOT                                                       SUM029
      SMM3=SMM3/TOT                                                       SUM030
      SPSOPO=SPSOPO/TOT                                                   SUM031
      SPS1P1=SPS1P1/TOT                                                   SUM032
      SPMOSO=SPMOSO/TOT                                                   SUM033
      SWSP=SWSP/TOT                                                       SUM034
      WRITE(6,30) SMS1,SMM3,SPSOPO,SPS1P1,SPMOSO,SWSP                     SUM035
   30 FORMAT(///,10X,"THE MEAN VALUES OVER A PRESSURE CYCLE ARE:",//,     SUM036
     &10X,"MS1=",F10.4,10X,"MM3=",F9.4,11X,"PSOPO=",F7.4,//,10X,         SUM037
     &"PS1P1=",F8.4,10X,"PMOSO=",F8.4,10X,"WSP=",F8.4)                   SUM038
      RETURN                                                              SUM039
      END                                                                 SUM040
```

A.2 SAMPLE PROGRAM INPUT AND OUTPUT

THE INPUT IS:

```
$IOCAE MP1=2.0,AP1M3=.333,MMAX=3.3,PM3SOI=2.34$
```

THE OUTPUT IS:

```
     INPUT DATA FOR CASE NO.  1

     GS= 1.4000        GP= 1.4000        MWSP= 1.0000

     PSOPO= 1.0000     AP1M3=  .3330     MP1= 2.0000

     PM3SOI=  2.3400

     FOR THIS CASE, MCRIT=  .8014     PCRIT=  .1951

     FOR THE SINUSOIDAL PRESSURE RATIO CURVE:
     AMP=   .100          PAVG=  .1000          NCYC=   10 TIME SLUGS/CYCLE
```

TIME SLUG DATA

SLUG	REGIME	PSOPO	WSP	MS1	PS1P1	MM3	PMOSO	PM3SO
1	SR	.1059	.2465	.4487	.7215	.5435	2.9384	2.4036
2	MR	.1095	.2577	.4551	.7434	.5446	2.8627	2.3398
3	MR	.1095	.2577	.4551	.7434	.5446	2.8627	2.3398
4	SR	.1059	.2465	.4487	.7215	.5435	2.9384	2.4036
5	SR	.1000	.2205	.4186	.6935	.5362	3.0744	2.5280
6	SR	.0941	.1946	.3867	.6643	.5287	3.2275	2.6679
7	SR	.0905	.1786	.3659	.6454	.5240	3.3328	2.7640
8	SR	.0905	.1786	.3659	.6454	.5240	3.3328	2.7640
9	SR	.0941	.1946	.3867	.6643	.5287	3.2275	2.6679
10	SR	.1000	.2205	.4186	.6935	.5362	3.0744	2.5280

```
     THE MEAN VALUES OVER A PRESSURE CYCLE ARE:

     MS1=      .4150          MM3=     .5354          PSOPO=  .1000

     PS1P1=    .6936          PMOSO=  3.0872          WSP=    .2196

     THE TOTAL NUMBER OF TIME SLUGS READ WAS   10
```

APPENDIX B

The initial phases of this research effort were concerned with the development of a large-scale, cold-flow, air fluidic oscillator to provide a periodic ejector driver flow and an investigation of the potential use of fluidic devices to enhance mixing between multiple supersonic streams.

B.1 WATER TABLE EXPERIMENTS

The preliminary stages of this investigation were based on the hydraulic analogy and were conducted entirely on the water table. With this approach, simple and inexpensive experimental models could be rapidly fabricated which would provide a qualitative insight into the factors influencing the flow.

The use of the hydraulic analogy is generally accepted for modeling one-dimensional or plane two-dimensional, compressible flow; however, the analogy for unsteady, compressible flow modeling is not as well understood or accepted. Loh [40] derives the constitutive equations governing one-dimensional channel flow of a liquid and makes a comparison with the corresponding equations governing unsteady, compressible, isentropic flow. He concluded that qualitatively the analogy exists although the relationships between the two flows are considerably more complex.

All preliminary water table experimentation was done with styrofoam models. These models were cut with an electrically heated nichrome wire from four inch thick styrofoam blocks. To improve motion pictures of the

flow, a black polymer film was bonded to the styrofoam blocks prior to cutting so that the upper surface of all models would be highly visible against the white bedplate of the water table. The styrofoam models were mounted on a wooden bedplate with specially fabricated spiked clamps. The bedplate was clamped in position on the water table surface; gates and ports on the bedplate controlled the flow of water to the oscillator models.

Three basic fluidic oscillator geometries were investigated and are shown in Figs. B.1-1, B.1-2, and B.1-3. The principles of operation of the single-jet oscillator are discussed fully in Section 3.1; in a similar fashion, the balance-ended oscillator exploits the bistability of a jet impinging on a knife-edge. The middle jet of the three-jet interleaved oscillator is steady and is supplied through a port on the surface of the water table bedplate. These oscillator configurations were selected because of their simplicity and adaptability to the problems of interest. A flip-flop jet oscillator similar to Viets' configuration [30,31] was not considered because of the potential for high flow losses and its relative complexity.

The experimental procedure during the hydraulic analogy experiments was to gradually increase the height of the water in the large plenum upstream of the oscillator model being investigated until a desired level was reached and then the observations were made. The individual styrofoam pieces of the model could be repositioned easily so that the effects of the relative positions of the pieces could be investigated quickly.

The objectives of these preliminary hydraulic analogy experiments were:

1. To investigate the operational characteristics of these oscillator configurations;
2. To determine the factors influencing their behavior;
3. To determine if the pulsations of the three-jet oscillator enhanced mixing between interleaved supersonic streams; and
4. To examine a supersonic-subsonic ejector configuration on the water table which is driven by the single-jet oscillator in order to gain insight into the flow phenomena involved.

The single-jet oscillator configuration shown in Fig. B.1-1 performed very poorly. The motion of the jet was extremely irregular, moving only slightly left or right of the knife-edge and producing nearly negligible pressure pulses. The centerbody forming the feedback loop was recontoured as shown in Fig. B.1-4. The tendency of a jet to attach to a nearby wall, the *Coanda* effect, tends to pull the inlet jet away from the knife-edge so that it is directed into the feedback loop. The narrower feedback loop channel and the now vigorous action of the jet resulted in a strong pressure pulse moving through the feedback loop. The proximity of the feedback loop centerbody to the inlet jet also causes the inlet jet to flip well across the knife-edge into the resonance chamber when the feedback loop pulse reaches the inlet. This is because the surge of flow in the feedback loop can exit the loop only by deflecting the inlet jet toward the resonance chamber.

Figure B.1-5 is a photograph of a plexiglass model with the feedback loop centerbody moved away from the inlet jet. Figure B.1-6 is the same model with the centerbody moved slightly towards the jet. The jet action in the latter figure is much more pronounced and stable.

The balance-ended oscillator exhibited stability problems. If the stagnation height of the water in the plenum was gradually and carefully increased during start-up, the oscillator operated at about .44 Hz. A rapid start-up of the oscillator or a disturbance in the oscillator would result in the oscillator operating at approximately twice the previous frequency, about .90 Hz, and at half of the previous amplitude. Apparently the lack of surfaces near the jet leave it free to oscillate in higher frequency modes. If the resonance chambers are capable of sustaining these higher frequency modes, the oscillator will be somewhat unpredictable and unstable operation will be observed. Control vanes were positioned in the vicinity of the jet inlet as shown in Fig. B.1-7. The tendency for the jet to attach to these surfaces caused the jet to flip further to the left and right. This action prevented the jet from oscillating in higher frequency modes and increased the amplitude of the pulses.

Figure B.1-8 is the flow field produced by the three-jet oscillator. The large undulations in the steady jet at the center were absent when all three jets were steady.

The single-jet oscillator was also used to drive a supersonic-subsonic configuration during the hydraulic analogy experiments. Not much time was spent on this model due to leakage and secondary flow control problems.

The effects of the pulsed driver on the shock wave structure within the mixing duct and the rapid mixing of primary and secondary streams after the disintegration of the supersonic core, see Section 3.3.2, were observed.

A Super-8 color film detailing the above experiments is available upon request from Professor A. L. Addy.

The final series of hydraulic analogy experiments were performed with a plexiglass model of the single-jet oscillator; this is shown in Fig. B.1-9.[†] The plexiglass model has greater dimensional stability and control than the styrofoam model. The experiments with the styrofoam model gave only a crude picture of what factors affected oscillator performance and how. Features incorporated into the plexiglass model included (1) adjustable inlet and outlet jet widths, (2) adjustable inlet to knife-edge separation distance, and (3) a movable feedback loop centerbody. Leakage, which had been a problem with the styrofoam model, was prevented by using o-rings and a vacuum hold-down system.

Frequency, waveform, and amplitude characteristics of the single-jet oscillator model were accurately determined by videotaping, through the transparent glass and plexiglass walls of the water table and resonance chamber of the oscillator model, the passage of waves in the resonance chamber. A ruled scale and timer were located within the camera's view. Stop action, single-frame advance, and slow motion features of the video system aided accurate waveform and amplitude determination.

[†]This series of experiments and the design of the plexiglass oscillator model were performed by T. R. Stover [42], former graduate student.

A series of experiments were conducted with this oscillator model following a classical experiment sequence. The variables of interest were the ratio of the outlet jet to inlet jet width, the ratio of the inlet to knife-edge separation distance to the inlet jet width, and the ratio of the inlet jet width to the oscillator resonance chamber length. These ratios will be referred to as R_1, R_2, and R_3, respectively.

Oscillator frequencies were found to be 12% less than what surface wave theory suggests. This is certainly due in part to the time required for the jet to flip across the knife-edge and then back again. Also, the ratio of the wave amplitude to mean water height was not negligible.

Amplitudes were found to rapidly increase with the ratio of knife-edge separation distance to inlet jet width, R_2, to some maximum value and then to gradually decrease as this ratio was further increased. The value of R_2 at which the maximum amplitudes occurred was insensitive to R_1 but increased slightly as R_3 was decreased.

The ratio of the mean height of the water in the resonance chamber to the plenum chamber stagnation height was linearly proportional to R_1. Wave amplitudes were found to increase with R_1 up to $R_1 = 1.0$. Lesser amplitudes were always observed when R_1 was further increased to $R_1 = 1.3$. Generally amplitudes were found to increase with R_3 too. These facts suggest that the maximum amplitudes are obtained at the maximum mass flowrate; i.e., when the inlet jet has the most energy as it flip-flops. Choking at the inlet appears to occur if $R_1 > 1.0$.

The waveform was not significantly altered by changes of any of these geometric ratios. The waveform rise times decreased slightly as the mass

flowrate was increased. A higher frequency beat was always noticed at the peak of each pulse. This was due to transverse oscillations of the jet while it resided in the resonance chamber. This is believed to be the cause of the high frequency beats seen in the air flow oscillator, see Fig. 3.3.2-29.

The results of these experiments were used to design the air flow oscillator. A value of R_1 was selected that was sufficiently small to ensure, beyond any doubt, that the C-D primary flow nozzle at the ejector inlet was always choked but R_1 was still sufficiently close to a value of 1.0 such that the maximum amplitude pressure pulses were approached; R_1 = 2/3 was used. The oscillator design incorporated a movable knife-edge so that amplitudes could be adjusted. It was assumed that the mass flowrate through the oscillator would be large enough so that the optimum value of R_2 would not be too large. A moderate value of R_2 was used to determine the maximum knife-edge separation given the inlet jet width. Unless this value of R_2 was far too small, the amplitude of the pulses obtained at the maximum knife-edge separation would be near the maximum obtainable for the previously selected value of R_1.

Details concerning the design and performance of the large-scale air flow oscillator can be found in Sections 3.1 and 3.3 of this report.

B.2 AIR FLOW FLUIDIC OSCILLATOR EXPERIMENTS

A series of cold air flow experiments were run with the fluidic oscillator prior to all ejector experiments. Frequencies from 75 Hz to 250 Hz were examined; the highest frequency was limited by the minimum possible lengths of the feedback loop and resonance chamber.

The operating frequencies of the oscillator were about 25% less than the estimates made assuming pulses moved at the estimated sonic speed. By changing the resonance chamber length while keeping the feedback loop length constant and measuring the resulting frequencies, it was possible to estimate pulse propagation speeds. Propagation speeds were in excess of the sonic velocity as expected. Thus, it appears the time it takes the inlet jet to flip-flop is the cause for the low operating frequency limits.

The ratio of the resonance chamber to feedback loop lengths were varied over a wide range with no apparent effects other than frequency effects.

The results of these experiments were used to determine which operating frequencies and oscillator configurations would be used in the ejector experiments. The knife-edge setting was left at the maximum R_2 or separation distance. Pressure pulses were considered to be sufficiently large and extending the knife could have caused vibration or leakage problems.

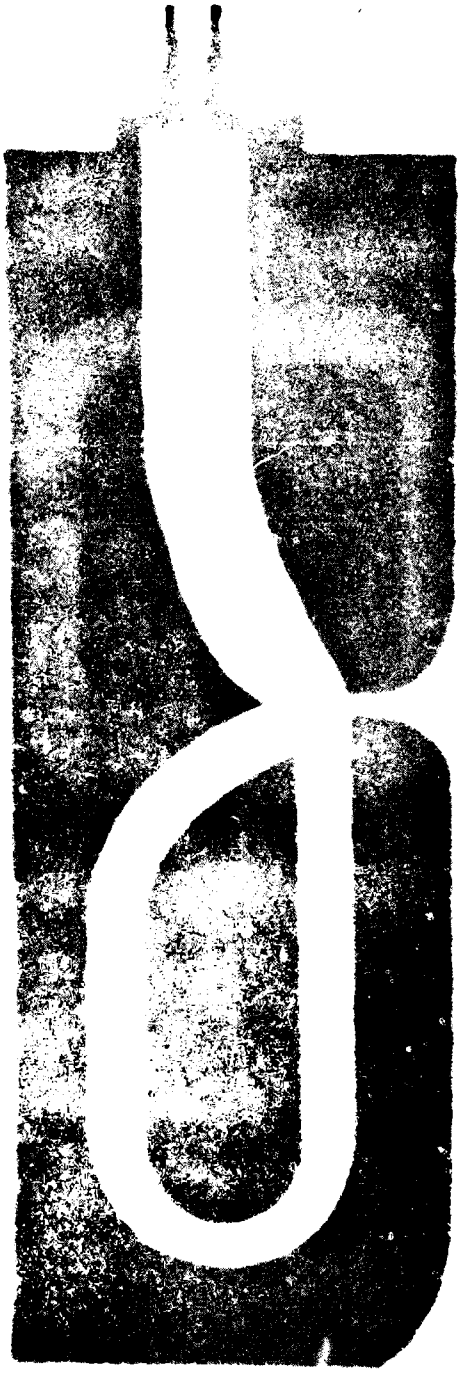

Figure B.1-1 The single-jet oscillator

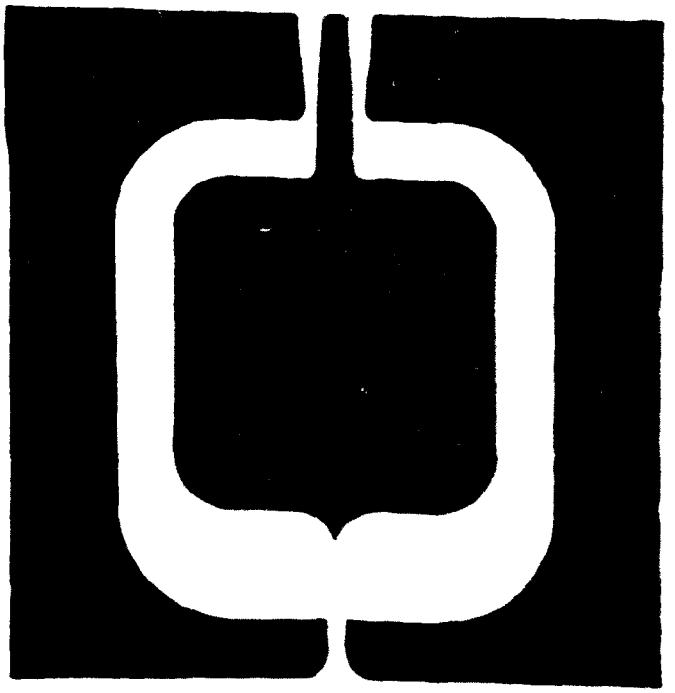

Figure B.1-2 The balance-ended oscillator

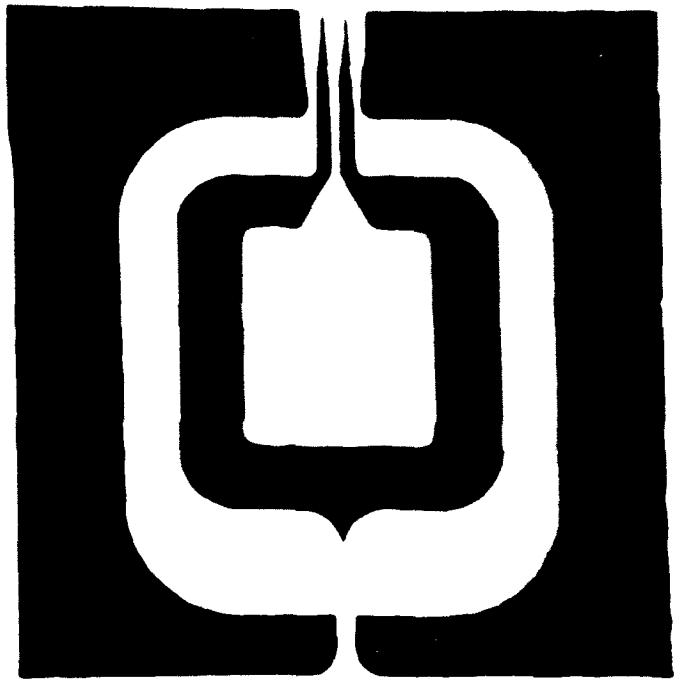

Figure B.1-3 The three-jet interleaved oscillator

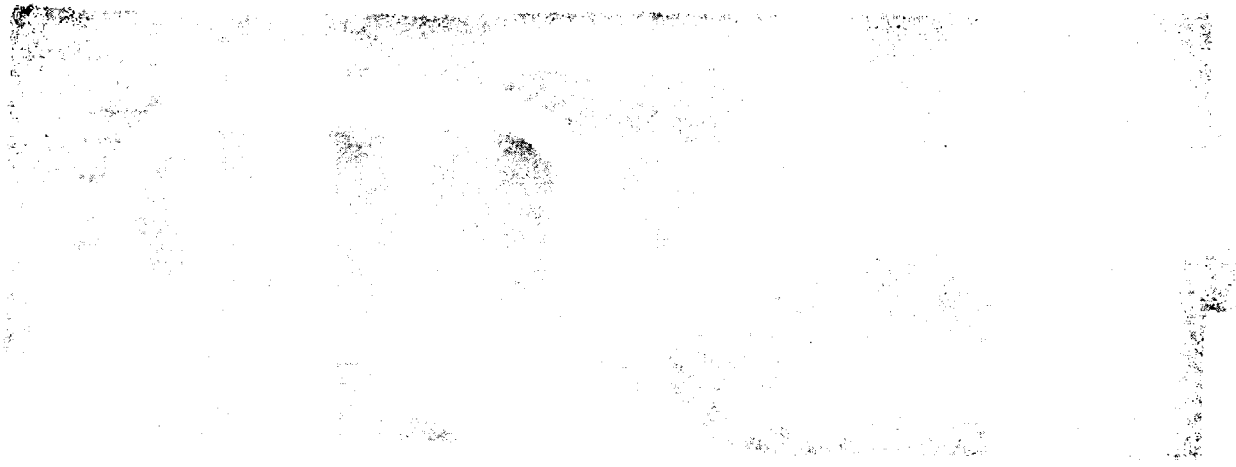

Figure B.1-4 The improved single-jet oscillator configuration

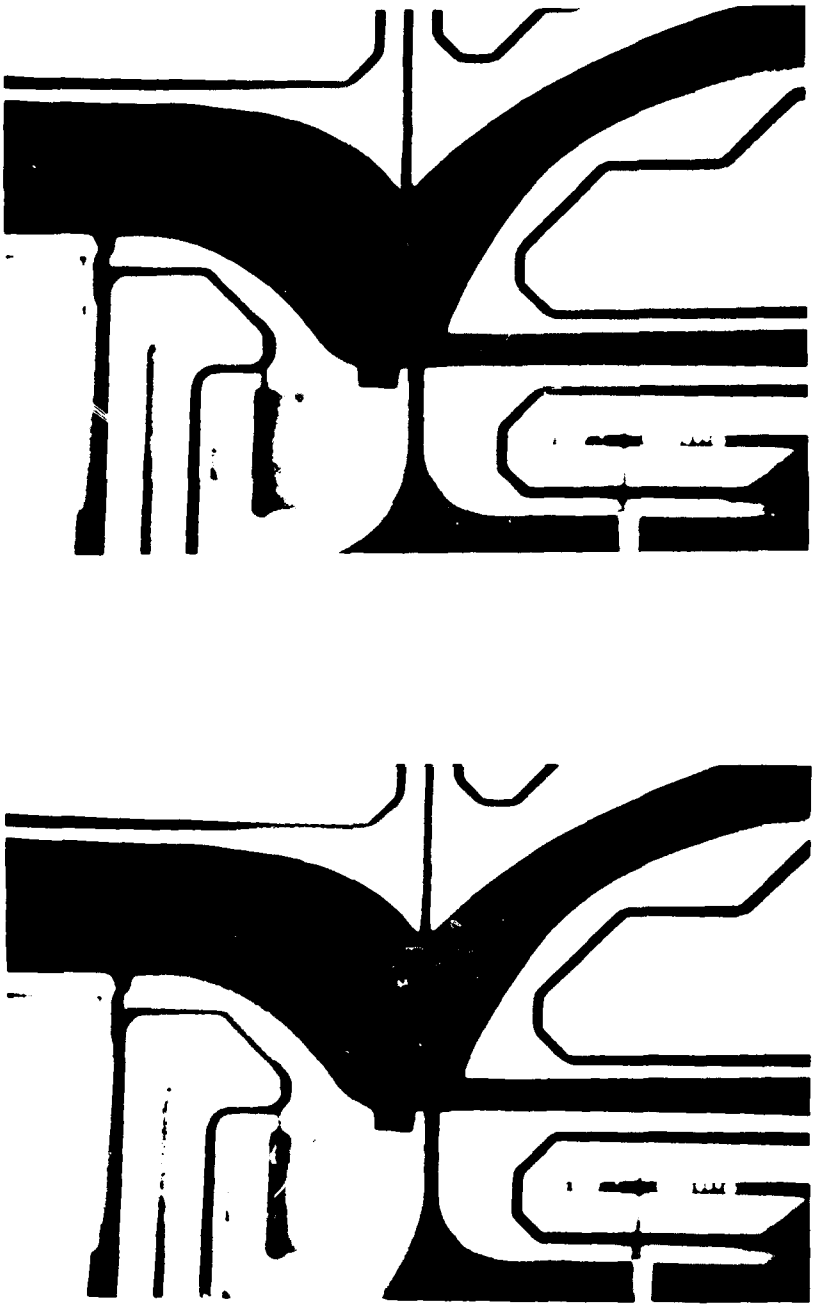

Figure B.1-5 Single-jet oscillator with centerbody moved away from inlet jet

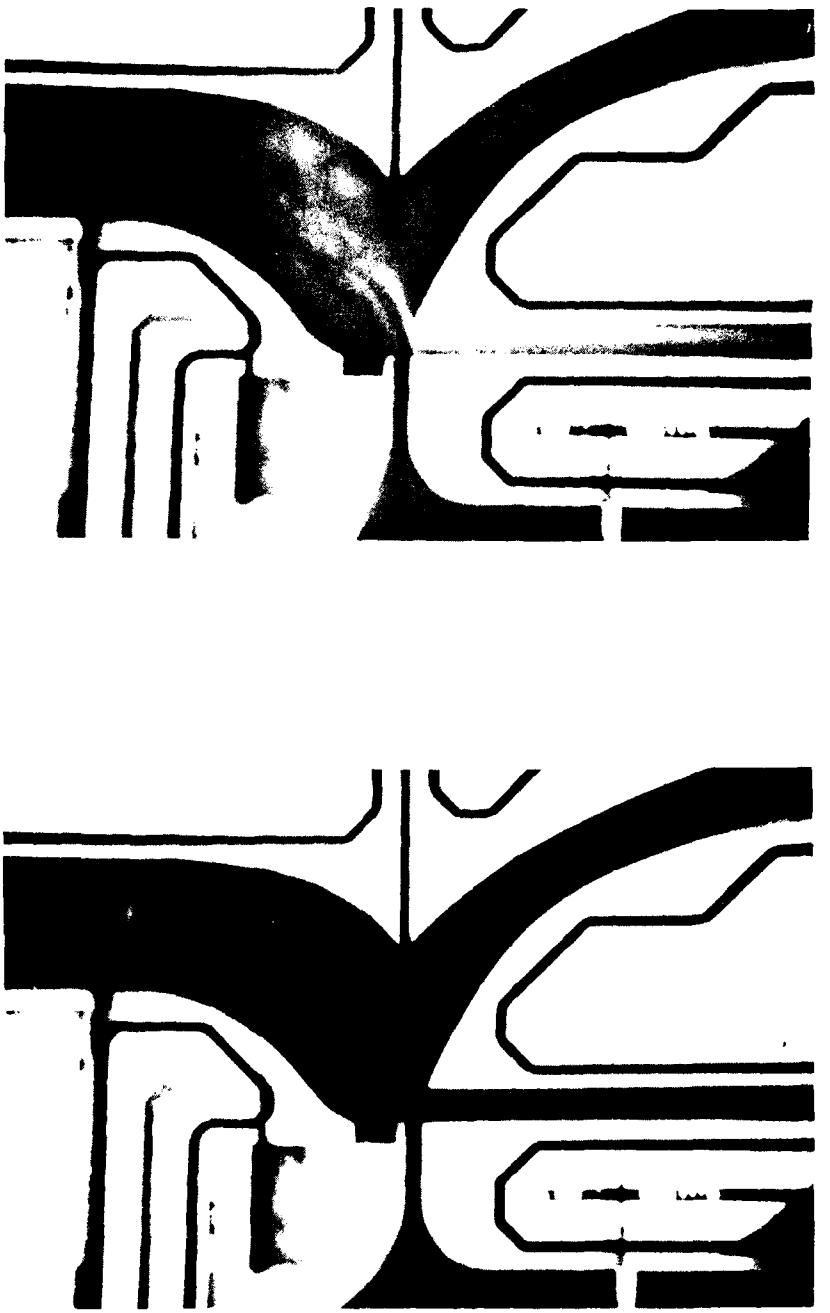

Figure B.1-6 Single-jet oscillator with centerbody in position for jet attachment

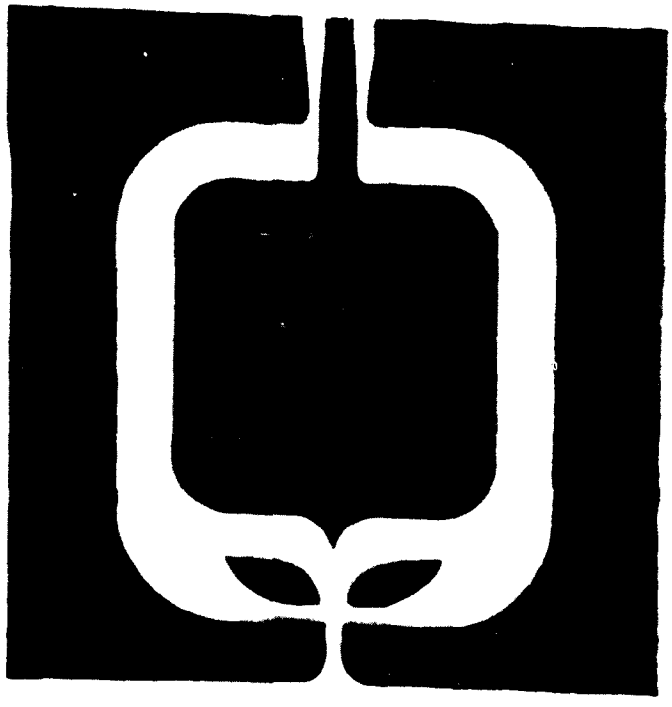

Figure B.1-7 Balance-ended oscillator with flow control vanes in position

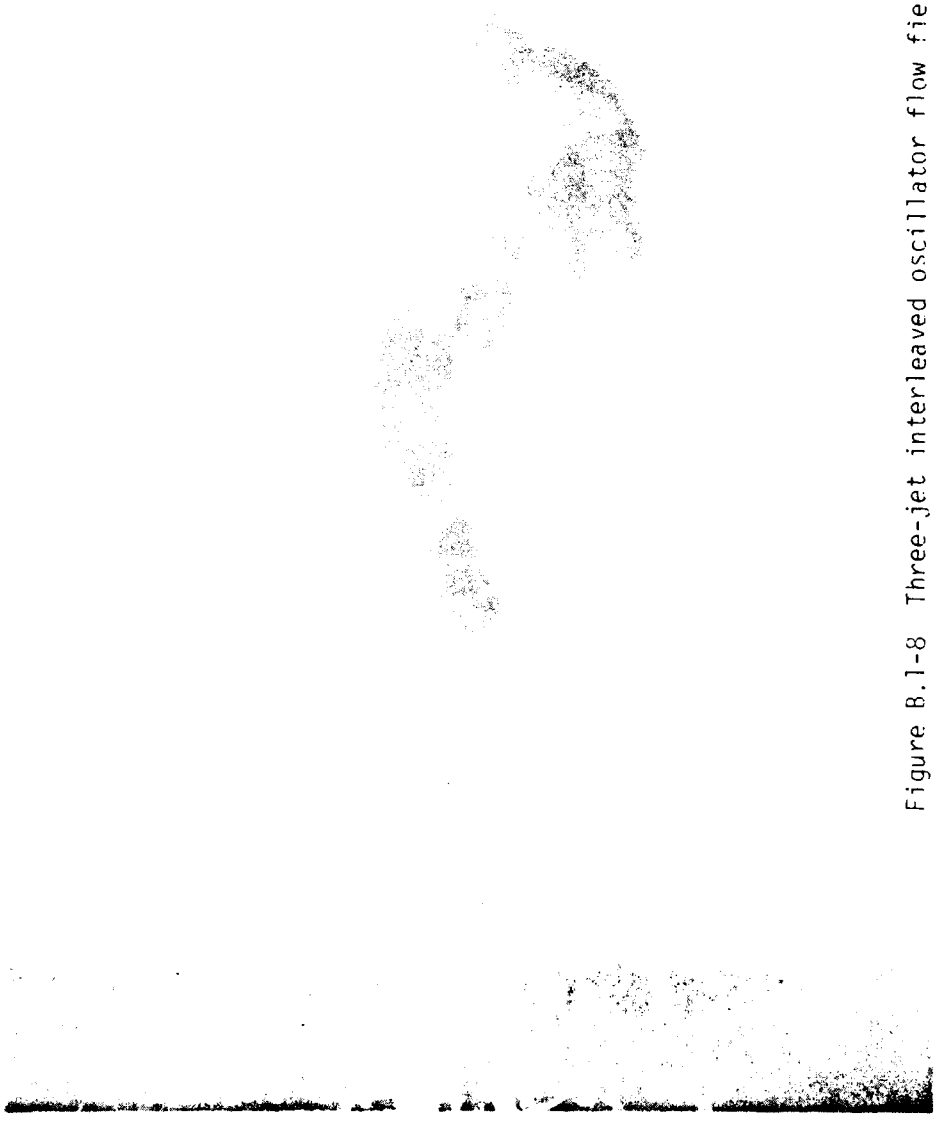

Figure B.1-8 Three-jet interleaved oscillator flow field

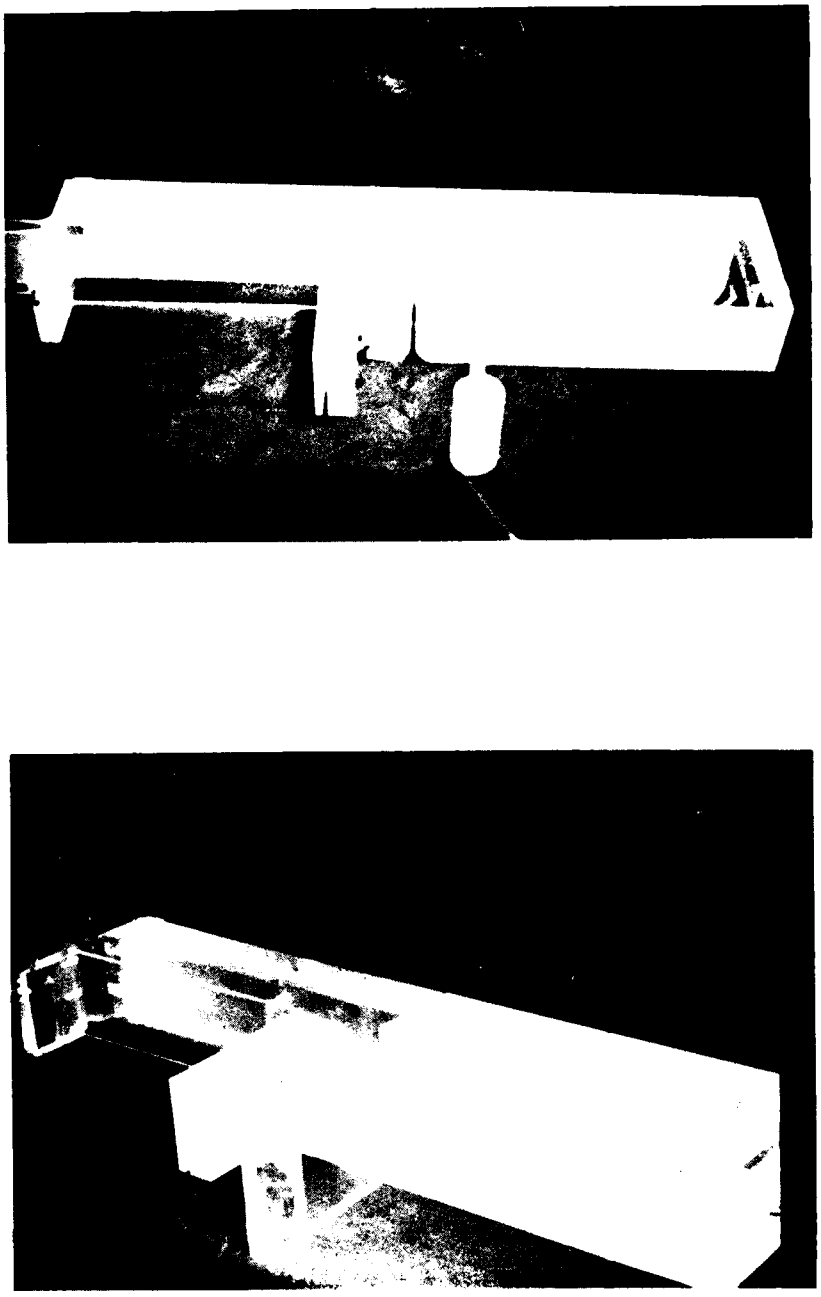

Figure B.1-9 Plexiglass model of the single-jet oscillator

APPENDIX C

This appendix lists the faculty, graduate students, and support staff who participated on a part-time basis during the performance of this research grant.

FACULTY

A. L. Addy
Principal Investigator
Professor of Mechanical Engineering

GRADUATE STUDENTS

J. C. Dutton
Ph.D. 1979
Lawrence Livermore Laboratories

H. L. Petrie
M.S. 1979
Ph.D. Candidate

S. H. White
M.S. 1978
E. I. Du Pont De Nemours

T. R. Stover
M.S. 1978
Cummins Diesel

M. R. Sandberg
M.S. 1977
Petro-Marine, Inc.

V. Amatucci
M.S. Candidate

D. Kuntz
M.S. Candidate

SUPPORT STAFF

Karen Bryan
Clerk-Stenographer III

Allen F. Stephens
Research Machine Shop Supervisor

Leroy Westendorf
Instrument Maker